CAPITAL UNIVERSITY OF SCIENCE AND TECHNOLOGY, ISLAMABAD

MHD Inclined Magnetic Field with Joule Heating and Thermal Radiation with Stagnation Point Flow

by

Ayesha Maqbool

A thesis submitted in partial fulfillment for the degree of Master of Philosophy

in the

Faculty of Computing
Department of Mathematics

2021

I dedicate my thesis to my idolized father ***Maqbool Ahmed*** *and my mother* ***Shahida Perveen*** *who always stand by my side.*

CERTIFICATE OF APPROVAL

MHD Inclined Magnetic Field with Joule Heating and Thermal Radiation with Stagnation Point Flow

by

Ayesha Maqbool

(MMT183019)

THESIS EXAMINING COMMITTEE

S. No.	Examiner	Name	Organization
(a)	External Examiner	Dr. Iftikhar Ahmad	UOG, Gujrat
(b)	Internal Examiner	Dr. Muhammad Afzal	CUST, Islamabad
(c)	Supervisor	Dr. Shafqat Hussain	CUST, Islamabad

Dr. Shafqat Hussain
Thesis Supervisor
March, 2021

Dr. Muhammad Sagheer
Head
Dept. of Mathematics
March, 2021

Dr. Muhammad. Abdul Qadir
Dean
Faculty of Computing
March, 2021

Author's Declaration

I, **Ayesha Maqbool** hereby state that my MS thesis titled "**MHD Inclined Magnetic Field with Joule Heating and Thermal Radiation with Stagnation Point Flow**" is my own work and has not been submitted previously by me for taking any degree from Capital University of Science and Technology, Islamabad or anywhere else in the country/abroad.

At any time if my statement is found to be incorrect even after my graduation, the University has the right to withdraw my M.Phil Degree.

(Ayesha Maqbool)

Registration No: MMT183019

Plagiarism Undertaking

I solemnly declare that research work presented in this thesis titled "**MHD Inclined Magnetic Field with Joule Heating and Thermal Radiation with Stagnation Point Flow**" is solely my research work with no significant contribution from any other person. Small contribution/help wherever taken has been duly acknowledged and that complete thesis has been written by me.

I understand the zero tolerance policy of the HEC and Capital University of Science and Technology towards plagiarism. Therefore, I as an author of the above titled thesis declare that no portion of my thesis has been plagiarized and any material used as reference is properly referred/cited.

I undertake that if I am found guilty of any formal plagiarism in the above titled thesis even after award of M.Phil Degree, the University reserves the right to withdraw/revoke my M.Phil degree and that HEC and the University have the right to publish my name on the HEC/University website on which names of students are placed who submitted plagiarized work.

(Ayesha Maqbool)
Registration No: MMT183019

Acknowledgement

Starting with the name of Almighty **ALLAH** who is most gracious and omnipresent, who makes the mankind and created this world to reveal what is veiled. Also, the **Prophet Muhammad (Peace Be Upon Him)** who is a guidance in every aspect of life for the betterment of Humanity.

Firstly, I would like to express my deepest appreciation to my supervisor **Dr. Shafqat Hussain** for the continual support of my M.Phil research and also for his immense knowledge and enthusiasm. Without his tireless help, I would have not been able to commence this present research work. I could not have imagined having a better mentor and supervisor for my M.Phil thesis.

Besides my supervisor, I would like to thank the rest of my M.Phil course work teachers for their great vision and motivation. Therefore, I want to thank my seniors and fellow labmates, for their stimulating discussion.

Further on, I am grateful to my friends and my family: my parents and sibling for supporting me spirituality all over my life.

(Ayesha Maqbool)

Abstract

This investigation is undertaken to explore the impact of thermal radiation on the development of Magnetohydrodynamic with stagnation point and inclined magnetic field with Joule heating, laminar, incompressible two dimensional steady flow through a stretching surface. A mathematical model that resembles the physical flow problem has been developed. Impact of stretching ratio parameter, inclined magnetic field with Joule heating and thermal radiation have been incorporated. Meanwhile, a system of non-linear ordinary differential equations are obtained by using appropriate similarity transformation on the governing partial differential equations. The resulting system of ordinary differential equations is solved numerically by utilizing a shooting technique coupled with Range Kutta fourth order method, implemented in the computational software MATLAB. Influence of different physical parameters on velocity, temperature and concentration profiles are analyzed through graphs. Numerical values of skin fraction coefficient, Nusselt number, and Sherwood number are also computed and discussed.

Contents

List of Figures

List of Tables

Abbreviations

CFD	Computational fluid dynamics
PDEs	Partial differential equations
ODEs	Ordinary differential equations
MHD	Magnetohydrodynamics
RK	Range Kutta
IVP	Initial value problem
BVP	Boundary value problem

Symbols

U_w	Fluid velocity at wall
T_w	Wall temperature
C_w	Nanoparticle concentration on the surface
S	Cauchy stress tensor
p	Pressure
I	Identity tensor
μ_0	Limiting viscosity at zero shear rate
μ_∞	Limiting viscosity at infinite shear rate
A_1	Rivlin Ericson tensor
u	Velocity component in the x-direction
v	Velocity component in the y-direction
ρ_{nf}	Nanofluid density
$(\rho C_p)_f$	Heat capacitance of fluid
$(\rho C_p)_{nf}$	Heat capacitance of nanofluid
T	Fluid temperature
T_∞	Ambient fluid temperature
C_∞	Ambient fluid concentration
B_0	Strength of magnetic field
A, B	Constants
l	Characteristic length
α_{nf}	Thermal diffusivity of the nanofluid
μ_{nf}	Dynamic viscosity of the nanofluid
ρ_s	Density of the nanoparticles

$(\rho C_p)_s$	Heat capacitance of the nanoparticles
$g(\eta)$	Dimensionless temperature
$\varphi(\eta)$	Dimensionless concentration
M	Magnetic parameter
P_r	Prandtl number
E_c	Eckert number
K	Porosity parameter
H_e	Heat generation rate parameter
N_b	Brownian motion parameter
N_t	Thermophoresis parameter
S_c	Schmidt number
K_1	Chemical reaction parameter
D_u	Dufour number
S_r	Soret number
Q	Radiation absorption parameter

Greek symbols

τ	Extra stress tensor
π	Second invariant tensor
η	Similarity variable
λ	Non-Newtonian parameter
ϕ	Volume fraction of nanoparticles

Subscripts

f	Fluid
nf	Nanofluid
s	Nanoparticles

Chapter 1

Introduction and Literature Survey

This chapter provides introduction of computational fluid dynamics related to various respective aspects. A review on the fluid flow and the heat distribution process shall be done in accordance with the stretching surface. A brief introduction and significance of boundary layer, magnetohydrodynamics, thermal radiation, Joule heating, stagnation point and inclined magnetic field flow are described.

1.1 Computational Fluid Dynamics (CFD)

Computational fluid dynamics, now known as CFD, is described as a collection of methodologies that allow the computer to provide us with a numerical simulation of fluid flows [1]. The object of a flow simulation is to figure out how the flow in a given system behaves under a given set of inlet and outlet conditions. These states are commonly referred to as boundary conditions [2]. The cornerstone of CFD is the fundamental governing equations of fluid dynamics - energy equation (energy is conserved), momentum equation ($F = ma$) and the continuity equation (mass is conserved) [3]. In our daily life, examples of fluid flow are apparent in different

applications like meteorology, air conditioning, aerodynamic design, engine combustion, industrial process, also blood flow in human body and so on. Archimedes was a Greek mathematician, who first inspected the fluid statics and buoyancy, then composed the famous law known as the Archimedes principle. Computational fluid dynamics has been a field of significant research and development since the early 20th century. Leonardo da Vinci (1452 - 1519) introduced the equation of mass for one dimensional steady-state flow. Isaac Newton (1642 -1727) stated the laws of motion and the law of viscosity. Leonhard Euler (1707-1783) postulated the integral and differential form of equations of motion, known as Bernoulli equation.

Navier (1785 - 1836) and Stokes (1819 - 1903) included viscous term in the equation of motion. Ludwig Prandtl (1875 - 1953) noted that with limited viscosity fluid flows, such as water flows and air flows can be divided into thin boundary layers close to the solid surfaces. Fluid dynamics has a wide range of applications, including the calculation of forces on aircraft [4], predicting weather patterns [5], magnetic cell separation [6] and in various metallurgical procedures [7].

1.2 Magnetohydrodynamics (MHD)

The magnetohydrodynamics is the branch of mechanics which deals with magnetic behavior and properties of electrically conducting fluid. When a conducting fluid moves through a magnetic field, it induces current, as a result Lorentz force is produced which changes the movement of the fluid. The MHD factor has a fundamental role in controlling the cooling rate and for achieving the desired quality of the product. It is of concern that applications of MHD flows occur in a variety of industrial fields, such as electrical propulsion for space travel, crystal development in liquids, cooling of nuclear reactors, etc. To the author's understanding, Pavlov [8] was first who study the MHD flow over a stretched wall. Furthermore, addressed the analysis in the presence of a uniform magnetic field and obtained an accurate analytical approach. Kabir et al. [9] investigated the impact of viscous dissipation on MHD natural convectional flow with a vertical wavy surface. They

concluded that the temperature and velocity profiles enlarge by mounting the variation of Eckert number. Hayat et al. [10] explored the impact of chemical reaction in MHD flow through a nonlinear over stretching surface. Moreover, highlights the flow analysis is considered under the action of applied magnetic field.

1.3 Stagnation Point

The stagnation point is defined as a point in the flow field where the local velocity of the fluid is zero and exists on the surface of the objects in the flow field where the fluid is brought to rest by the object. The stagnation point flow to the stretching sheet is very useful and significant from a functional point of view. There are different mathematical methods used to solve nonlinear differential equations [11]. Initially, Hiemenz [12] suggested the idea of a stagnation point flow. According to his theory, the stagnation point flow describes the motion of fluid particles adjacent to the stagnation area of a solid surface for both fixed and moving bodies. Grosan et al. [13] worked on the MHD oblique stagnation point flow. Markin and Pop [14] reported the effect of exothermic surface reaction is considered in the presence of a stagnation point flow on a stretching/shrinking surface. Weidman [15] studied planar stagnation point flow normally impinging a rotating plate. Mahapatra and Gupta [16] are currently analysing Homann stagnation point flow for non-axisymmetric viscoelastic liquid numerically. Lok et al. [17] recently investigated electrically conductive and viscous fluid with the presence of a uniform magnetic field over a stretching/shrinking surface in the sense of a non-orthogonal stagnation point flow.

1.4 Inclined Magnetic Field

Inclined magnetic field is basically the non-zero inclination of magnetic field. Inclination is the angle between the direction of vector and another preferred direction in the problem [18]. Further, Hayat et al. [19] deliberated with the impact of

inclined magnetic field on peristaltic flow of an incompressible Williamson fluid in an inclined channel with heat and mass transfer. It was observed that the velocity profile enhances for increase in inclined magnetic field. Sandeep and Sugunamma [20] scrutinized the influences of radiation and inclined magnetic field on free convective flow of viscous dissipative fluid over a vertical sheet via porous medium in existence of heat source. It was found that declination of inclination angle diminish the magnetic field effect. As a result at $\omega = \pi/6$, the fluid velocity and temperature were increased slightly.

1.5 Joule Heating

The movement of electrical current produces heat that is known as the Joule heat phenomenon. Joule heating is often known as Ohmic heating. Joule heating has a regular set of built-up and technological advancement, such as electrical fires, electrical heaters, radiant light bulbs, electrical fuses, and electronic fag. Some studies are provided here for the principle of Joule heating. Rahman [21] discussed the micropolar fluids of convective flows from radiative isothermal porous surfaces with Joule heating and viscous dissipation also considered the cooling process. Khan et al. [22] analyzed the features of heterogeneous and homogeneous reactions in magneto Casson liquid flow induced by slandering surface. Dissipation and Joule heating aspects were also accounted.

1.6 Thermal Radiation

Thermal radiation is described as the amount of energy emitted depend on the temperature of the surface. Recently, thermal radiation has a significant effect on the thermal transport properties in the dynamics and manufacturing area, interstellar science, high temperature advances. Thermal radiation characterises the thermal heat forming the surface and diffusing in both directions. In addition, it has an important role to play in improving the thermal transport characteristics of

polymer dispensing industry. Ilbas [23] addressed the impact of thermal radiation in the presence combustion modeling that will be very useful in this pattern and numerous performances to boost radiation have been sought. Waqas et al. [24] discussed the effect of radiation and MHD in the updated nanofluid relationship numerically and explored that thermal radiation characterizes the heat transfer process.

Many aspects in this study are important to explore for a thorough understanding of computational fluid dynamics. Some of the characteristics related to fluid flow phenomena are encountered from literature with the references in this Chapter.

1.7 Thesis Contribution

In this dissertation, the main objective is to reformulate the review work by MHD inclined magnetic field with Joule heating and thermal radiation with stagnation point flow. In this research, PDEs are transformed into dimensionless ODEs by means of an similarity transformation. The numerical values are determined by using the shooting technique with Range Kutta fourth order. The impact of distinct physical parameters on flow of fluid are explained via tables, and graph.

1.8 Thesis Layout

A brief description of contents of the thesis is presented as follows:

The fundamentals of fluid dynamics are explained in Chapter 2. A brief review has been outlined on the basic definitions, fundamental laws and governing equations. The shooting technique and dimensionless physical quantities are classified. A comprehensive review of the numerical analysis of Shawky et al. [25] research paper is presented. By using the shooting process, as similar to the review work in Chapter 3 is repeated. The non linear combined system of PDEs has been converted into an ODEs system. The impacts of various parameters are shown and discussed graphically.

The effect of the inclined magnetic field, Joule heating, stretching ratio and thermal radiation of MHD including stagnation point flow is updated in Chapter 4. The system of ODEs is derived by appropriate similarity transformation discussed numerically. Behavior of physical parameters has been presented in tabular form and through graphs. In this thesis, we also computed the numerical values of local Nusselt number, skin-friction coefficient and Sherwood number.

The summary of the whole study is presented with concluding remarks and forthcoming implementation in Chapter 5.

All the references used in the research work are listed in Bibliography.

Chapter 2

Fundamental Concepts and Basic Equations of Flow

A few simple concepts, governing laws and dimensional quantities are presented in this Chapter. It also addresses dimensional quantities that have been used in subsequent chapters. In addition, a brief explanation for the shooting system used to find the numerical results was conducted.

2.1 Important Definitions

2.1.1 Magnetohydrodynamics

"Magnetohydrodynamics is focused on the hydrodynamics of electrically conductive fluids on plasma and liquid metals, especially" [26].

2.1.2 Fluid Mechanics

"Fluid mechanics is the branch of science which deals with the behavior of the fluids (liquids or gases) at rest as well as in motion. Thus this branch of science deals with the static, kinematics and dynamic aspects of fluids" [27].

2.1.3 Fluid Statics

"The study fluids at rest is called fluid statics" [27].

2.1.4 Fluid Kinematics and Fluid Dynamics

"The study of the fluids in motion, where pressure forces are not considered, is called fluid kinematics and if the pressure forces are also considered for this fluids in motion, that branch of science is called fluid dynamics" [27].

2.1.5 Fluid

"A substance exists in three primary phases. Solid, Liquid and Gas (at very high temperatures, it also exists as plasma). A substance in the liquid or gas phase is referred to as a fluid. Distinction between a solid and fluid is made on the basis of substances ability to resist an applied shear or (tangential) stress that tends to change its shape" [28].

2.2 Physical Properties of the Fluid

There are certain physical property of fluid which is described below

2.2.1 Specific Volume

"Specific volume of a fluid occupied by a unit mass or volume per unit mass of a fluid is called specific volume. Mathematically, it is expressed as

$$\text{Specific volume} = \frac{\text{Volume of fluid}}{\text{Mass of fluid}} = \frac{1}{\frac{\text{Mass of fluid}}{\text{Volume of fluid}}} = \frac{1}{\rho}$$

Thus specific volume is the reciprocal of mass density. It is expressed as m^3/kg. It is commonly applied to gases" [27].

2.2.2 Specific Weight

"The specific weight of a fluid, denoted by γ (lowercase Greek gamma), is its weight per unit volume" [29].

2.2.3 Temperature

"Temperature T is a measure of the internal energy level of a fluid. It may vary considerably during high-speed flow of a gas" [29].

2.2.4 Pressure

"Pressure is the (compression) stress at a point in a static fluid. Next to velocity, the pressure p is the most dynamic variable in fluid mechanics. Differences or gradients in pressure often drive a fluid flow, especially in ducts. In low-speed flows, the actual magnitude of the pressure is often not important, unless it drops so low as to cause vapor bubbles to form in a liquid" [29].

2.2.5 Density

"The density of a fluid, denoted by ρ (lowercase Greek rho), is its mass per unit volume . Density is highly variable in gases and increases nearly proportionally to the pressure level" [29].

2.2.6 Viscosity

"The most important of these is viscosity, which relates the local stresses in a moving fluid to the strain rate of the fluid element. When a fluid is sheared, it begins to move at a strain rate inversely proportional to a property called its coefficient of viscosity μ" [29].

2.2.7 Kinematic Viscosity

"The second form of Re illustrates that the ratio of μ to ρ has its own name, the kinematic viscosity :

$$\nu = \frac{\mu}{\rho}$$

It is called kinematic because the mass units cancel, leaving only the dimensions L^2/T" [29].

2.2.8 Newton Law of Viscosity

"It states that the shear stress (τ) on a fluid element layer is directly proportional to the rate of shear strain. The constant of proportionality is called the coefficient of viscosity. Mathematically, it is expressed as

$$\tau_{xy} = \mu \frac{du}{dy}.$$

Fluids which obey the above relation are known as Newtonian fluids and the fluids which do not obey the above relation are called Non-Newtonian fluids" [27].

2.3 Types of Fluid Flow

2.3.1 Steady and Unsteady Flow

"If the flow characteristics such as depth of flow, velocity of flow, rate of flow at any point in open channel flow do not change with respect to time, the flow is said to be steady flow, mathematically, we have

$$\left(\frac{\partial v}{\partial t}\right)_{(x_0,y_0,z_0)} = 0, \left(\frac{\partial p}{\partial t}\right)_{(x_0,y_0,z_0)} = 0, \left(\frac{\partial \rho}{\partial t}\right)_{(x_0,y_0,z_0)} = 0, \tag{2.1}$$

where (x_0, y_0, z_0) is a fixed point in fluid field. Unsteady flow is that type at any in which the velocity, pressure or density at a point changes with respect to time.

Thus, mathematically, for unsteady flow

$$\left(\frac{\partial v}{\partial t}\right)_{(x_0,y_0,z_0)} \neq 0, \left(\frac{\partial \rho}{\partial t}\right)_{(x_0,y_0,z_0)} \neq 0 \text{ etc"} \text{ [27]}. \tag{2.2}$$

2.3.2 Uniform and Non-uniform Flow

"Uniform flow is defined as that type of flow in which the velocity at any given time does not change with respect to space (i.e., length of direction of the flow). Mathematically, for uniform flow

$$\left(\frac{\partial \mathbf{v}}{\partial s}\right)_{t\ =\ constant} = 0,$$

where $\partial \mathbf{v}$ = Change of velocity
∂s = Length of flow in the direction s. Non-uniform flow is that type of flow in which the velocity at any given time changes with respect to space. Thus, mathematically, for non-uniform flow

$$\left(\frac{\partial \mathbf{v}}{\partial s}\right)_{t\ =\ constant} \neq 0\text{"} \text{ [27]}.$$

2.3.3 Compressible and Incompressible Flows

"Compressible flow is that type of flow in which the density of the fluid changes from point to point or in other words the density (ρ) is not constant for the fluid. Thus, mathematically, for compressible flow

$$\rho \neq constant$$

Incompressible flow is that type of flow in which the density is constant for the fluid flow. Liquids are generally incompressible while gases are compressible. Mathematically, for incompressible flow

$$\rho = constant\text{"} \text{ [27]}.$$

2.3.4 Laminar and Turbulent Flow

"Laminar flow is defined as that type of flow in which the fluid particles move along well-defined paths or stream line and all the stream-lines are straight and parallel. Thus the particles move in laminas or layers gliding smoothly over the adjacent layer. This type of flow is also called stream-line flow or viscous flow. Turbulent flow is that type of flow in which the fluid particles move in a zig-zag way. Due to the movement of fluid particles in a zig-zag way, the eddies formation takes place which are responsible for high energy loss" [27].

2.3.5 Rotational and Irrotational Flows

"Rotational flow is that type of flow in which the fluid particles while flowing along stream-lines, also rotate about their own axis. And if the fluid particle while flowing along stream-lines, do not rotate about their own axis then that type of flow is called irrotational flow" [27].

2.4 Classification of Fluids

2.4.1 Types of Fluid

"The fluids may be classified into the following five types:

1. Ideal fluid,
2. Real fluid,
3. Newtonian fluid,
4. Non-Newtonian fluid, and
5. Ideal Plastic Fluid" [27].

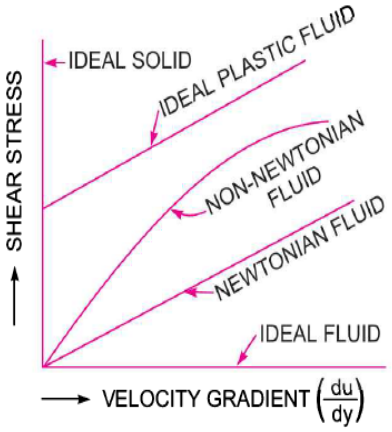

FIGURE 2.1: Types of fluids.

2.4.2 Ideal Fluid

"A fluid which is incompressible and is having no viscosity, is known an ideal fluid . Ideal fluid is only an imaginary fluid as all the fluids, which exist, have some viscosity" [27].

2.4.3 Real Fluid

"A fluid, which possesses viscosity, is known as real fluid. All the fluids, in actual practice, are real fluids" [27].

2.4.4 Ideal plastic fluid

"A fluid, in which shear stress is more than the yield value and shear stress is proportional to the rate of shear strain (or velocity gradient), is known as ideal plastic fluid" [27].

2.4.5 Newtonian Fluid

"A real fluid, in which the shear stress is directly proportional to the rate of shear strain (or velocity gradient), is known as a Newtonian fluid" [27].

2.4.6 Non-Newtonian Fluid

"A real fluid, in which the shear stress is not proportional to the rate of shear strain (or velocity gradient), is known as a Non-Newtonian fluid" [27].

2.5 Modes of Heat Transfer and Related Properties

2.5.1 Heat Transfer

"Heat transfer is that section of engineering science that studies the energy transport between material bodies due to a temperature difference" [30].

2.5.2 Modes of Heat Transfer

"There are three modes of heat transfer namely conduction, convection and radiation.

1. Conduction
2. Convection
3. Radiation" [30].

2.5.3 Conduction

"The conduction mode of heat transfer occurs either because of an exchange of energy from one molecule to another, without the actual motion of the molecules, or because of the motion of the free electrons of they are present. Therefore, this form of heat transport depends heavily on the properties of the medium and takes place in solids, liquids and gases if a difference in temperature exists" [30].

2.5.4 Convection

"Molecules present in liquids and gases have freedom of motion, and by moving from hot to cold region, they carry energy with them. The transfer of heat from one region to another, due to such macroscopic motion in a liquid and gas, added to the energy transfer by conduction within the fluid, is called heat transfer by convection" [30].

2.5.5 Mixed Convection

"A mixed convection state is one in which both natural and forced convection are present. Convection heat transfer also occurs in boiling and condensation processes" [30].

2.5.6 Natural Convection

"When fluid motion occurs because of a density variation caused by temperature differences, the situation is said to be a free, or natural, convection" [30].

2.5.7 Forced Convection

"When fluid motion is caused by external force, such as pumping or blowing, the state is defined as being one of forced convection" [30].

2.5.8 Radiation

"All bodies emit thermal radiation at all temperature. This is the only mode in which both does not require a material medium for heat transfer to occur. The nature of thermal radiation is such that a propagation of energy, carried by electromagnetic waves, is emitted from the surface of the body. When these

electromagnetic waves strike other body surface, a part is reflected, a part is transmitted and the remaining part absorbed" [30].

2.6 Some Main Definition

2.6.1 Stream Lines and Stream Function

"The lines with constant stream function values, are referred to as streamlines. The stream function is defined by the following relationships:

$$u_2 = \frac{\partial \psi}{\partial x_2}$$

$$u_1 = \frac{\partial \psi}{\partial x_1}$$

where ψ is the stream function. If we differentiate the first relation with respect to x_2 and the second with respect to x_1 and then sum, we get the differential equation for the stream function as

$$\frac{\partial^2 \psi}{\partial x_2^2} + \frac{\partial^2 \psi}{\partial x_1^2} = \frac{\partial u_1}{\partial x_1} - \frac{\partial u_2}{\partial x_2}$$," [30].

2.6.2 Isothermal Process

"If the change in density occurs at constant temperature, then the process is called isothermal and relationship between pressure (p) and density (ρ) is given by $\frac{p}{\rho} =$ constant" [27].

2.6.3 Adiabatic Process

"If the change in density occurs with no heat exchange to and from the gas, the process is called adiabatic. And if no heat is generated within the gas due to friction, the relationship between pressure and density is given by $\frac{p}{\rho^k} =$ constant

where k =Ratio of the specific heat of a gas at constant pressure and constant volume" [27].

2.6.4 Stagnation

"For high-speed flows, such as those encountered in jet engines, the potential energy of the fluid is still negligible, but the kinetic energy is not. In such cases, it is convenient to combine the enthalpy and the kinetic energy of the fluid into a single term called stagnation (or total) enthalpy h_0, defined per unit mass

$$h_0 = h + \frac{V^2}{2}$$

When the potential energy of the fluid is negligible, the stagnation enthalpy represents the total energy of a flowing fluid stream per unit mass. Thus it simplifies the thermodynamic analysis of high-speed flows" [28].

2.7 Boundary Layer

"Viscous effects are particularly important near the solid surfaces, where the strong interaction of the molecules of the fluid with molecules of the solid causes the relative velocity between the fluid and the solid to become almost exactly zero. For a stationary surface, therefore, the fluid velocity in the region near the wall must reduce to zero. This is called no slip condition. We see this effect in nature when a dust cloud driven by the wind moves along the ground. Not all the dust particles are moving at the same speed; close to the ground they move more slowly than further away. If we were to look in the region very close to the ground we would see that the dust particles there are almost stationary, no matter how strong the wind. Right at the ground, the dust particles do not move at all, indicating that the air has zero velocity at this point." [31].

2.8 Law of Conservation and Fundamental Equations of Flow

2.8.1 Conservation of Mass

"The principle of conservation of mass can be stated as the time rate of change of mass is fixed volume is equal to the net rate of flow of mass across the surface. The mathematical statement of the principal result in the following equation, known as the continuity of (mass) equation

$$\frac{\partial \rho}{\partial t} + \nabla.(\rho\ \mathbf{v}) = 0. \tag{2.3}$$

where ρ is the density (kg/m^3) of the medium, $\mathbf{v}$ the velocity vector (m/s), and ∇ is the nabla or del operator. The continuity equation (2.3) is in conservation (or divergence) form since it can be derived directly from an integral statement of mass conservation. By introducing the material derivative or Eulerian derivative operator $\frac{D}{DT}$

$$\frac{D}{Dt} = \frac{\partial}{\partial t} + \mathbf{v}.\nabla, \tag{2.4}$$

the continuity equation (2.3) can be expressed in the alternative, non- conservation (or advective) form

$$\frac{\partial \rho}{\partial t} + \mathbf{v}.\nabla\rho + \rho\nabla.\mathbf{v} = \frac{D\rho}{DT} + \rho\nabla.\mathbf{v}, \tag{2.5}$$

For steady-state conditions, the continuity equation becomes

$$\nabla.(\rho\mathbf{v}) = 0 \tag{2.6}$$

when the density changes following a fluid particle are negligible, the continum is termed incompressible and we have $\frac{D\rho}{Dt} = 0$. The continuity equation (2.5) then becomes

$$\nabla.\mathbf{v} = 0 \tag{2.7}$$

which is often referred to as the incompressibility condition or incompressibility constraint" [32].

2.8.2 Conservation of Momentum

"The principle of conservation of linear momentum equation states that the time rate of change of linear momentum of a given set of particles is equal to the vector sum of all the external forces acting on the particles of the set, provided Newton's Third Law of action and reaction governs the internal forces. Newton's Second Law can be written as:

$$\frac{\partial \rho \mathbf{v}}{\partial t} + \nabla.(\rho \otimes \mathbf{v}) = \nabla.\sigma + \rho \mathbf{f}. \tag{2.8}$$

where $\otimes$ is the tensor (or dyadic) product of two vectors, σ is the cauchy stress tensor (N/m^2) and $\mathbf{f}$ is the body force vector, measured per unit mass and normally taken to be the gravity vector. Equation (2.8) describe the motion of a continuous medium, and in fluid mechanics they are also known as Navier equations.
The form of the momentum equation shown in (2.8) is the conservation (divergence) form that is most often utilized for compressible flows. This equation may be simplified to a form more commonly used with incompressible flows. Expanding the first two derivatives and collecting terms

$$\rho \left(\frac{\partial \mathbf{v}}{\partial t} + \mathbf{v} \nabla.\mathbf{v} \right) + \mathbf{v} \rho \left(\frac{\partial \rho}{\partial T} + \nabla.\rho \mathbf{v} \right) = \nabla.\sigma + \rho \mathbf{f} \tag{2.9}$$

The second term in parentheses is the continuity equation (2.3) and neglecting this term allows (2.9) to reduce to the non-conservation (advective) form

$$\rho \frac{D\mathbf{v}}{Dt} = \nabla.\sigma + \rho \mathbf{f} \tag{2.10}$$

where the material derivative (2.4) has been employed.
The principle of conservation of angular momentum can be stated as the time rate of change of the total moment of a given set of particles is equal to the vector

sum of the moments of the external forces acting on the system. In the absence of distributed couples, the principle leads to the symmetry of the stress tensor:

$$\sigma = (\sigma)^T \tag{2.11}$$

where the superscript T denotes the transpose of the enclosed quantity" [32].

2.8.3 Conservation of Energy

"The law of conservation of energy is equal to the sum of the rate of work done by applied forces and the change of heat content per unit time. In the general case, the First Law of Thermodynamics can be expressed in conservation form as

$$\frac{\partial \rho e^t}{\partial t} + \nabla.\rho \mathbf{v} e^t = -\nabla.\mathbf{q} + \nabla.(\sigma.\mathbf{v}) + Q + \rho \mathbf{f}.\mathbf{v} \tag{2.12}$$

where $e^t = e + 1/2v.v$ is the total energy (J/m^3), e is the internal energy, $\mathbf{q}$ is the heat flux vector (W/m^2) and Q is the internal heat generation (W/m^3). The total energy equation (2.8.3) is useful for high speed compressible flows where the kinetic energy is significant. For incompressible flows, an internal energy equation is more appropriate and can be derived (2.8.3) from with use of the momentum equation (2.8). Taking the dot product of the velocity vector with the momentum equation produces an equation for the kinetic energy; this equation is subtracted from the total energy equation to produce the conservation (divergence) form of the internal energy equation

$$\frac{\partial \rho e}{\partial t} + \nabla.\rho \mathbf{v} e = -\nabla.\mathbf{q} + Q + \Phi \tag{2.13}$$

where Φ is a dissipation function that is defined by

$$\Phi = \sigma : \nabla \mathbf{v} \tag{2.14}$$

In Eq. (2.14) $\nabla \mathbf{v}$ is the velocity gradient tensor which will be defined more completely in the following sections.

The thermal energy equation (2.13) can be simplified further by expanding the

derivatives on the left-hand side of the equation and using the continuity equation. The resulting equation is the non-conservative (advective) form of the energy equation

$$\rho \frac{De}{Dt} = -\nabla.\mathbf{q} + Q + \Phi \tag{2.15}$$

which is the standard form used for incompressible flows" [32].

2.9 Dimensionless Quantities

According to Josef Kunes some dimensionless quantities of fluid mechanics are given as

2.9.1 Prandtl Number

"This number expresses the ratio of the momentum diffusivity (viscosity) to the thermal diffusivity. It characterizes the physical properties of a fluid with convective and diffusive heat transfers" [26].

2.9.2 Nusselt Number

"It expresses the ratio of the total heat transfer in a system to the heat transfer by conduction. In characterizes the heat transfer by convection between a fluid and the environment close to it or, alternatively, the connection between the heat transfer intensity and the temperature field in a flow boundary layer" [26].

2.9.3 Dufour Number

"It characterizes the ratio of the diffuse heat and mass transfers, in a binary mixture of gases under isotropic conditions, to the enthalpy of the unit mixture mass, provided the linear diffusion rate equals that of conduction. Thermodiffusion" [26].

2.9.4 Schmidt Number

"This number expresses the ratio of the kinematic viscosity, or momentum transfer by internal friction, to the molecular diffusivity. It characterizes the relation between the material and momentum transfers in mass transfer" [26].

2.9.5 Sherwood Number

"It expresses the ratio of the heat transfer to the molecular diffusion. It characterizes the mass transfer intensity at the interface of phases" [26].

2.10 Solution Methodology

We have used shooting technique to deal with the nonlinear ordinary differential equations by using MATLAB software.

2.10.1 Shooting Method with RK4 Scheme

"In a shooting method, the missing (unspecified) initial condition at the initial point of the interval is assumed, and the differential equation is then integrated numerically as an initial value problem to the terminal point. The accuracy of the assumed missing initial condition is then checked by comparing the calculated value of the dependent variable at the terminal point with its given value there. If a difference exists, another value of the missing initial condition must be assumed and the process is repeated. This process is continued until the agreement between the calculated and the given condition at the terminal point is within the specified degree of accuracy. For this type of iterative approach, one naturally inquires whether or not there is systematic way of finding each succeeding (assumed) value of the missing initial condition.

2.10.2 Newton's Method

In this method, the differential equation is kept in its nonlinear form and the missing slope is found systematically by Newton's method. This method provides quadratic convergence of the iteration and is far better than the usual cut-and-try methods. Consider the second-order differential equation

$$z''(x) = f\,(x, z, z') \tag{2.16}$$

subject to the boundary conditions

$$z(0) = 0, \quad z(l) = W. \tag{2.17}$$

By denoting z by z_1 and z_1' by z_2, Eq. (2.16) can be written as the following system of first order equations.

$$\left.\begin{aligned} z_1' &= z_2, & z_1 &= 0, \\ z_2' &= f(x, z_1, z_2), & z_1(l) &= W. \end{aligned}\right\} \tag{2.18}$$

We denote the missing initial slope $z_2(0)$ by s, to have

$$\left.\begin{aligned} z_1' &= z_2, & z_1(0) &= 0, \\ z_2' &= f(x, z_1, z_2), & z_2(0) &= s. \end{aligned}\right\} \tag{2.19}$$

The problem is to find s such that the solution of the IVP Eq. (2.19) satisfies the boundary condition $z(l) = W$. In other words, if the solutions of the initial value problem are denoted by $z_1(x, s)$ and $z_2(x, s)$, one searches for the value of s such that

$$z_1(l, s) - W = \phi(s) = 0 \tag{2.20}$$

For the Newton's method, the iteration formula for s is given by

$$s^{(n+1)} = s^{(n)} - \frac{\phi(s^{(n)})}{\frac{d\phi(s^{(n)})}{ds}} \tag{2.21}$$

or

$$s^{(n+1)} = s^{(n)} - \frac{z_1(l, s^n) - W}{\frac{\partial z_1(l,s^n)}{\partial s}} \tag{2.22}$$

To find the derivative of z_1 with respect to s, differentiate (2.19) with respect to s. For simplification, use the following notations,

$$\frac{dz_1}{ds} = z_3, \quad \frac{dz_2}{ds} = z_4 \tag{2.23}$$

This process results in the following IVP.

$$\left.\begin{aligned} z_3' &= z_4, & z_3(0) &= 0, \\ z_4' &= \frac{\partial f}{\partial z_1} z_3 + \frac{\partial f}{\partial z_2} z_4, & z_4(0) &= 1. \end{aligned}\right\} \tag{2.24}$$

The solution of Eq. (2.24), the value of z_3 at l can be computed. This value is actually the derivative of z_1 with respect of s computed at l. This value is actually the derivative of z_1 with respect of s computed at l. Setting the value of $z_3(l, s)$ in Eq. (2.22), the modified value of s can be achieved. This new value of s is used to solve the Eq. (2.19) and the process is repeated until the value of s is within a described degree of accuracy" [33].

Chapter 3

Numerical Analysis of MHD Williamson Nanofluid Flow Induced by Stretching Surface

3.1 Introduction

In this chapter, we are interested to investigate the magnetohydrodynamics (MHD) Williamson nanofluid flow with heat and mass transfer in a boundary layer through porous medium over a stretching sheet placed horizontally. Using the appropriate similarity transformation the governing PDEs are converted into ODEs and shooting technique has been used to obtain the numerical results. The effects of different physical parameters on concentration, velocity and temperature of nanofluid flow have been presented graphically and discussed in detail. This chapter provides the review study of Shawky et al. [25].

3.2 Problem Formulation

We consider the incompressible two-dimensional steady flow of Williamson viscous dissipative nanofluid through a stretching sheet using the Cartesian coordinates

(x, y) depicted in Figure 3.1. Along x-axis sheet is stretched with a Bx velocity, where $B > 0$ indicates the stretching parameter. Note that U_w, T_w and C_w, are the fluid velocity, temperature and nanoparticle concentration on the surface(wall), respectively. The Williamson fluid model is [34, 35]

$$S = -pI + \tau, \tag{3.1}$$

$$\tau = \left[\mu_\infty + \frac{(\mu_0 - \mu_\infty)}{1 - \Gamma\dot{\gamma}}\right] A_1, \tag{3.2}$$

where S the Cauchy stress tensor, while τ is extra stress tensor, p indicates the pressure, I represents the identity tensor, μ_0 shows at zero shear rate limiting viscosity and μ_∞ known as at infinite shear rate limiting viscosity, $\lambda > 0$ expresses the time constant, A_1 represents the first Rivlin Erickson tensor and $\dot{\gamma}$ interpreted as follows:

$$\dot{\gamma} = \sqrt{\frac{1}{2}\pi},$$

$$\pi = \text{trace}(A_1^2), \tag{3.3}$$

$$\dot{\gamma} = \left[\left(\frac{\partial u}{\partial x}\right)^2 + \frac{1}{2}\left(\frac{\partial u}{\partial y} + \frac{\partial v}{\partial x}\right)^2 + \left(\frac{\partial v}{\partial y}\right)^2\right]^{\frac{1}{2}}, \tag{3.4}$$

where π denotes the second invariant strain tensor. Here only evaluated the case for which $\mu_\infty = 0$ and $\lambda\ \dot{\gamma} < 1$. Thus Eq. (3.2) can be written as

$$\tau = \left[\frac{\mu_0}{1 - \Gamma\dot{\gamma}}\right] A_1. \tag{3.5}$$

By manipulating Binomial expansion then

$$\tau = \mu_0[1 + \Gamma\dot{\gamma}]A_1, \tag{3.6}$$

and the components of the extra stressed tensor are :

$$\tau_{xx} = 2\mu_0[1 + \Gamma\dot{\gamma}]\frac{\partial u}{\partial x}, \tag{3.7}$$

$$\tau_{xy} = \tau_{yx} = \mu_0[1 + \Gamma\dot{\gamma}]\left(\frac{\partial u}{\partial y} + \frac{\partial v}{\partial x}\right), \tag{3.8}$$

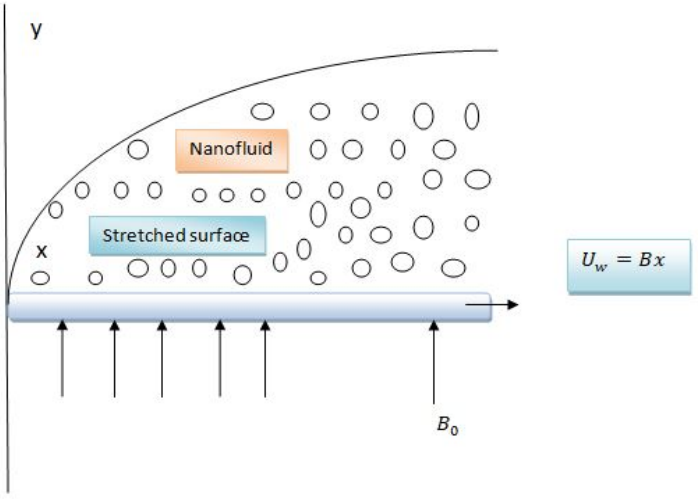

FIGURE 3.1: Schematic diagram of the physical problem.

$$\tau_{yy} = 2\mu_0[1 + \Gamma\dot{\gamma}]\frac{\partial v}{\partial y}, \tag{3.9}$$

$$\tau_{xz} = \tau_{yz} = \tau_{zx} = \tau_{zy} = \tau_{zz} = 0. \tag{3.10}$$

3.2.1 The Governing Equations

Under the aforementioned assumptions the boundary layer equations are

- Continuity Equation:

$$\frac{\partial u}{\partial x} + \frac{\partial v}{\partial y} = 0. \tag{3.11}$$

- Momentum Equation:

$$u\frac{\partial u}{\partial x} + v\frac{\partial u}{\partial y} = \frac{\mu_{nf}}{\rho_{nf}}\frac{\partial^2 u}{\partial y^2} + \sqrt{2}\frac{\mu_{nf}}{\rho_{nf}}\Gamma\frac{\partial u}{\partial y}\frac{\partial^2 u}{\partial y^2} - \frac{\mu_{nf}}{\rho_{nf}k}u - \frac{\sigma B_0^2}{\rho_{nf}}u. \tag{3.12}$$

- Concentration Equation:

$$u\frac{\partial C}{\partial x} + v\frac{\partial C}{\partial y} = D_B\frac{\partial^2 C}{\partial y^2} + \frac{D_T}{T_\infty}\frac{\partial^2 T}{\partial y^2} - k_1(C - C_\infty) + \frac{D_m K_T}{T_m}\left(\frac{\partial^2 T}{\partial y^2}\right). \tag{3.13}$$

- Energy Equation:

$$\begin{aligned} u\frac{\partial T}{\partial x}+v\frac{\partial T}{\partial y} &= \alpha_{nf}\frac{\partial^2 T}{\partial y^2}+\frac{\mu_{nf}}{(\rho C_p)_{nf}}\left(\frac{\partial u}{\partial y}\right)^2+\frac{1}{\sqrt{2}}\frac{\mu_{nf}}{(\rho C_p)_{nf}}\Gamma\left(\frac{\partial u}{\partial y}\right)^3 \\ &+\frac{(\rho C_p)_f}{(\rho C_p)_{nf}}\left[D_B\frac{\partial C}{\partial y}\frac{\partial T}{\partial y}+\frac{D_T}{T_\infty}\left(\frac{\partial T}{\partial y}\right)^2\right]+\frac{\sigma B_0^2}{(\rho C_p)_{nf}}u^2 \\ &-\frac{Q_0}{(\rho C_p)_{nf}}(T-T_\infty)-Q_1(C-C_\infty) \\ &+\frac{D_m K_T}{C_s(\rho C_p)_{nf}}\frac{\partial^2 C}{\partial y^2}. \end{aligned} \tag{3.14}$$

In the above equations u the velocity component in the $x-$direction and v symbol for the velocity component in the $y-$direction. $(\rho C_p)_{nf}$ represents the heat capacitance of nanofluid, T stands for the temperature of fluid, K_{nf} shows thermal conductivity of nanofluid, D_B represents coefficient of Brownian diffusion, C shows volumetric fraction of nanoparticles, $(\rho C_p)_f$ shows the heat capacity of fluid, D_T represents the coefficient of thermophoretic diffusion, D_m represents the diffusitivity of mass, C_s shows the susceptability of concentration, T_m represents the temperature at mean level, T_∞ shows the temperature fluid at infinite level and C_∞ denotes the ambient fluid concentration, while Q_0 indicates the rate of heat generation, Q_1 is known as radiation absorption, ρ_{nf} is density of nanofluid, K_1 stands for coefficient of chemical reaction, B_0 shows the strength of magnetic field, and σ denotes the electrical conductivity.

3.2.2 Dimensional Boundary Conditions

The dimensional form of the boundary conditions is given as:

$$\left.\begin{aligned} u=U_w=Bx,\ v=0,\ T=T_w=T_\infty+A\left(\frac{x}{l}\right)^2,\ C=C_w,\ \text{at } y=0, \\ u\to 0,\ T\to T_\infty,\ C=C_\infty,\ \text{as } y\to\ \infty, \end{aligned}\right\} \tag{3.15}$$

where A and B expressed as constants, l shows characteristic length, α_{nf} stands for thermal diffusivity, ρ_{nf} represents density of nanofluid and μ_{nf} indicates dynamic

viscosity of the nanofluid. These fluid properties are given by (Hady et al. [36]) and (Tiwari and Das [37]):

$$\left.\begin{aligned}
&\mu_{nf} = \frac{\mu_f}{(1-\phi)^{2.5}}, \quad \nu_f = \frac{\mu_f}{\rho_f},\\
&\rho_{nf} = (1-\phi)\rho_f + \phi\rho_s,\\
&\alpha_{nf} = \frac{k_{nf}}{(\rho C_p)_{nf}}, \quad k_{nf} = k_f\left(\frac{k_s + 2k_f - 2\phi(k_f - k_s)}{k_s + 2k_f + \phi(k_f - k_s)}\right),\\
&(\rho C_p)_{nf} = (1-\phi)(\rho C_p)_f + \phi(\rho C_p)_s,
\end{aligned}\right\} \tag{3.16}$$

where k_{nf} shows the nanofluid thermal conductivity, ϕ denotes the volume fraction of nanoparticle.

3.3 Similarity Transformation

The following transformation has been used to get ODEs from PDEs [25]

$$\left.\begin{aligned}
u = Bxf'(\eta), \quad v = -\sqrt{B\nu_f}f(\eta), \quad \eta = y\sqrt{\frac{B}{\nu_f}}\\
g(\eta) = \frac{T - T_\infty}{T_w - T_\infty}, \quad \varphi(\eta) = \frac{C - C_\infty}{C_w - C_\infty},
\end{aligned}\right\} \tag{3.17}$$

where η is the similarity variable, $g(\eta)$ denotes the dimensionless temperature, $\varphi(\eta)$ represents the dimensionless concentration.

Detailed procedure for the conversion of PDEs into ODEs in the dimensionless form has been discussed as follows:

Let the velocity components and there partial derivative

$$\begin{aligned}
\frac{\partial u}{\partial x} &= \frac{\partial}{\partial x}(Bxf'(\eta)),\\
&= Bf'(\eta),\\
\frac{\partial v}{\partial y} &= \frac{\partial}{\partial y}(-\sqrt{B\nu_f}f(\eta)),\\
&= -Bf'(\eta).
\end{aligned}$$

Verification of continuity equation has been carried out as:

$$\frac{\partial u}{\partial x}+\frac{\partial v}{\partial y} = Bf'(\eta)-Bf'(\eta)=0. \tag{3.18}$$

Next, momentum equation will be converted into the dimensionless form. The procedure includes the following conversion of different terms from dimensional to the non-dimensional form.

$$\begin{aligned} u\frac{\partial u}{\partial x} &= (Bxf'(\eta))\frac{\partial}{\partial x}(Bxf'(\eta), \\ &= B^2xf'^2(\eta). \\ v\frac{\partial u}{\partial y} &= (-\sqrt{B\nu_f}f(\eta))\frac{\partial}{\partial y}(Bxf'(\eta), \\ &= -B^2xf(\eta)f''(\eta). \end{aligned}$$

Taking the left hand side of Eq. (3.12), the following form become

$$\begin{aligned} u\left(\frac{\partial u}{\partial x}\right)+v\left(\frac{\partial v}{\partial y}\right) &= B^2xf'^2-B^2xff'', \\ &= B^2x(f'^2-ff''). \end{aligned}$$

Next, the right hand side of equation includes

$$\begin{aligned} \frac{\mu_{nf}}{\rho_{nf}}\left(\frac{\partial^2 u}{\partial y^2}\right) &= \frac{\mu_{nf}}{\rho_{nf}}\frac{\partial}{\partial y}(Bxf''(\eta))\sqrt{\frac{B}{\nu_f}}, \\ &= \frac{\mu_{nf}}{\rho_{nf}}\frac{B^2x}{\nu_f}f'''(\eta). \end{aligned}$$

$$\begin{aligned} \sqrt{2}\frac{\mu_{nf}}{\rho_{nf}}\Gamma\frac{\partial u}{\partial y}\frac{\partial^2 u}{\partial y^2} &= \sqrt{2}\frac{\mu_{nf}}{\rho_{nf}}\Gamma\left(Bxf''\sqrt{\frac{B}{\nu_f}}\right)\left(\frac{B^2x}{\nu_f}f'''\right), \\ &= \sqrt{2}\frac{\mu_{nf}}{\rho_{nf}}\Gamma\frac{B^{\frac{7}{2}}x^2}{\nu_f^{\frac{3}{2}}}f''f'''. \end{aligned}$$

Similarly,

$$\begin{aligned} -\frac{\mu_{nf}}{\rho_{nf}k}u &= -\frac{\mu_{nf}}{\rho_{nf}k}(Bxf'), \\ -\frac{\sigma B_0^2}{\rho_{nf}}u &= -\frac{\sigma B_0^2}{\rho_{nf}}(Bxf'). \end{aligned}$$

Using these values in Eq. (3.12),

$$B^2x(f'^2 - ff'') = \frac{\mu_{nf}}{\rho_{nf}}\frac{B^2x}{\nu_f}f''' + \sqrt{2}\frac{\mu_{nf}}{\rho_{nf}}\Gamma f'''f''\frac{B^{\frac{7}{2}}x^2}{\nu_f^{\frac{3}{2}}}$$
$$-\frac{\mu_{nf}}{\rho_{nf}k}(Bxf') - \frac{\sigma B_0^2}{\rho_{nf}}(Bxf').$$

Rearrange the equation

$$\frac{\mu_{nf}}{\rho_{nf}}\frac{B^2x}{\nu_f}f''' + \sqrt{2}\frac{\mu_{nf}}{\rho_{nf}}\Gamma f'''f''\frac{B^{\frac{7}{2}}x^2}{\nu_f^{\frac{3}{2}}} - \frac{\mu_{nf}}{\rho_{nf}k}(Bxf')$$
$$-\frac{\sigma B_0^2}{\rho_{nf}}(Bxf') - B^2x(f'^2 - ff'') = 0.$$

Dividing each term of previous equation by $\left(B\frac{\mu_{nf}}{\rho_{nf}}\right)$, it becomes

$$\frac{Bx}{\nu_f}f''' + \sqrt{\frac{2B^3}{\nu_f}}\Gamma xf'''f''\frac{Bx}{\nu_f} - \frac{x}{k}(f') - \frac{\sigma B_0^2}{\rho_{nf}}(xf')\frac{\rho_{nf}}{\mu_{nf}}$$
$$-Bxf'^2\frac{\rho_{nf}}{\mu_{nf}} + Bxff''\frac{\rho_{nf}}{\mu_{nf}} = 0.$$

Multiplying each term of prior equation by (ν_f)

$$Bxf''' + \lambda f'''f''Bx - \frac{x\nu_f}{k}(f') - \frac{\sigma B_0^2}{\rho_{nf}}(xf'\nu_f)\frac{\rho_{nf}}{\mu_{nf}}$$
$$-Bxf'^2\frac{\rho_{nf}}{\mu_{nf}}\nu_f + Bxff''\frac{\rho_{nf}}{\mu_{nf}}\nu_f = 0. \tag{3.19}$$

Using these

- $$\frac{\rho_{nf}}{\mu_{nf}}\nu_f = \frac{\rho_{nf}}{\rho_f}\frac{\mu_f}{\mu_{nf}}\frac{\rho_f}{\mu_f}\nu_f$$
$$= \frac{\left[(1-\phi) + \phi\frac{\rho_s}{\rho_f}\right]}{\frac{\rho_f}{\rho_f}}\frac{\mu_f}{\frac{\mu_f}{(1-\phi)^{2.5}}}$$
$$= \left[(1-\phi) + \phi\frac{\rho_s}{\rho_f}\right](1-\phi)^{2.5}$$
$$= \phi_1 \tag{3.20}$$
- $\rho_{nf} = [(1-\phi)\rho_f + \phi\rho_s]$

$$= \frac{\left[(1-\phi)+\phi\frac{\rho_s}{\rho_f}\right]}{\rho_f}$$
$$= \frac{\phi_2}{\rho_f} \tag{3.21}$$

and dividing each term of Eq. (3.19) by Bx

$$f''' + \lambda f''' f'' - \frac{1}{K}(f') - M\frac{\phi_1}{\phi_2}f' - f'^2\phi_1 + ff''\phi_1 = 0.$$

Finally the dimensionless form of momentum equation reduced as

$$f''' + \lambda f''' f'' - \phi_1\left(f'^2 - ff'' + \frac{M}{\phi_2}f'\right) - \frac{1}{K}f' = 0. \tag{3.22}$$

Next, we use the following detailed procedure to convert Eq. (3.14) into the dimensionless form

$$\begin{aligned}
u\frac{\partial T}{\partial x} &= (Bxf'(\eta))\frac{\partial}{\partial x}\left[g(\eta)(T_w - T_\infty) + T_\infty\right], \\
&= (Bxf'(\eta))\frac{\partial}{\partial x}\left[g(\eta)A\left(\frac{x}{l}\right)^2 + T_\infty\right], \\
&= (Bxf'(\eta))\left[g(\eta)2Ax\left(\frac{1}{l}\right)^2\right], \\
&= 2AB\left(\frac{x}{l}\right)^2 f'g. \\
v\frac{\partial T}{\partial y} &= (-\sqrt{Bv_f}f(\eta))\frac{\partial}{\partial y}\left[g(\eta)A\left(\frac{x}{l}\right)^2 + T_\infty\right], \\
&= (-\sqrt{Bv_f}f(\eta))g'(\eta)A\left(\frac{x}{l}\right)^2\sqrt{\frac{B}{\nu_f}}, \\
&= -ABfg'\left(\frac{x}{l}\right)^2.
\end{aligned}$$

Left hand side of Eq. (3.14) yields

$$\begin{aligned}
u\frac{\partial T}{\partial x} + v\frac{\partial T}{\partial y} &= 2AB\left(\frac{x}{l}\right)^2 f'g - ABfg'\left(\frac{x}{l}\right)^2, \\
&= AB\left(\frac{x}{l}\right)^2(2f'g - fg').
\end{aligned}$$

The following derivatives will help to convert

the right side of Eq. (3.14) into the dimensionless form

$$\begin{aligned}
\alpha_{nf}\frac{\partial^2 T}{\partial y^2} &= \alpha_{nf} g''(\eta)\frac{B}{\nu_f}A\left(\frac{x}{l}\right)^2,\\
\frac{\mu_{nf}}{(\rho C_p)_{nf}}\left(\frac{\partial u}{\partial y}\right)^2 &= \frac{\mu_{nf}}{(\rho C_p)_{nf}}\frac{B^3x^2}{\nu_f}f''^2,\\
\frac{1}{\sqrt{2}}\frac{\mu_{nf}}{(\rho C_p)_{nf}}\Gamma\left(\frac{\partial u}{\partial y}\right)^3 &= \frac{1}{\sqrt{2}}\frac{\mu_{nf}}{(\rho C_p)_{nf}}\Gamma\frac{B^{\frac{9}{2}}x^3}{\nu_f^{\frac{3}{2}}}f''^3,\\
\frac{(\rho C_p)_f}{(\rho C_p)_{nf}}D_B\frac{\partial C}{\partial y}\frac{\partial T}{\partial y} &= \frac{(\rho C_p)_f}{(\rho C_p)_{nf}}D_B\frac{B}{\nu_f}(C_w-C_\infty)(T_w-T_\infty)\varphi' g',\\
\frac{(\rho C_p)_f}{(\rho C_p)_{nf}}\frac{D_T}{T_\infty}\left(\frac{\partial T}{\partial y}\right)^2 &= \frac{(\rho C_p)_f}{(\rho C_p)_{nf}}\frac{D_T}{T_\infty}g'^2(T_w-T_\infty)^2\frac{B}{\nu_f},\\
\frac{\sigma B_0^2}{(\rho C_p)_{nf}}u^2 &= \frac{\sigma B_0^2}{(\rho C_p)_{nf}}B^2x^2f'^2,\\
-\frac{Q_0}{(\rho C_p)_{nf}}(T-T_\infty) &= -\frac{Q_0}{(\rho C_p)_{nf}}g(\eta)(T_w-T_\infty)\\
-Q_1(C-C_\infty) &= -Q_1(C_w-C_\infty)\varphi(\eta),\\
\frac{D_mK_T}{C_s(\rho C_p)_{nf}}\frac{\partial^2 C}{\partial y^2} &= \frac{D_mK_T}{C_s(\rho C_p)_{nf}}\frac{B}{\nu_f}(C_w-C_\infty)\varphi''.
\end{aligned}$$

Substituting these values in Eq. (3.14),

$$\begin{aligned}
AB\left(\frac{x}{l}\right)^2(2f'g-fg') &= \alpha_{nf}g''(\eta)\frac{B}{\nu_f}A\left(\frac{x}{l}\right)^2\\
&+\frac{\mu_{nf}}{(\rho C_p)_{nf}}\frac{B^3x^2}{\nu_f}f''^2\\
&+\frac{1}{\sqrt{2}}\frac{\mu_{nf}}{(\rho C_p)_{nf}}\Gamma\frac{B^{\frac{9}{2}}x^3}{\nu_f^{\frac{3}{2}}}f''^3\\
&+\frac{(\rho C_p)_f}{(\rho C_p)_{nf}}\left[D_B\frac{B}{v_f}(C_w-C_\infty)(T_w-T_\infty)\varphi' g'\right.\\
&\left.+\frac{D_T}{T_\infty}g'^2(T_w-T_\infty)^2\frac{B}{\nu_f}\right]\\
&+\frac{\sigma B_0^2}{(\rho C_p)_{nf}}B^2x^2f'^2-\frac{Q_0}{(\rho C_p)_{nf}}g(\eta)(T_w-T_\infty)\\
&-Q_1(C_w-C_\infty)\varphi(\eta)+\frac{D_mK_T}{C_s(\rho C_p)_{nf}}\frac{B}{\nu_f}(C_w-C_\infty)\varphi''.
\end{aligned}$$

Dividing each term by $\left(AB\left(\frac{x}{l}\right)^2\right)$ on both sides,

$$(2f'g-fg') = \frac{\alpha_{nf}}{\nu_f}g''+\frac{\mu_{nf}}{(\nu_f\rho C_p)_{nf}}\frac{B^2l^2}{A}f''^2$$

$$
\begin{aligned}
&+\frac{\Gamma}{\sqrt{2}}\frac{\mu_{nf}}{(\rho C_p)_{nf}}\frac{B^{\frac{7}{2}}x}{\nu_f^{\frac{3}{2}}}f'^3\\
&+\frac{(\rho C_p)_f}{\nu_f(\rho C_p)_{nf}}\left[D_B(C_w-C_\infty)(T_w-T_\infty)\varphi' g'\right.\\
&\left.+\frac{D_T}{T_\infty}g'^2(T_w-T_\infty)^2\right]\frac{l^2B}{ABx^2}\\
&+\frac{\sigma B_0^2}{(\rho C_p)_{nf}}\frac{Bl^2}{A}f'^2-\frac{Q_0}{(\rho C_p)_{nf}}g(\eta)(T_w-T_\infty)\frac{l^2}{AB}\\
&-Q_1(C_w-C_\infty)\varphi(\eta)\frac{l^2}{ABx^2}\\
&+\frac{D_mK_T}{C_s(\rho C_p)_{nf}}\frac{l^2}{\nu_f Ax^2}(C_w-C_\infty)\varphi''.
\end{aligned}
$$

Putting the value of α_{nf} it becomes,

$$
\begin{aligned}
(2f'g-fg') \;=\;& \frac{k_{nf}}{\nu_f(\rho C_p)_{nf}}g''+\frac{\mu_{nf}}{(\nu_f\rho C_p)_{nf}}\frac{B^2l^2}{A}f''^2\\
&+\frac{\Gamma}{\sqrt{2}}\frac{\mu_{nf}}{(\rho C_p)_{nf}}\frac{B^{\frac{7}{2}}x}{\nu_f^{\frac{3}{2}}}f''^3+\frac{(\rho C_p)_f}{\nu_f(\rho C_p)_{nf}}\left[D_B(C_w-C_\infty)\varphi' g'\right.\\
&\left.+\frac{D_T}{T_\infty}g'^2(T_w-T_\infty)\right]\frac{l^2B}{ABx^2}(T_w-T_\infty)+\frac{\sigma B_0^2}{(\rho C_p)_{nf}}\frac{Bl^2}{A}f'^2\\
&-\frac{Q_0(T_w-T_\infty)}{(\rho C_p)_{nf}}g(\eta)-Q_1\varphi(\eta)\frac{(C_w-C_\infty)}{B(T_w-T_\infty)}\\
&+\frac{D_mK_T}{C_s(\rho C_p)_{nf}\nu_f}\frac{(C_w-C_\infty)}{(T_w-T_\infty)}\varphi''. \qquad (3.23)
\end{aligned}
$$

Multiplying the term $\frac{(\rho C_p)_{nf}}{(\rho C_p)_f}$ on both sides of Eq. (3.23)

$$
\begin{aligned}
\frac{(\rho C_p)_{nf}}{(\rho C_p)_f}(2f'g-fg') \;=\;& \frac{k_{nf}}{k_f}\left(\frac{k_f\rho_f}{\mu_f(\rho C_p)_f}\right)g''\\
&+\frac{(\rho C_p)_{nf}}{(\rho C_p)_f}\frac{\mu_{nf}}{(\nu_f\rho C_p)_{nf}}\frac{B^2l^2}{A}f''^2\\
&+\frac{(\rho C_p)_{nf}}{(\rho C_p)_f}\frac{\Gamma}{\sqrt{2}}\frac{\mu_{nf}}{(\rho C_p)_{nf}}\frac{B^{\frac{7}{2}}x}{\nu_f^{\frac{3}{2}}}f''^3\\
&+\frac{(\rho C_p)_{nf}}{(\rho C_p)_f}\frac{(\rho C_p)_f}{\nu_f(\rho C_p)_{nf}}\left[D_B(C_w-C_\infty)\varphi' g'\right.\\
&\left.+\frac{D_T}{T_\infty}g'^2(T_w-T_\infty)\right]\\
&+\frac{(\rho C_p)_{nf}}{(\rho C_p)_f}\frac{\sigma B_0^2}{(\rho C_p)_{nf}}\frac{Bl^2}{A}f'^2
\end{aligned}
$$

$$
\begin{aligned}
&-\frac{(\rho C_p)_{nf}}{(\rho C_p)_f}\frac{Q_0(T_w-T_\infty)}{(\rho C_p)_{nf}}g(\eta)\\
&-\frac{(\rho C_p)_{nf}}{(\rho C_p)_f}Q_1\varphi(\eta)\frac{(C_w-C_\infty)}{B(T_w-T_\infty)}\\
&+\frac{(\rho C_p)_{nf}}{(\rho C_p)_f}\frac{D_mK_T}{C_s(\rho C_p)_{nf}\nu_f}\frac{(C_w-C_\infty)}{(T_w-T_\infty)}\varphi''.
\end{aligned}
$$

$$
\begin{aligned}
\bullet\ \frac{(\rho Cp)_{nf}}{(\rho Cp)_f} &= \frac{[(1-\phi)(\rho Cp)_f+\phi(\rho Cp)_s]}{(\rho Cp)_f}\\
&= \left[(1-\phi)+\phi\frac{(\rho Cp)_s}{(\rho Cp)_f}\right]\\
&= \phi_3 \qquad (3.24)\\
\bullet\ \frac{\mu_n f}{\nu_f(\rho Cp)_{nf}} &= \frac{\mu_{nf}}{\mu_f}\frac{\rho}{(\rho Cp)_{nf}}\frac{\nu_f}{\nu_f}\\
&= \frac{\mu_f}{\frac{(1-\phi)^{2.5}}{\mu_f}}\frac{\rho_f}{[(1-\phi)(\rho Cp)_f+\phi(\rho Cp)_s]}\\
&= \frac{\mu_f}{\mu_f(1-\phi)^{2.5}}\frac{\frac{\rho_f}{(\rho Cp)_f}}{\left[(1-\phi)+\phi\frac{(\rho Cp)_s}{(\rho Cp)_f}\right]}\\
&= \frac{\rho_f}{\phi_4(\rho Cp)_f} \qquad (3.25)
\end{aligned}
$$

Now using the non-dimensional constants,

$$
\begin{aligned}
\phi_3(2f'g-fg') &= \frac{k_{nf}}{k_f}\left(\frac{1}{P_r}\right)g''+\frac{\phi_3}{\phi_4}E_cf''^2\\
&+\frac{\Gamma x}{2}\sqrt{\frac{2B^3}{\nu_f}}\frac{\mu_{nf}}{(\rho C_p)_{nf}}\frac{B^2x^2l^2}{x^2A\nu_f}f''^3\\
&+\frac{(\rho C_p)_{nf}}{(\rho C_p)_f}\frac{(\rho C_p)_f}{\nu_f(\rho C_p)_{nf}}D_B(C_w-C_\infty)\varphi'g'\\
&+\frac{(\rho C_p)_{nf}}{v(\rho C_p)_f}\frac{(\rho C_p)_f}{\nu_f(\rho C_p)_{nf}}\frac{D_T}{T_\infty}g'^2(T_w-T_\infty)\\
&+ME_cf'^2-H_eg+Q\varphi+D_u\varphi''.
\end{aligned}
$$

So, the required dimensionless equation of temperature equation,

$$
\begin{aligned}
\frac{1}{P_r}\left(\frac{k_{nf}}{k_f}\right)g''+\phi_3\left(\frac{E_c}{\phi_4}f''^2+\frac{E_c}{2\phi_4}\lambda f''^3+N_bg'\varphi'+N_tg'^2-2f'g+fg'\right)\\
+E_cMf'^2-H_eg+Q\varphi+D_u\varphi''=0. \qquad (3.26)
\end{aligned}
$$

Next, the concentration equation will be converted into the dimensionless form. The procedure includes the following conversion of different terms from dimensional to non-dimensional form. Consider left side of the concentration equation

$$\begin{aligned} u\frac{\partial C}{\partial x} &= (Bxf'(\eta))\frac{\partial}{\partial x}(\varphi(\eta)(C_w - C_\infty) + C_\infty), \\ &= Bxf'(\eta)(0), \\ &= 0. \\ v\frac{\partial C}{\partial y} &= -\sqrt{B\nu_f}f(\eta)\frac{\partial}{\partial y}(\varphi'(\eta)(C_w - C_\infty) + C_\infty), \\ &= -\sqrt{Bv_f}f(\eta)\varphi'(\eta)(C_w - C_\infty)\sqrt{\frac{B}{\nu_f}}, \\ &= -Bf(\eta)\varphi'(\eta)(C_w - C_\infty). \end{aligned} \tag{3.27}$$

The left hand side of Eq. (3.13) becomes

$$\begin{aligned} \frac{\partial C}{\partial x} + \frac{\partial C}{\partial y} &= 0 - Bf(\eta)\varphi'(\eta)(C_w - C_\infty), \\ &= -Bf(\eta)\varphi'(\eta)(C_w - C_\infty). \end{aligned}$$

Next taking the right side of Eq. (3.13).

$$\begin{aligned} D_B\frac{\partial^2 C}{\partial y^2} &= D_B\frac{\partial}{\partial y}\left(\varphi'(\eta)(C_w - C_\infty)\sqrt{\frac{B}{\nu_f}}\right), \\ &= D_B\varphi''(\eta)(C_w - C_\infty)\frac{B}{\nu_f}. \end{aligned}$$

Similarly derivation of the temperature term involving,

$$\begin{aligned} \frac{D_T}{T_\infty}\frac{\partial^2 T}{\partial y^2} &= \frac{D_T}{T_\infty}\frac{\partial^2}{\partial y^2}(g(\eta)(T_w - T_\infty) + T_\infty), \\ &= \frac{D_T}{T_\infty}g''(\eta)(T_w - T_\infty)\frac{B}{\nu_f}. \end{aligned}$$

Putting the value of C, it becomes

$$\begin{aligned} -k_1(C - C_\infty) &= -k_1(\varphi(\eta)(C_w - C_\infty) + C_\infty - C_\infty), \\ &= -k_1\varphi(\eta)(C_w - C_\infty). \end{aligned}$$

Next derivation of the concentration term with respect to $y-$axis,

$$\frac{D_m K_T}{T_m}\left(\frac{\partial^2 C}{\partial y^2}\right) = \frac{D_m K_T}{T_m} g''(\eta)(T_w - T_\infty)\frac{B}{\nu_f}.$$

Using these values in Eq. (3.13),

$$\begin{aligned} -Bf(\eta)\varphi'(\eta)(C_w - C_\infty) &= D_B\varphi''(\eta)(C_w - C_\infty)\frac{B}{v_f} + \frac{D_T}{T_\infty} g''(\eta)(T_w - T_\infty)\frac{B}{v_f} \\ &\quad -k_1\varphi(\eta)(C_w - C_\infty) + \frac{D_m K_T}{T_m} g''(\eta)(T_w - T_\infty)\frac{B}{\nu_f}. \end{aligned}$$

Dividing by $\left(D_B(C_w - C_\infty)\frac{B}{\nu_f}\right)$,

$$\begin{aligned} -f\varphi'\frac{v_f}{D_B} &= \varphi''(\eta) + \frac{D_T}{T_\infty D_B} g''(\eta)\frac{(T_w - T_\infty)}{C_w - C_\infty} \\ &\quad -\frac{k_1\nu_f}{D_B B}\varphi(\eta) + \frac{D_m K_T}{D_B T_m} g''(\eta)\frac{(T_w - T_\infty)}{(C_w - C_\infty)}. \end{aligned}$$

Substituting the non-dimensional constants,

$$\begin{aligned} \varphi'' + S_c f\varphi' - K_1\varphi + g'' S_r S_c + g''\frac{N_t}{N_b} &= 0, \\ \varphi'' + S_c f\varphi' + \left(\frac{N_t}{N_b} + S_r S_c\right) g'' - K_1\varphi &= 0. \end{aligned} \tag{3.28}$$

3.3.1 Boundary Conditions

For converting the associated boundary conditions into the dimensionless form, the following steps have been performed:

$$\begin{aligned} &u = U_w = Bx, \qquad \text{at} \quad y = 0, \\ &Bxf'(\eta) = Bx, \qquad \text{at} \quad \eta = 0, \\ &\Rightarrow f'(0) = 1. \\ &v = 0, \qquad \text{at} \quad y = 0, \\ &-\sqrt{B\nu_f} f(\eta) = 0, \qquad \text{at} \quad \eta = 0, \\ &T = T_w = T_\infty + A\left(\frac{x}{l}\right)^2, \qquad \text{at} \quad y = 0, \end{aligned}$$

$$\Rightarrow f(0) = 0.$$

$$(T_w - T_\infty)g(\eta) + T_\infty = T_w, \qquad \text{at} \quad \eta = 0,$$

$$(T_w - T_\infty)g(0) = (T_w - T_\infty)$$

$$\Rightarrow g(0) = 1.$$

$$C = C_w, \qquad \text{at} \quad y = 0,$$

$$\Rightarrow (C_w - C_\infty)\varphi(\eta) + C_\infty = C_w, \qquad \text{at} \quad \eta = 0,$$

$$\Rightarrow (C_w - C_\infty)\varphi(0) = (C_w - C_\infty)$$

$$\Rightarrow \varphi(0) = 1.$$

$$u \to 0 \qquad \text{as} \quad y \to \infty,$$

$$\Rightarrow Bxf'(\eta) \to 0, \qquad \text{as} \quad \eta \to \infty,$$

$$\Rightarrow f'(\infty) \to 0.$$

$$T \to T_\infty, \qquad \text{as} \quad y \to \infty,$$

$$\Rightarrow (T_w - T_\infty)g(\eta) + T_\infty \to T_\infty, \qquad \text{as} \quad \eta \to \infty,$$

$$\Rightarrow (T_w - T_\infty)g(\eta) + T_\infty - T_\infty \to T_\infty - T_\infty, \qquad \text{as} \quad \eta \to \infty,$$

$$\Rightarrow (T_w - T_\infty)g(\infty) \to 0$$

$$\Rightarrow g(\infty) \to 0.$$

$$C \to C_\infty, \qquad \text{as} \quad y \to \infty,$$

$$\Rightarrow (C_w - C_\infty)\varphi(\eta) + C_\infty \to C_\infty, \qquad \text{as} \quad \eta \to \infty,$$

$$\Rightarrow (C_w - C_\infty)\varphi(\infty) + C_\infty - C_\infty \to C_\infty - C_\infty$$

$$\Rightarrow (C_w - C_\infty)\varphi(\infty) \to 0$$

$$\Rightarrow \varphi(\infty) \to 0.$$

3.3.2 Non-Dimensional Equations

$$f''' + \lambda f''' f'' - \phi_1 \left(f'^2 - ff'' + \frac{M}{\phi_2} f' \right) - \frac{1}{K} f' = 0, \tag{3.29}$$

$$\frac{K_0}{P_r} g'' + \phi_3 \left(\frac{E_c}{\phi_4} f''^2 + \frac{E_c}{2\phi_4} \lambda f''^3 + N_b g'\varphi' + N_t g'^2 - 2f'g + fg' \right) + E_c M f'^2 - H_e g + Q\varphi + D_u \varphi'' = 0, \tag{3.30}$$

$$\varphi'' + S_c f\varphi' + \left(\frac{N_t}{N_b} + S_r S_c\right) g'' - K_1\varphi \;\; = \;\; 0, \tag{3.31}$$

with boundary conditions:

$$\begin{aligned} f(0) = 0,\ f'(0) = 1,\ g(0) = 1,\ \varphi(0) = 1, \\ g(\infty) \to 0,\ f'(\infty) \to 0,\ \varphi(\infty) \to 0. \end{aligned} \tag{3.32}$$

In the above equations M represents magnetic parameter, P_r shows the Prandtl number, λ stands for non-Newtonian parameter, E_c the Eckert number, K represents porosity number, H_e shows the heat generation rate parameter, N_b stands for Brownian motion parameter, N_t the thermopheroesis parameter, S_c known as Schmidt number, K_1 shows the chemical reaction parameter, D_u Dufour number, S_r Soret number and Q stands for radiation absorption parameter. The above mentioned parameters are defined as follow:

$$\begin{aligned} &M = \frac{x}{U_w}\frac{\sigma B_0^2}{\rho_f}, \quad \lambda = \Gamma x\sqrt{\frac{2B^3}{v_f}}, \quad P_r = \frac{v_f}{\alpha_f}, \quad E_c = \frac{U_w^2}{(C_p)_f(T_w - T_\infty)}, \quad K = \frac{kU_w}{v_f x}, \\ &H_e = \frac{xQ_0}{(\rho C_p)_f U_w}, \quad N_b = \frac{\tau D_B}{v_f}(C_w - C_\infty), \quad N_t = \frac{\tau D_T}{v_f T_\infty}, \quad S_c = \frac{v_f}{D_B}, \quad K_0 = \frac{k_{nf}}{k_f}\ , \\ &K_1 = \frac{k_1 v_f}{BD_B}, \quad D_u = \frac{D_m K_T(C_w - C_\infty)}{C_s v_f(\rho C_p)_f(T_w - T_\infty)}, \quad S_r = \frac{D_m K_T(T_w - T_\infty)}{T_m v_f(C_w - C_\infty)}, \\ &Q = \frac{Q_1(C_w - C_\infty)(\rho C_p)_{nf}}{B(T_w - T_\infty)(\rho C_P)_f}. \end{aligned}$$

Where,

$$\left.\begin{aligned} \phi_1 &= (1-\phi)^{2.5}\left[1 - \phi + \phi\left(\frac{\rho_s}{\rho_f}\right)\right], \\ \phi_2 &= \left[1 - \phi + \phi\left(\frac{\rho_s}{\rho_f}\right)\right], \\ \phi_3 &= \left[1 - \phi + \phi\left(\frac{(\rho C_p)_s}{(\rho C_p)_f}\right)\right], \\ \phi_4 &= (1-\phi)^{2.5}\left[1 - \phi + \phi\left(\frac{(\rho C_p)_s}{(\rho C_p)_f}\right)\right]. \end{aligned}\right\} \tag{3.33}$$

3.4 Physical Quantities of Interest

We are now interested in studying the skin friction coefficient C_f, the local Nusselt number Nu_x (heat transfer rate) and the Sherwood number Sh. The parameters defined as the amount rate of drag surface and heat transfer at wall. Such physical quantities are described as follow:
Mathematical form of skin coefficient friction is

$$C_f = \frac{\tau_w}{\rho_f U_w^2}. \tag{3.34}$$

Nusselt number is defined as

$$Nu_x = \frac{-x}{(T_w - T_\infty)} \left(\frac{\partial T}{\partial y}\right)_{y=0}. \tag{3.35}$$

The quantity of Sherwood number is

$$Sh = \frac{-x}{(C_w - C_\infty)} \left(\frac{\partial C}{\partial y}\right)_{y=0}. \tag{3.36}$$

The wall heat is defined as

$$\left(\frac{\partial T}{\partial y}\right)_{y=0} = g'(0)(T_w - T_\infty)\sqrt{\frac{B}{\nu_f}}, \tag{3.37}$$

and $(\frac{\partial C}{\partial y})_{y=0}$ denotes the mass transfer

$$\left(\frac{\partial C}{\partial y}\right)_{y=0} = \varphi'(0)(C_w - C_\infty)\sqrt{\frac{B}{v_f}}, \tag{3.38}$$

Shear stress at the surface is defined as

$$\tau_w = \mu_{nf}\left(\frac{\partial u}{\partial y} + \frac{\Gamma}{\sqrt{2}}\left(\frac{\partial u}{\partial y}\right)^2\right)_{y=0}. \tag{3.39}$$

Converting τ_w into dimensionless form as follows

$$\tau_w = \frac{\mu_f}{(1-\phi)^{2.5}}\left(Bx\sqrt{\frac{B}{\nu_f}}f''(0) + \frac{\Gamma}{\sqrt{2}}\left(Bx\sqrt{\frac{B}{\nu_f}}\right)^2 f''^2(0)\right). \tag{3.40}$$

Following dimensionless form obtained for Nusselt number, Sherwood number and skin friction coefficient by using equations (3.37), (3.38) and (3.40).

$$\begin{aligned}
C_f &= \frac{\tau_w}{\rho_f U_w^2}, \\
&= \frac{\mu_f}{\rho_f U_w^2 (1-\phi)^{2.5}} \left(Bx\sqrt{\frac{B}{\nu_f}} f''(0) + \frac{\Gamma}{\sqrt{2}} \left(Bx\sqrt{\frac{B}{\nu_f}} \right)^2 f''^2(0) \right), \\
&= \frac{\mu_f}{\rho_f U_w^2 (1-\phi)^{2.5}} \left(Bx\sqrt{\frac{B}{\nu_f}} f''(0) + \frac{2\Gamma}{2\sqrt{2}} B^2 x^2 \left(\sqrt{\frac{B}{\nu_f}} \right)^2 f''^2(0) \right), \\
&= \frac{\nu_f}{U_w^2 (1-\phi)^{2.5}} Bx\sqrt{\frac{B}{\nu_f}} \left(f''(0) + \frac{\sqrt{2}\Gamma x}{2} \sqrt{\frac{B^3}{\nu_f}} f''^2(0) \right),
\end{aligned}$$

Multiply both sides by $(1-\phi)^{2.5}$

$$\begin{aligned}
C_f(1-\phi)^{2.5} &= \frac{\nu_f}{U_w^2} Bx\sqrt{\frac{B}{\nu_f}} \left(f''(0) + \frac{\lambda}{2} f''^2(0) \right) \quad (\because \nu_f = \frac{\mu_f}{\rho_f}), \\
C_f(1-\phi)^{2.5} &= \frac{\nu_f}{B^2 x^2} Bx\sqrt{\frac{B}{\nu_f}} \left(f''(0) + \frac{\lambda}{2} f''^2(0) \right), \\
C_f(1-\phi)^{2.5} &= \sqrt{\frac{\nu_f}{U_w x}} \left(f''(0) + \frac{\lambda}{2} f''^2(0) \right) \qquad (\because U_w = Bx),
\end{aligned}$$

$$\Rightarrow \quad (Re_x)^{\frac{1}{2}} C_f (1-\phi)^{2.5} = \left(f''(0) + \frac{\lambda}{2} f''^2(0) \right). \tag{3.41}$$

Dimensionless Nusselt number is

$$\begin{aligned}
Nu_x &= \frac{-x}{(T_w - T_\infty)} \left(\frac{\partial T}{\partial y} \right)_{y=0}, \\
&= \frac{-x}{(T_w - T_\infty)} g'(0) \sqrt{\frac{B}{v_f}} (T_w - T_\infty), \\
&= -\sqrt{\frac{xU_w}{\nu_f}} g'(0) \qquad (\because U_w = Bx),
\end{aligned}$$

$$\Rightarrow \quad (Re_x)^{\frac{-1}{2}} Nu_x = -g'(0). \tag{3.42}$$

Non-dimensional Sherwood number is

$$\begin{aligned} Sh &= \frac{-x}{(C_w - C_\infty)}\left(\frac{\partial C}{\partial y}\right)_{y=0}, \\ &= \frac{-x}{(C_w - C_\infty)}\varphi'(0)\sqrt{\frac{B}{v_f}}(C_w - C_\infty), \\ &= -\sqrt{\frac{xU_w}{\nu_f}}\varphi'(0), \\ &\Rightarrow \quad (Re_x)^{\frac{-1}{2}} Sh = -\varphi'(0). \end{aligned} \tag{3.43}$$

The local Reynolds number is $Re_x = \frac{xU_w}{\nu_f}$.

3.5 Numerical Scheme

In this section, the shooting method has been used together with RK4 method to solve the system of nonlinear ordinary differential equations (3.29)-(3.31) along with boundary conditions (3.32). We adopt the following procedure:

$$f''' = \frac{\phi_1\left[f'^2 - f''f + f'\left(\frac{M}{\phi_2}\right)\right] - f'\left(\frac{1}{K}\right)}{(1+\lambda f'')}, \tag{3.44}$$

$$\begin{aligned} g'' = \quad & \frac{1}{\left(\frac{1}{P_r}\left(\frac{k_{nf}}{k_f}\right) - D_u\left(\frac{N_t}{N_b} + S_r S_c\right)\right)}\left[-\phi_3\left\{fg' - 2f'g + f''^2\left(\frac{E_c}{\phi_4}\right)\right.\right. \\ & \left.\left. + f''^3\left(\frac{\lambda E_c}{2\phi_4}\right) + N_b g'\varphi' + N_t g'^2\right\} + E_c M f'^2 - H_e g\right. \\ & \left. + Q\varphi - D_u S_c f\varphi' + D_u K_1\varphi\right], \end{aligned} \tag{3.45}$$

$$\varphi'' = -S_c f\varphi' - \left(\frac{N_t}{N_b} + S_r S_c\right) g'' + K_1\varphi. \tag{3.46}$$

$$\left.\begin{aligned} f(0) = 0,\ f'(0) = 1,\ g(0) = 1,\ \varphi(0) = 1, \\ g(\infty) \to 0,\ f'(\infty) \to 0,\ \varphi(\infty) \to 0. \end{aligned}\right\}$$

First Eq. (3.44) is numerically solved and then the calculated results for f, f', f'' will be used in Eq. (3.45) and Eq. (3.46) as a recognize input. By using shooting method Eq. (3.44) is solved independently. To apply shooting method, we convert the BVP into IVP by assuming the missing initial condition. We introduce the following notations for further simplification.

$$f = y_1,\ f' = y_2, f'' = y_3,\ \frac{\partial f}{\partial \chi} = y_4,\ \frac{\partial f'}{\partial \chi} = y_5,\ \frac{\partial f''}{\partial \chi} = y_6,$$

where χ is the assumed initial condition.

The system of first order ODEs and the corresponding initial condition can be written as

$$\begin{aligned}
y_1' &= y_2, && y_1(0) = 0,\\
y_2' &= y_3, && y_2(0) = 1,\\
y_3' &= \frac{\phi_1\left[y_2^2 - y_1 y_3 + y_2\left(\frac{M}{\phi_2}\right)\right] - y_2\left(\frac{1}{K}\right)}{(1+\lambda y_3)}, && y_3(0) = \chi,\\
y_4' &= y_5, && y_4(0) = 0,\\
y_5' &= y_6, && y_5(0) = 0,\\
y_6' &= \left[\phi_1\left\{2y_2y_5 - y_1y_6 - y_3y_4 + y_5\left(\frac{M}{\phi_2}\right)\right\} + y_5\left(\frac{1}{K}\right)(1+\lambda y_3)\right.\\
&\left.-(\lambda y_6)\left\{\phi_1\left(y_2^2 - y_1y_3 + y_2\left(\frac{M}{\phi_2}\right)\right) + y_2\left(\frac{1}{K}\right)\right\}\right]\frac{1}{(1+\lambda y_3)^2}, && y_6(0) = 1.
\end{aligned}$$

For the solution of above initial value problem we use Runge Kutta method of order four. The approximate solution of Eq. (3.44) can be obtained by converting the unbounded domain $[0, \infty)$ into bounded domain $[0, \eta_\infty]$, where η_∞ is an applicable finite positive real number with chosen initial guess χ such that

$$F(\chi) = y_2(\eta_\infty, \chi) - 1 = 0. \tag{3.47}$$

To solve the algebraic Eq. (3.47), we apply the Newton method which has the following iterative procedure:

$$\chi^{n+1} = \chi^n - \left(\frac{y_2(\eta_\infty, \chi) - 1}{\left(\frac{\partial y_2(\eta_\infty, \chi)}{\partial \chi}\right)}\right), n = 0, 1, 2, 3, .. \tag{3.48}$$

As a result of derivative notations $\frac{\partial y_2(\eta_\infty,\chi)}{\partial \chi}$, the Newton iterative scheme gets the form

$$\chi^{n+1} = \chi^n - \left(\frac{y_2(\eta_\infty,\chi)-1}{y_5(\eta_\infty)}\right). \tag{3.49}$$

The threshold for the shooting method is defined as follows:

$$|y_2(\eta_\infty)-1| < \epsilon, \tag{3.50}$$

where ϵ is taken as 10^{-6}. The method has been repeated until this criteria is fulfilled. In order to apply numerical method for the solution of Eq. (3.45) and Eq. (3.46), we denote the missing initial condition $g(0)$ and $\varphi(0)$ by q and r, respectively and different notations have been used which are given below

$$\left.\begin{aligned} g=Y_1,\ g'=Y_2,\ \phi=Y_3,\ \phi'=Y_4,\ \frac{\partial g}{\partial q}=Y_5,\ \frac{\partial g'}{\partial q}=Y_6,\ \frac{\partial \phi}{\partial q}=Y_7,\\ \frac{\partial \varphi'}{\partial q}=Y_8,\ \frac{\partial g}{\partial r}=Y_9,\ \frac{\partial g'}{\partial r}=Y_{10},\ \frac{\partial \varphi}{\partial r}=Y_{11},\ \frac{\partial \varphi'}{\partial r}=Y_{12} \end{aligned}\right\} \tag{3.51}$$

Using these notations, we get a system of first order ODEs which are given below

$$Y_1' = Y_2,$$

$$Y_2' = \frac{1}{\left(\frac{1}{P_r}\left(\frac{k_{nf}}{k_f}\right) - D_u\left(\frac{N_t}{N_b}+S_rS_c\right)\right)}\left[-\phi_3\left(y_1Y_2 - 2y_2Y_1 + y_3^2\left(\frac{E_c}{\phi_4}\right) + y_3^3\left(\frac{\lambda E_c}{2\phi_4}\right)\right.\right.$$
$$\left.\left. + N_bY_2Y_4 + N_tY_2^2\right) - E_cMy_2^2 + H_eY_1 - QY_3 + D_uS_cy_1Y_4 - D_uK_1Y_3\right],$$

$$Y_3' = Y_4,$$

$$Y_4' = -S_cy_1Y_4 + \left(\frac{\left(\frac{N_t}{N_b}+S_rS_c\right)}{\frac{1}{P_r}\left(\frac{k_{nf}}{k_f}\right) - D_u\left(\frac{N_t}{N_b}+S_rS_c\right)}\right)\left[-\phi_3\left\{y_1Y_2 - 2y_2Y_1 + y_3^2\left(\frac{E_c}{\phi_4}\right)\right.\right.$$
$$\left.\left. + y_3^3\left(\frac{\lambda E_c}{2\phi_4}\right) + N_bY_2Y_4 + N_tY_2^2\right\} - E_cMy_2^2 + H_eY_1 - QY_3\right.$$
$$\left. + D_uS_cy_1Y_4 - D_uK_1Y_3)\right] + K_1Y_3,$$

$$Y_5' = Y_6,$$

$$Y_6' = \left(\frac{1}{\frac{1}{P_r}\left(\frac{k_{nf}}{k_f}\right) - D_u\left(\frac{N_t}{N_b} + S_rS_c\right)}\right)[-\phi_3\{y_1Y_6 - 2y_2Y_5 + N_b(Y_6Y_4 + Y_2Y_8)\}$$
$$+N_t(2Y_2Y_6) + H_eY_5 - QY_7 + D_uS_cy_1Y_8 - D_uK_1Y_7],$$
$$Y_7' = Y_8,$$
$$Y_8' = -S_cy_1Y_8 + \left(\frac{\left(\frac{N_t}{N_b} + S_rS_c\right)}{\frac{1}{P_r}\left(\frac{k_{nf}}{k_f}\right) - D_u\left(\frac{N_t}{N_b} + S_rS_c\right)}\right)[-\phi_3\{y_1Y_6 - 2y_2Y_5$$
$$+N_b(Y_6Y_4 + Y_2Y_8) + N_t(2Y_2Y_6)\} + H_eY_5 - QY_7$$
$$+D_uS_cy_1Y_8 - D_uK_1Y_7) + K_1Y_7],$$
$$Y_9' = Y_{10},$$
$$Y_{10}' = \left(\frac{1}{\frac{1}{P_r}\left(\frac{k_{nf}}{k_f}\right) - D_u\left(\frac{N_t}{N_b} + S_rS_c\right)}\right)[-\phi_3\{y_1Y_{10} - 2y_2Y_9 + N_b(Y_{10}Y_4 + Y_2Y_{11})\}$$
$$+N_t(2Y_2Y_{10}) + H_eY_5 - QY_{11} + D_uS_cy_1Y_{12} - D_uK_1Y_{11}],$$
$$Y_{11}' = Y_{12},$$
$$Y_{12}' = -S_cy_1Y_{12} + \left(\frac{\left(\frac{N_t}{N_b} + S_rS_c\right)}{\frac{1}{P_r}\left(\frac{k_{nf}}{k_f}\right) - D_u\left(\frac{N_t}{N_b} + S_rS_c\right)}\right)[-\phi_3\{y_1Y_{10} - 2y_2Y_9$$
$$+N_b(Y_{10}Y_4 + Y_2Y_{12}) + N_t(2Y_2Y_{10})\} + H_eY_9 - QY_{11}$$
$$+D_uS_cy_1Y_{12} - D_uK_1Y_{11}] + K_1Y_{11},$$

The resulting form of boundary conditions is

$$Y_1(0) = 1,\ Y_2(0) = q,\ Y_3(0) = 1,\ Y_4(0) = r,\ Y_5(0) = 0,\ Y_6(0) = 1,$$
$$Y_7(0) = 0,\ Y_8(0) = 0,\ Y_9(0) = 0,\ Y_{10}(0) = 0,\ Y_{11}(0) = 0,\ Y_{12}(0) = 1.$$

In order to solve the above initial value problem, we used RK4 method and selected the missing conditions in such a way that

$$(Y_1(q,r))_{\eta=\eta_\infty} = 0, \quad (Y_3(q,r))_{\eta=\eta_\infty} = 0. \tag{3.52}$$

The above set of equations can be solved by Newton method with following iterative formula:

$$\begin{bmatrix} q^{n+1} \\ r^{n+1} \end{bmatrix} = \begin{bmatrix} q^{n} \\ r^{n} \end{bmatrix} - \begin{bmatrix} \frac{\partial Y_1(q,r)}{\partial q} & \frac{\partial Y_1(q,r)}{\partial r} \\ \frac{\partial Y_3(q,r)}{\partial q} & \frac{\partial Y_3(q,r)}{\partial r} \end{bmatrix}^{-1} \begin{bmatrix} Y_1 \\ Y_3 \end{bmatrix}_{(q^n, r^n, \eta_\infty)}$$

We utilize the derivative notation as follows

$$\begin{bmatrix} q^{n+1} \\ r^{n+1} \end{bmatrix} = \begin{bmatrix} q^{n} \\ r^{n} \end{bmatrix} - \begin{bmatrix} Y_5 & Y_9 \\ Y_7 & Y_1 1 \end{bmatrix}^{-1} \begin{bmatrix} Y_1 \\ Y_3 \end{bmatrix}_{(q^n, r^n, \eta_\infty)}$$

where n = 0,1,2,3,....

The terminating process for the shooting method is adjusted as:

$$max\{|Y_1(\eta_\infty)|,\ |Y_3(\eta_\infty)|\} < \epsilon,$$

where ϵ is a small positive number. From now onward ϵ has been taken as 10^{-6} whereas η_∞ set as 5.

3.6 Graphical Discussion

The numerical results of the equations in the preceding sections are discussed using the graphs in this section. The numerical calculations are performed for the influence of various important parameters, including porosity parameter K, non-Newtonian Williamson parameter λ, magnetic parameter M, Prandtl number P_r, radiation absorption parameter Q, Eckert number E_c, chemical reaction parameter K_1, heat generation rate parameter H_e, Soret number S_r, Dufour number D_u, thermophoresis parameter N_t, Brownian motion parameter N_b, and Schmidt number S_c. These parameters have a direct influence on the distribution of concentration, temperature, and velocity.

3.6.1 Effect of Porosity Parameter K

Figure 3.2 shows that the influence of the porosity parameter on the field of velocity, and it is noticed that the fluid velocity increases by increasing the values of K.

Physically the boosting behavior of the porous medium is expressed by increasing the values of K. Furthermore, the lower resistance in the flow finally going to rise the velocity profile.

3.6.2 Effect of Non-Newtonian Williamson Parameter λ

The impact of non-Newtonian Williamson parameter on the velocity profile is shown in Figure 3.3. The fluid velocity is reduced by an increase in λ. It is obvious that an increase in non-Newtonian fluid the elasticity contributes to decrease in the fluid flow. It is elucidated that the velocity fluid and boundary layer thickness diminish with the increment in non-Newtonian Williamson variable λ.

3.6.3 Effect of Magnetic Parameter M

The transverse magnetic field effect on the field of velocity is sketched in Figure 3.4. It is illustrated that the velocity diminishes while the M values increases. Physical significance, the existence of a transverse magnetic field ultimately leads to a drag force called Lorentz force that will cause retardation in the distribution of velocity. With the increase of M, the concentration profiles increase as seen in Figure 3.5. As the value of M increases, it excites the motion of fluid particles which is due to enhance the Brownian motion, can spread rapidly into the neighbouring fluid layers.

3.6.4 Effect of Radiation Absorption Parameter Q

It can be seen from Figure 3.8 that the temperature field increases with Q. This is because the high Q values lead to increased conduction domination. The influence of radiation absorption parameter Q on the dimensionless concentration field $\phi(\eta)$ is expressed in Figure 3.9. By enlarging the radiation absorption parameter on the concentration profile make the thickness of boundary layer decreases.

3.6.5 Effect of Volume Fraction of Nanoparticles ϕ_1

Figure 3.6 displays the impact of volume fraction of nanoparticles on the velocity profiles ϕ_1. From the figure it is apparent that the rise in volume fraction of nanoparticles depreciates the fluid velocity. Figure 3.7 indicates that the fluid concentration is increased by an increase in the nanoparticles of volume fraction.

3.6.6 Effect of Prandtl Number P_r

Figure 3.10 illustrates that decreasing temperature with the P_r. Basically, Prandtl number restraint the comparative thickness of the thermal and momentum boundary layer. Moreover, graph portrays the behavior of $g(\eta)$ for diverse values of P_r. It stands noted that as the values of P_r rise, the temperature falls. Once there is a rise in P_r, a marked reduction in the thermal boundary-layer is noted. In other words, higher P_r results lower thermal diffusivity. However, a higher estimation value of P_r makes lowers diffusivity, while increases the thermal characteristics. Figure 3.11 explores that the finding of prandtl number on the concentration distribution, which certainly reveals that profile of concentration of the nanofluid increase with prandtl number P_r.

3.6.7 Effect of Eckert Number E_c

Figure 3.12 is specified to show that the thickness of the temperature field and the thermal boundary layer is expanded as boosting values of the Eckert number. Due to the fact that the dissipation rises by increasing the values of E_c because of this in higher dissipation the fluid internal energy also enhanced. Figure 3.13 is plotted that the influence of E_c on the concentration field $\phi(\eta)$. Actually, Eckert number can be written as a ratio of kinetic energy of the fluid particle and thermal energy. Concentration of the fluid decreases by increasing the E_c Eckert number. Physically, by the growth of thermal energy it will decrease the kinetic energy of the fluid particle so the distribution of concentration becomes lower.

3.6.8 Effect of Chemical Reaction Parameter K_1

Figure 3.14 is graphed to demonstrate the influence of the K_1 on the profile of the temperature $g(\eta)$, g is observed to decrease with boosting values of K_1. The effect of the chemical reaction parameter over the non-dimensional concentration field is expressed in Figure 3.15. Graph is illuminated by the larger variation of chemical reaction parameter reduces the fluid concentration. It can happen because chemical reaction assists to facilitate the transfer of mass and decreases the boundary layer thickness.

3.6.9 Effect of Dufour Number D_u

Figure 3.18 indulges the impact of Dufour number on the dimensionless temperature field. It is evident that for the higher values of D_u, the temperature of fluid decreases up to a certain value close to the wall of stretching sheet, but the opposite pattern is observed beyond this point. Figure 3.19 shows that raising the Dufour number D_u values initially leads to a deep enhancement in the field of concentration with a little bit decline. Nearby the stretching the surface concentration of fluid increases with increasing D_u Dufour number hence the opposite trend is noticed that is away from the wall.

3.6.10 Effect of Soret Number S_r

Figure 3.22 explores that with the increment of S_r the concentration boundary layer thickness ultimately contributes to an increase in the concentration field φ as the mass flux generated by the temperature gradient to enhance the profiles. The graph illustrates to analyze the influence of S_r Soret number on non dimensional $\varphi(\eta)$ concentration distribution. For higher estimation of $(S_r = 0.2, 0.8, 1.3)$ concentration field $\varphi(\eta)$ and the boundary layer thickness increases. It is on account to the validity for higher S_r temperature gradient of fluid shoot up which

corresponds to elevated the convective flow. Thus non dimensional concentration of fluid $\varphi(\eta)$ increases.

3.6.11 Effect of Thermophoresis Parameter N_t

The effect of thermophoresis parameter N_t on $g(\eta)$ is shown in Figure 3.20. The temperature of fluid upgrades and therefore the opacity of the thermal boundary region rises while the N_t thermophoresis parameter escalates. Figure 3.24 exhibits the visualization of thermophoresis parameter N_t on the concentration field. Generally, in the presence of thermophoresis parameter particles of fluid moving from hotter to colder area of the fluid by exert forces. So because of this transportation the dimensionless concentration of the fluid φ increases.

3.6.12 Effect of Heat Sink Parameter H_e

Figure 3.16 is graphed to demonstrate the influence of the heat sink parameter on the profile of the temperature $g(\eta)$, temperature boundary layer is observed to decrease with the increasing values of H_e. Figure 3.17 reflects the impact of H_e on the concentration field $\varphi(\eta)$. It is noted that by increasing H_e, the concentration field increases.

3.6.13 Effect of Schmidt Number S_c

Figure 3.23 illustrates that the alteration of the S_c on concentration profiles. Actually, Schmidt number is the relation between the momentum diffusivity to Bornian diffusivity. It is shown that near the stretching sheet wall, the concentration profiles increase with increasing S_c up to a certain value of η but apart from this point the opposite pattern is observed.

3.6.14 Effect of Brownian Motion N_b

Figure 3.21 elucidates that the concentration distribution decrease with larger values of the Brownian motion N_b. Essentially, that holds since the collision of the fluid macroscopic particles and random motion rises with the increment of N_b. Due to this lower the non-dimensional concentration of fluid φ can be visualized.

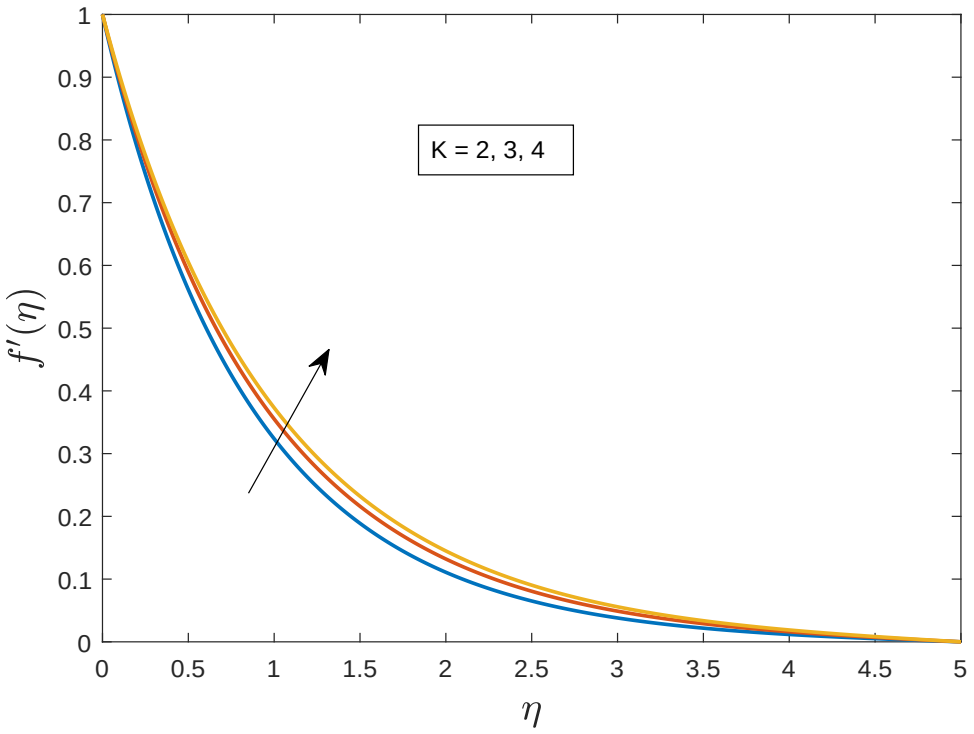

FIGURE 3.2: The effect of K is plotted against η on velocity profile.

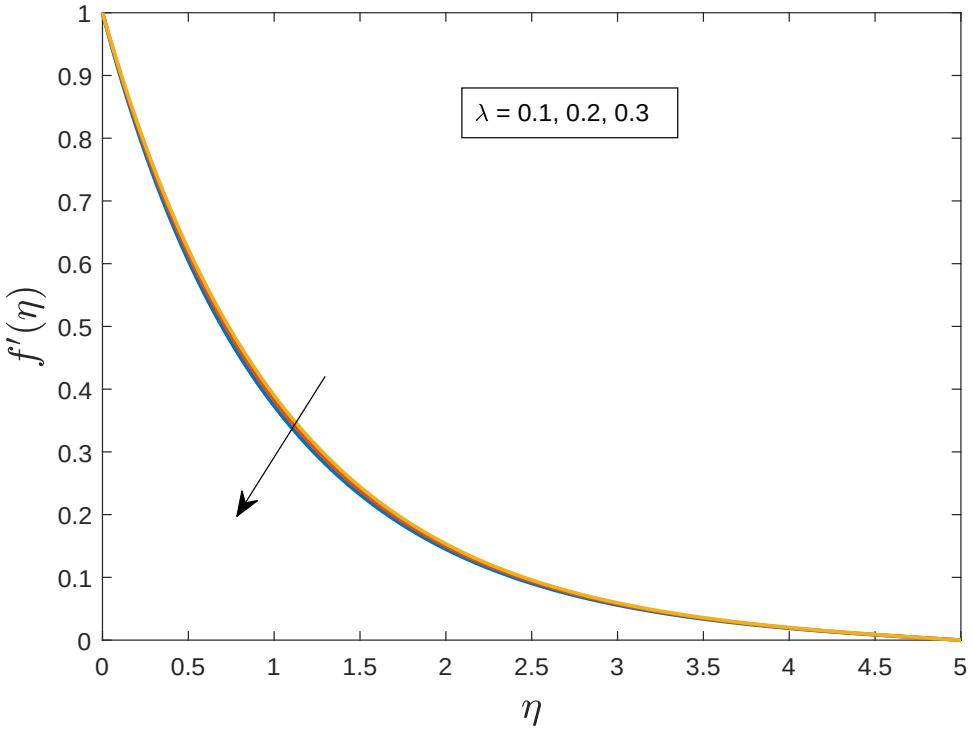

FIGURE 3.3: The effect of λ is plotted against η on velocity profile.

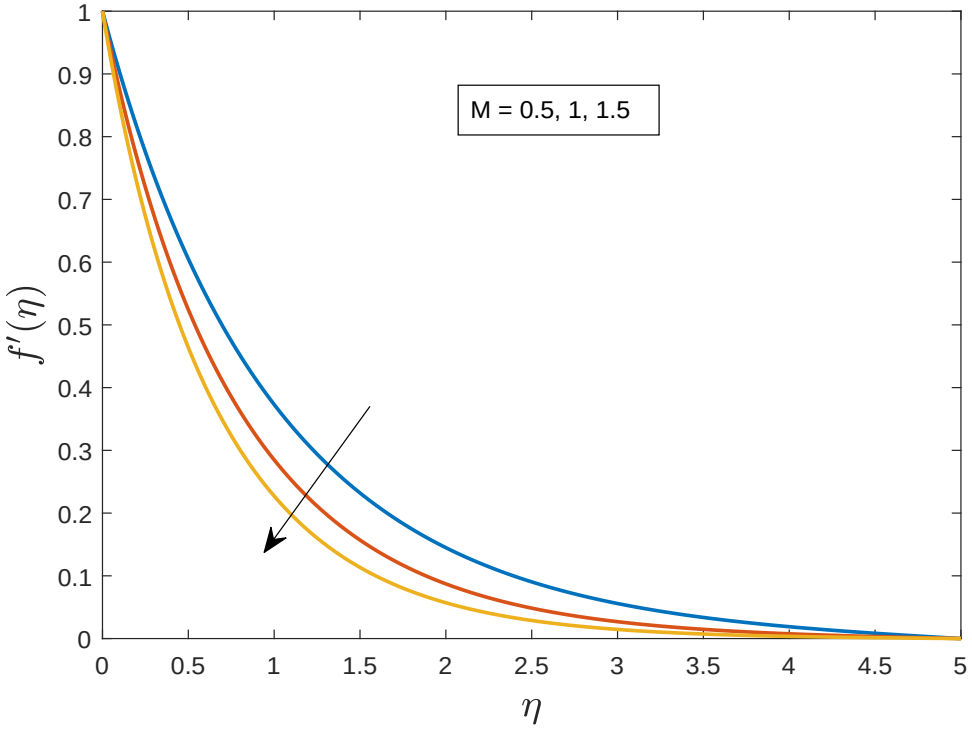

FIGURE 3.4: The effect of M is plotted against η on velocity profile.

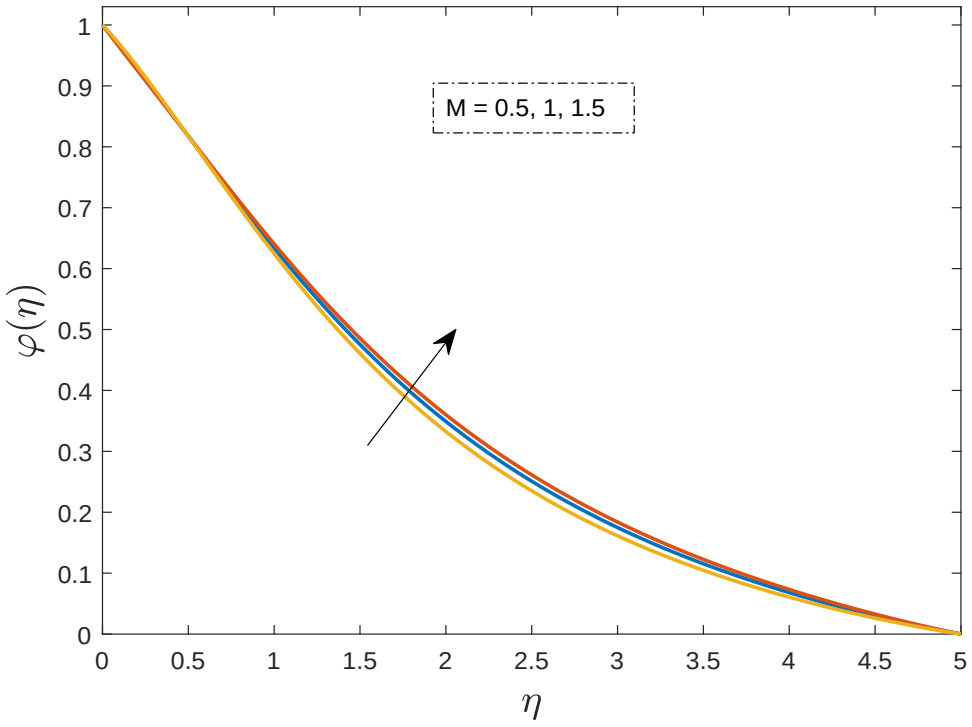

FIGURE 3.5: The effect of M is plotted against η on nanoparticles concentration profile for different values.

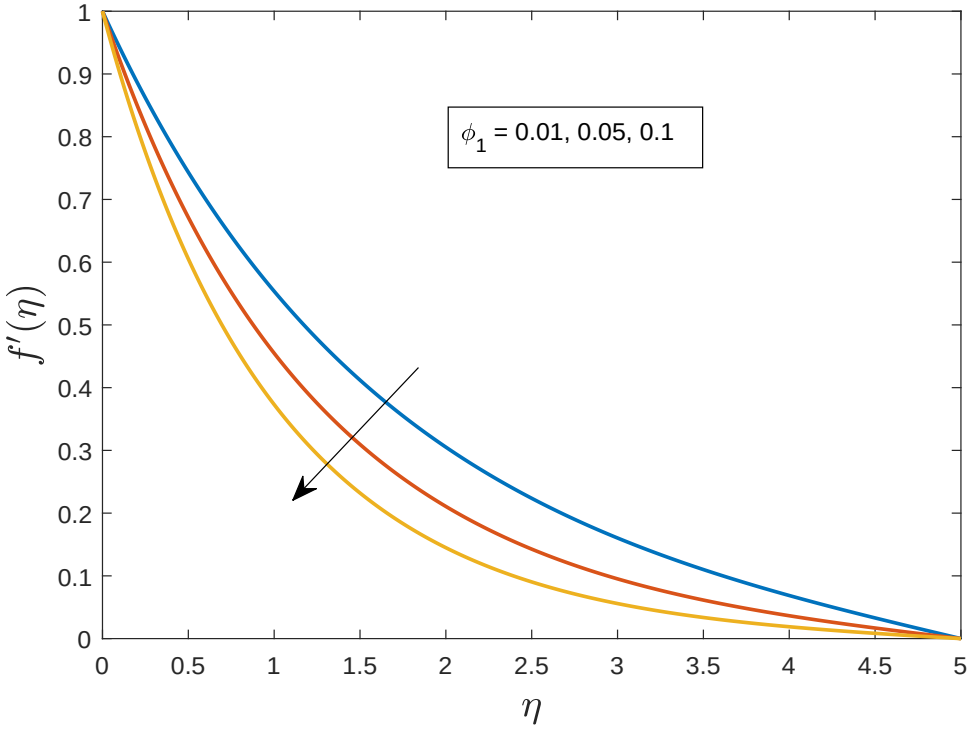

FIGURE 3.6: The effect of ϕ_1 is plotted against η on velocity profile.

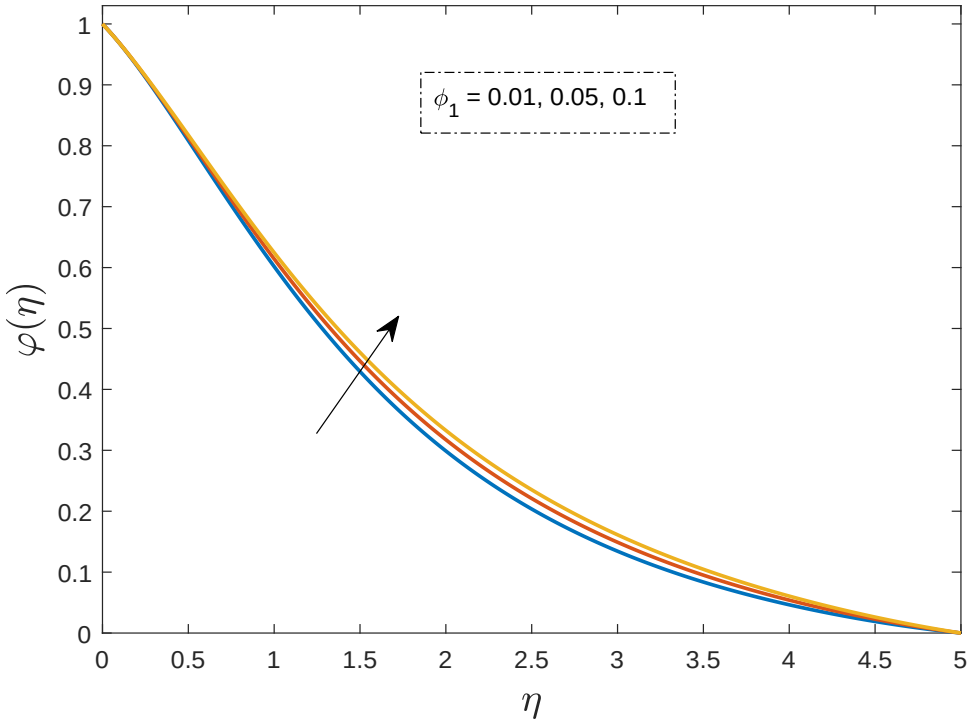

FIGURE 3.7: The effect of ϕ_1 is plotted against η on nanoparticles concentration profile.

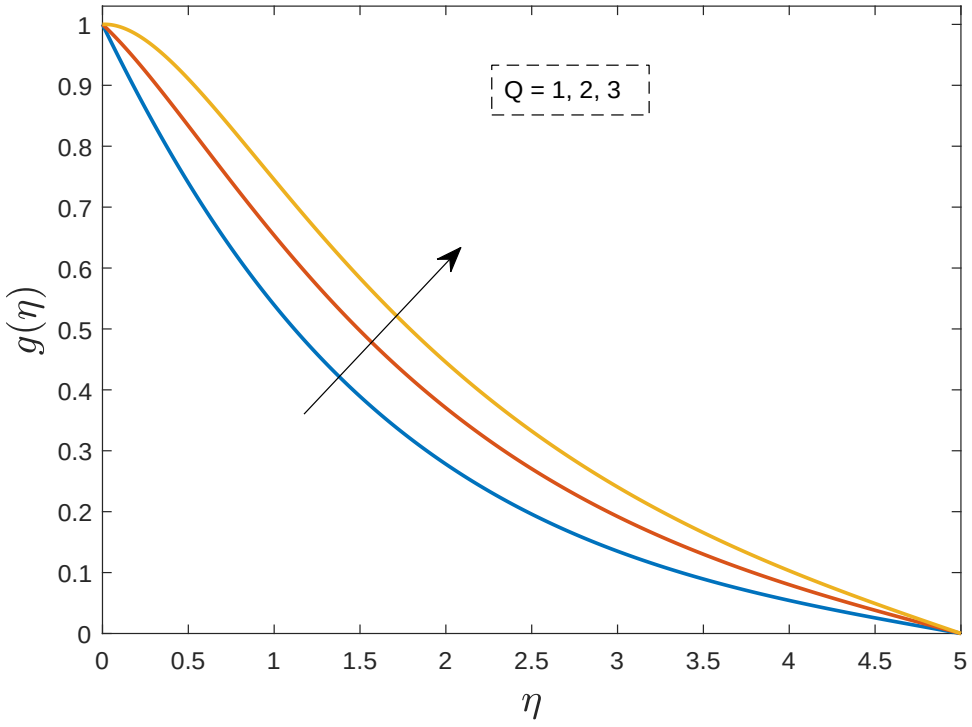

FIGURE 3.8: The effect of Q is plotted against η on temperature profile for different values.

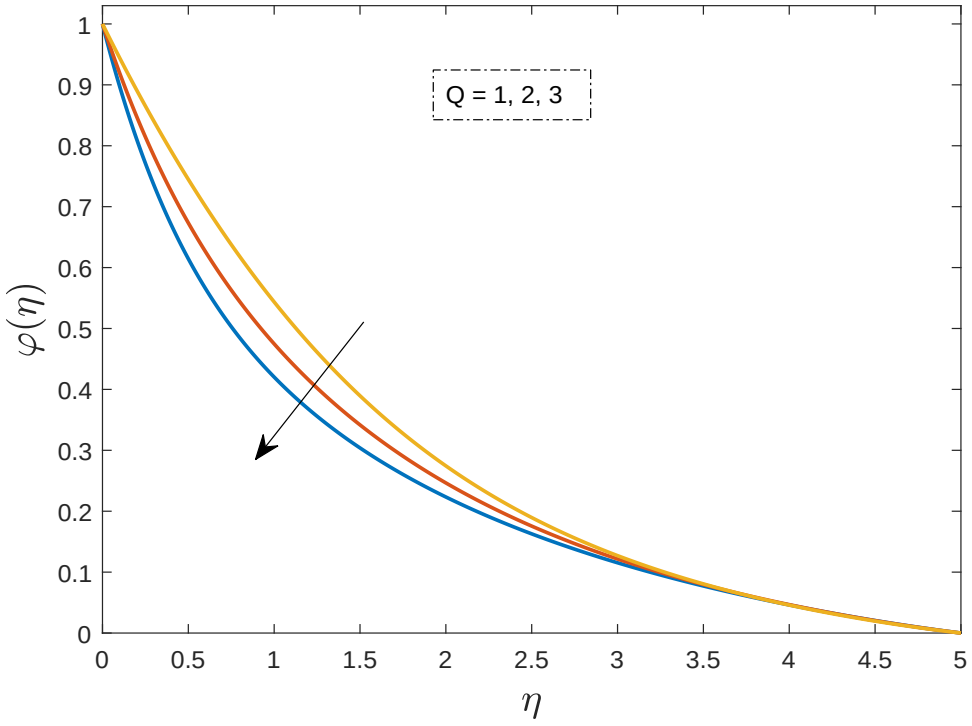

FIGURE 3.9: The effect of Q is plotted against η on nanoparticles concentration profile for different values.

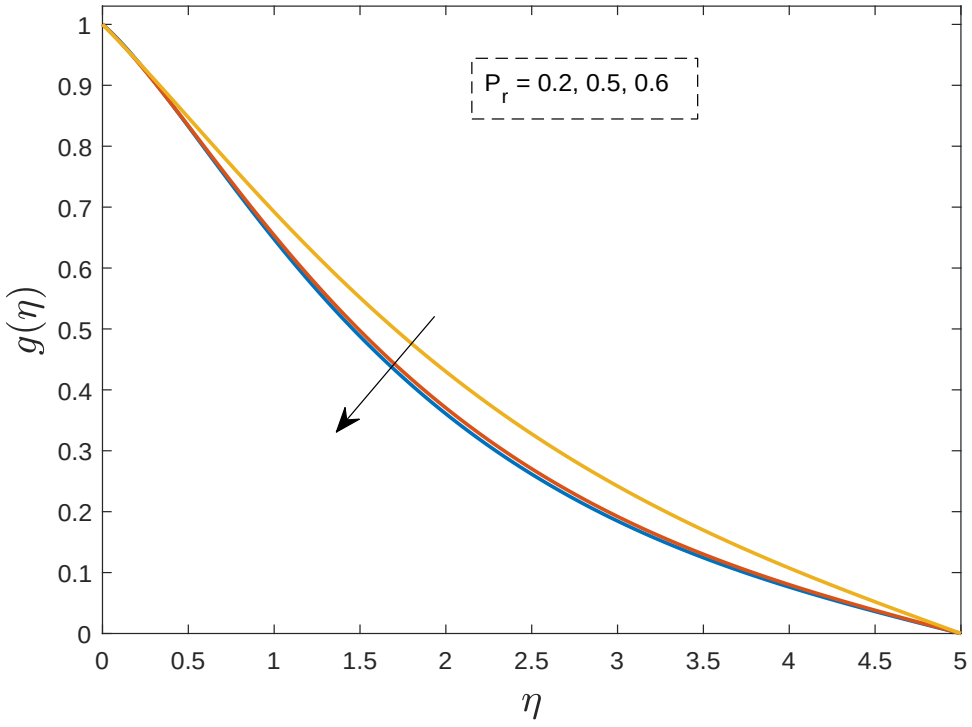

FIGURE 3.10: The effect of P_r is plotted against η on temperature profile for different values.

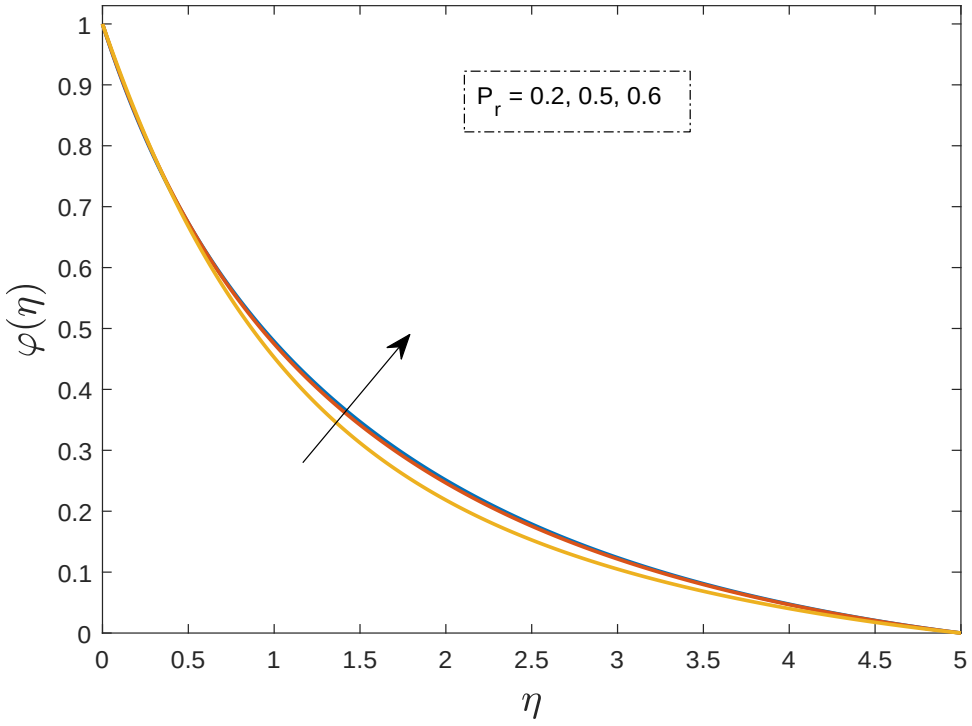

FIGURE 3.11: The effect of P_r is plotted against η on nanoparticles concentration profile for different values.

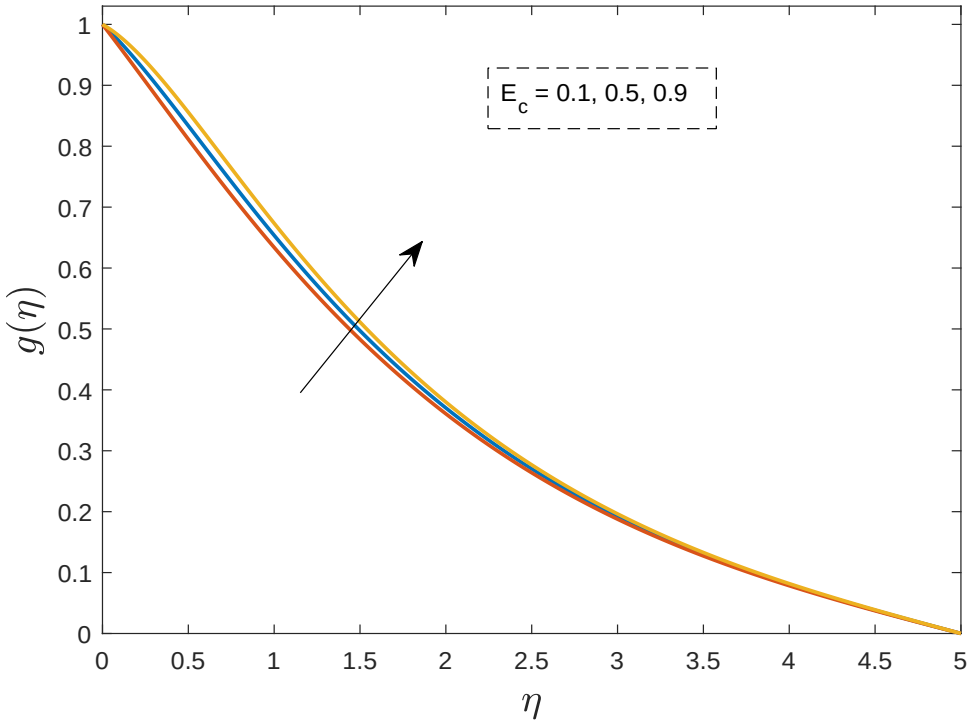

FIGURE 3.12: The effect of E_c is plotted against η on temperature profile for different values.

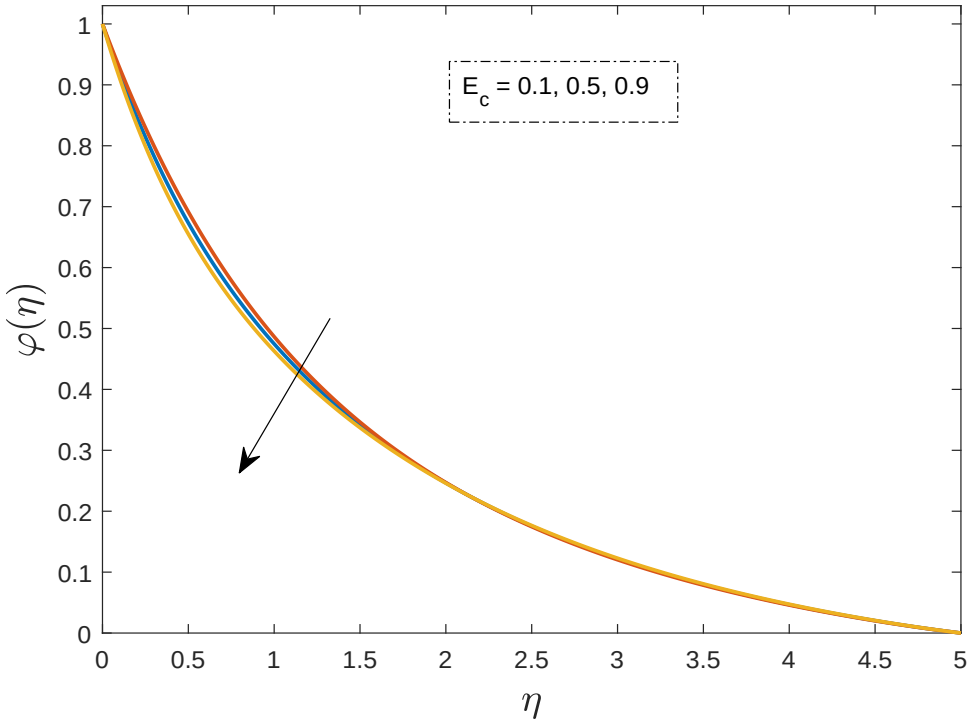

FIGURE 3.13: The effect of E_c is plotted against η on nanoparticles concentration profile.

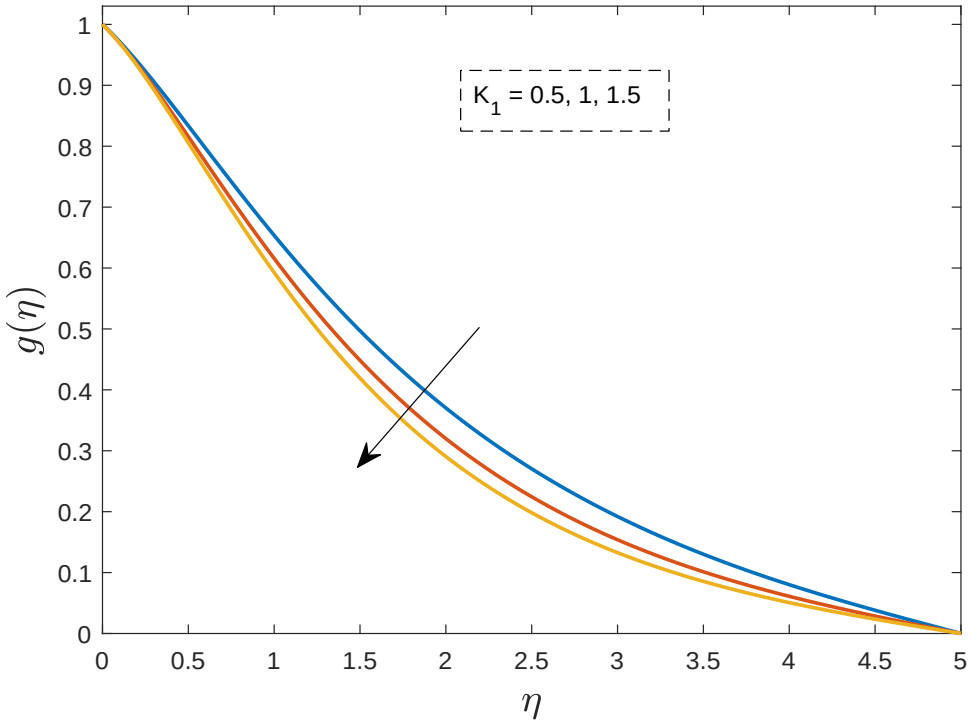

FIGURE 3.14: The effect of K_1 is plotted against η on temperature profile for different values.

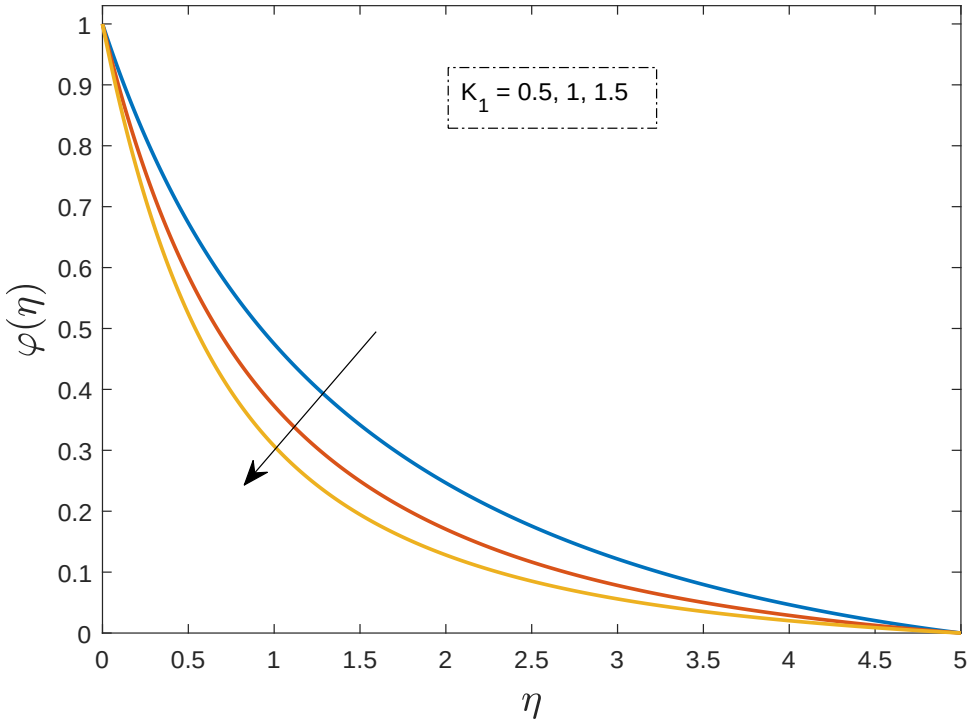

FIGURE 3.15: The effect of K_1 is plotted against η on nanoparticles concentration profile for different values.

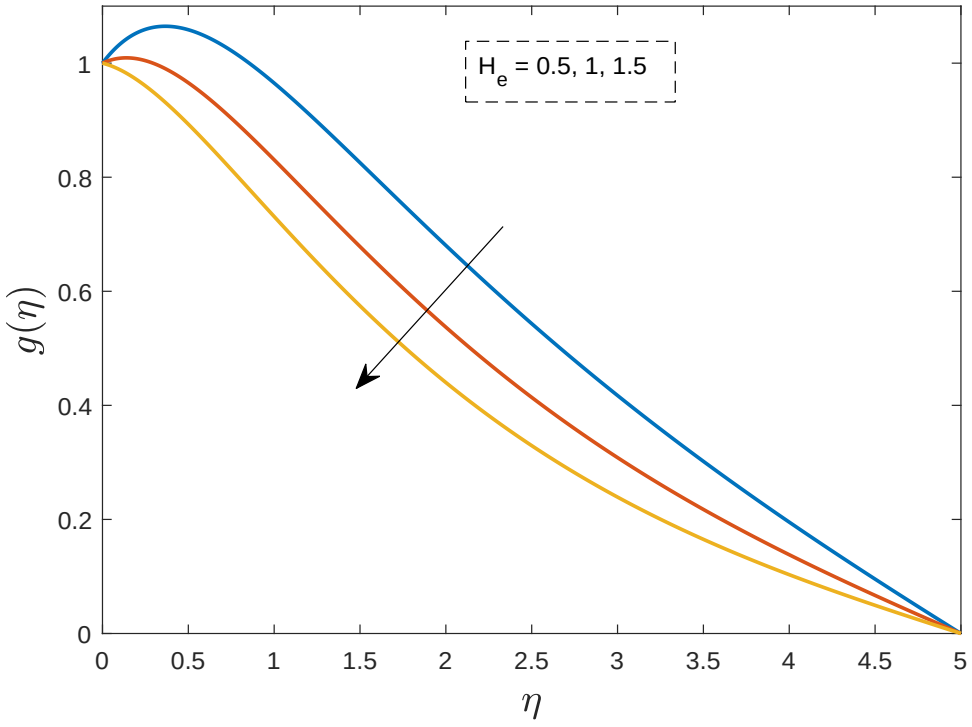

FIGURE 3.16: The effect of H_e is plotted against η on temperature profile for different values.

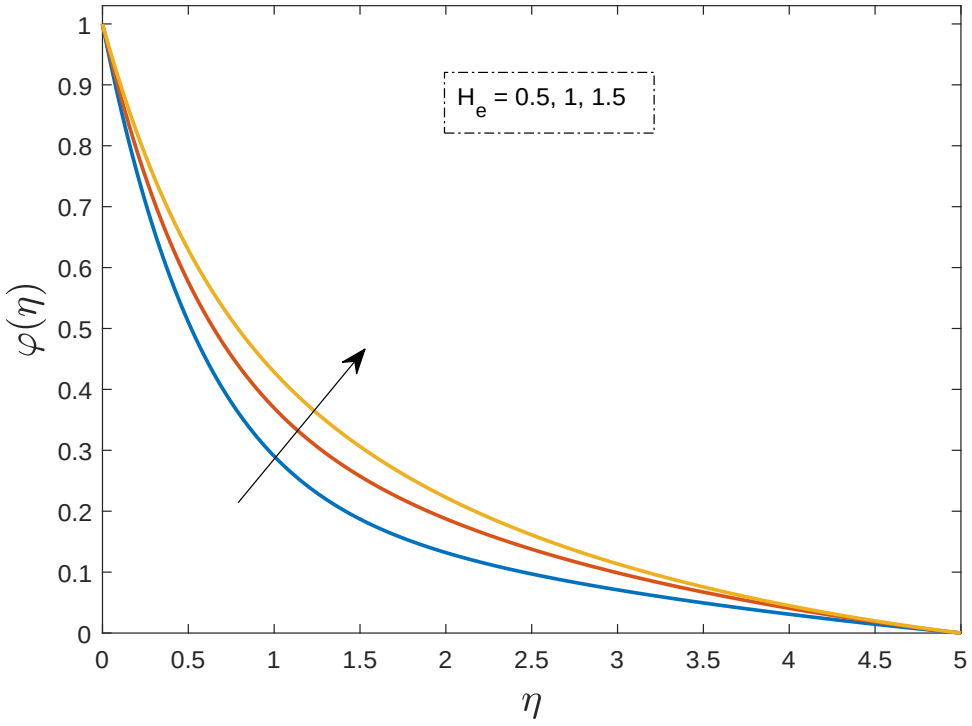

FIGURE 3.17: The effect of H_e is plotted against η on nanoparticles concentration profile for different values.

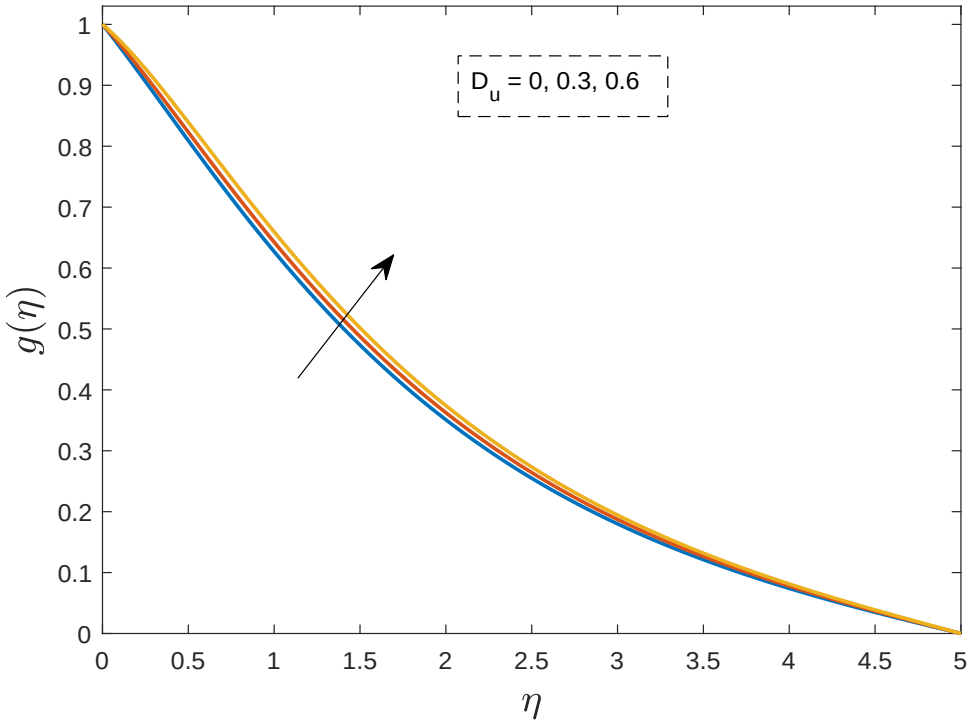

FIGURE 3.18: The effect of D_u is plotted against η on temperature profile for different values.

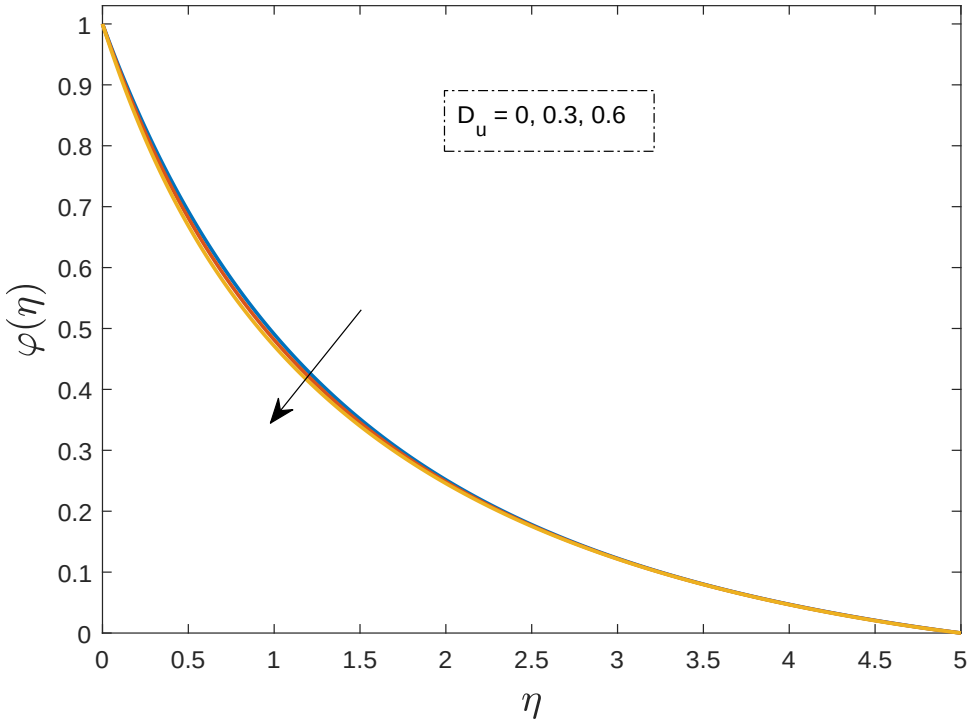

FIGURE 3.19: The effect of D_u is plotted against η on nanoparticles concentration profile for different values.

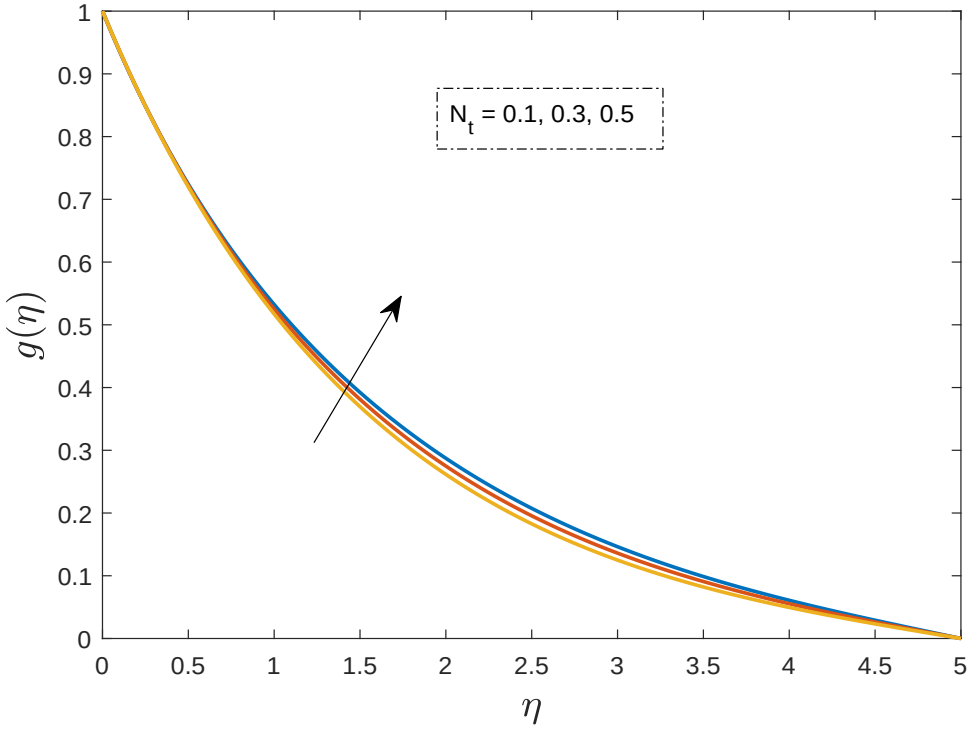

FIGURE 3.20: The effect of N_t is plotted against η on temperature profile for different values.

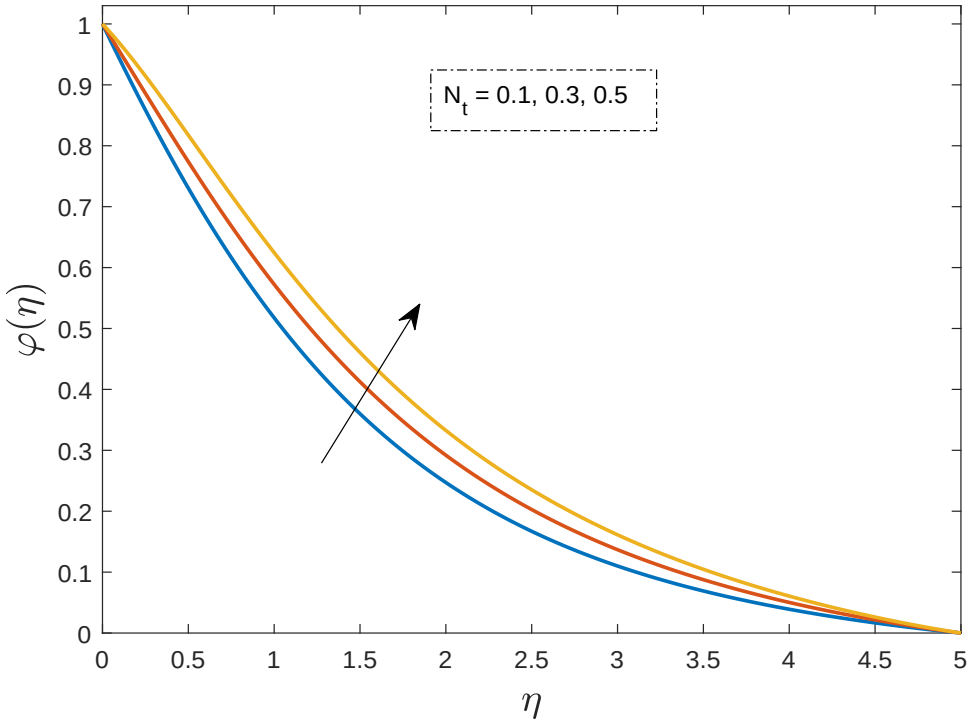

FIGURE 3.21: The effect of N_t is plotted against η on nanoparticles concentration profile.

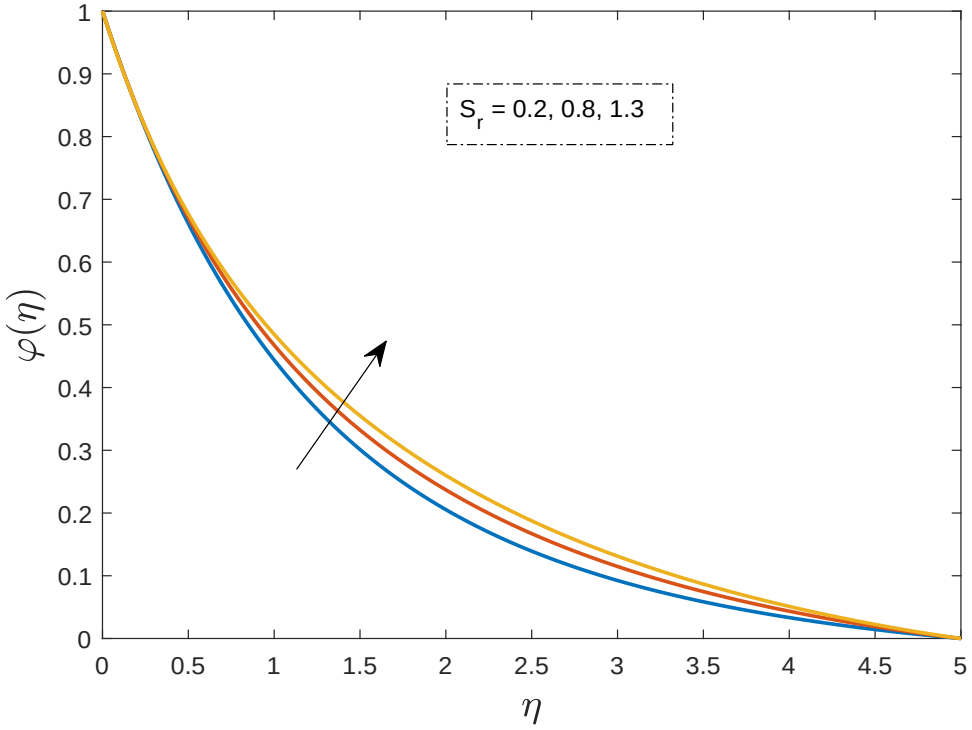

FIGURE 3.22: The effect of S_r is plotted against η on nanoparticles concentration profile for different values.

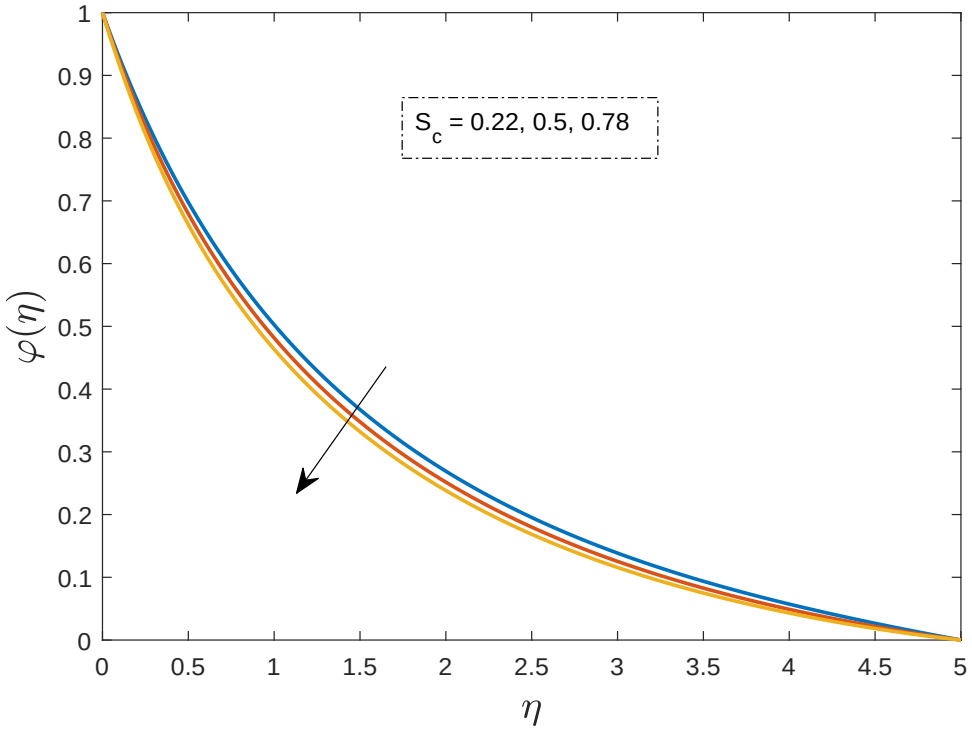

FIGURE 3.23: The effect of S_c is plotted against η on nanoparticles concentration profile for different values.

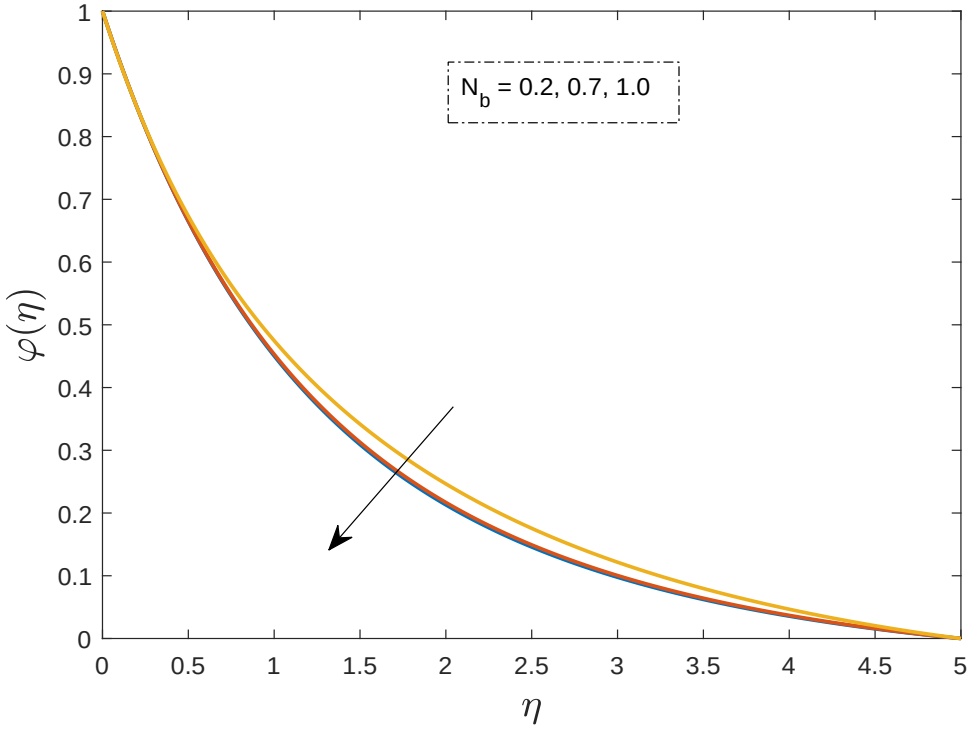

FIGURE 3.24: The effect of N_b is plotted against η on nanoparticles concentration profile.

Chapter 4

MHD Stagnation Point Flow with Effect of Inclined Magnetic Field, Joule Heating and Thermal Radiation

In the modern industry, the analysis of MHD stagnation point flow has been investigated by many researchers due to its many applications. This chapter comprises the solution for boundary layer stagnation point flow over stretching sheet with influence of thermal radiation and inclined magnetic field with Joule heating taking into account. Non-linear partial differential equations for the conservation of mass, momentum and concentration are converted into the ordinary differential equation by utilizing appropriate similarity transformation. Numerical solution of these ordinary differential equations is attained by manipulating shooting technique together with RK4 scheme. Eventually the results are discussed for different parameters affecting the flow fluid and heat transfer. Impact of distinct physical parameters across dimensionless temperature, concentration and velocity profiles are illustrated by graphs. The numerical values of skin friction coefficient, Nusselt number and Sherwood number are computed in tabular form.

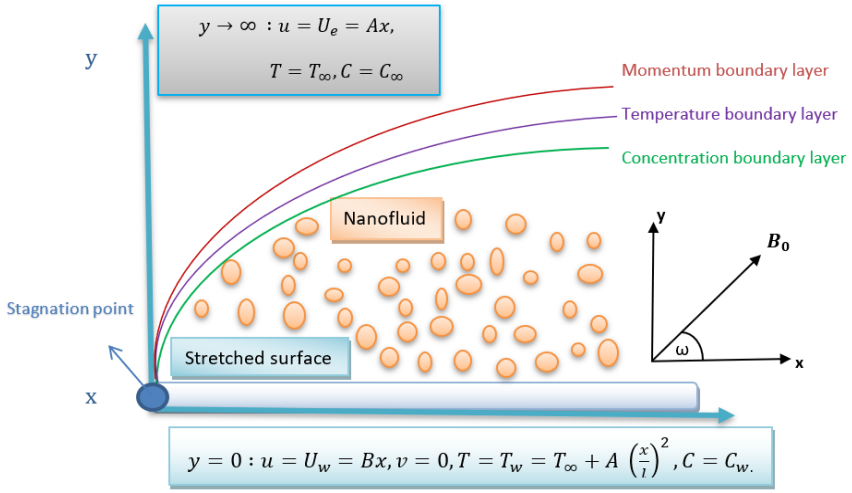

FIGURE 4.1: Schematic diagram of the physical model

4.1 Mathematical Modeling

Consider the laminar, two dimensional steady and incompressible MHD stagnation point flow of a fluid with inclined magnetic field and thermal radiation over a stretching sheet through porous medium. This sheet is placed in the plane $y = 0$, such that $y-$axis is normal and perpendicular to the sheet. The flow of nanofluid is constrained to the surface $y > 0$, the origin is kept fixed while the sheet is stretching with velocity $u = U_w = Bx$ and $U_e = Ax$ is the free stream velocity where B and A are two positive constants. The inclined magnetic field is applied to the sheet with an acute angle ω, $(0 \leq \omega \leq \frac{\pi}{2})$. Moreover, the direction of uniform magnetic field is chosen in such a manner that it is normal and perpendicular to the surface of the fluid flow. The nanoparticles concentration is C_w and for $y \to \infty$, the ambient temperature of fluid is T_∞ and ambient concentration of fluid is C_∞. Under the light of above assumptions, the governing equations are described as:

$$\frac{\partial u}{\partial x} + \frac{\partial v}{\partial y} = 0, \tag{4.1}$$

$$u\frac{\partial u}{\partial x} + v\frac{\partial u}{\partial y} = \frac{\mu_{nf}}{\rho_{nf}}\frac{\partial^2 u}{\partial y^2} + \sqrt{2}\frac{\mu_{nf}}{\rho_{nf}}\Gamma\frac{\partial u}{\partial y}\frac{\partial^2 u}{\partial y^2} - \frac{\mu_{nf}}{\rho_{nf}k_p}(U_e - u) + U_e\frac{\partial U_e}{\partial x}$$

$$+\frac{\sigma B_0^2}{\rho_{nf}}(U_e-u)\sin^2\omega, \tag{4.2}$$

$$\begin{aligned} u\frac{\partial T}{\partial x}+v\frac{\partial T}{\partial y} &= \alpha_{nf}\frac{\partial^2 T}{\partial y^2}+\frac{\mu_{nf}}{(\rho C_p)_{nf}}\left(\frac{\partial u}{\partial y}\right)^2+\frac{1}{\sqrt{2}}\frac{\mu_{nf}}{(\rho C_p)_{nf}}\Gamma\left(\frac{\partial u}{\partial y}\right)^3 \\ &+\frac{(\rho C_p)_f}{(\rho C_p)_{nf}}\left[D_B\frac{\partial C}{\partial y}\frac{\partial T}{\partial y}+\frac{D_T}{T_\infty}\left(\frac{\partial T}{\partial y}\right)^2\right] \\ &-\frac{1}{(\rho C_p)_{nf}}\frac{\partial q_r}{\partial y}+\frac{\sigma B_0^2}{(\rho C_p)_{nf}}(U_e-u)^2\sin^2\omega, \end{aligned} \tag{4.3}$$

$$u\frac{\partial C}{\partial x}+v\frac{\partial C}{\partial y}=D_B\frac{\partial^2 C}{\partial y^2}+\frac{D_T}{T_\infty}\frac{\partial^2 T}{\partial y^2}-k_1(C-C_\infty). \tag{4.4}$$

The associated boundary conditions are:

$$\left.\begin{aligned} &u=U_w=Bx,\ v=0,\ U_e=Ax,\ T=T_w=T_\infty \\ &+A\left(\frac{x}{l}\right),\ C=C_w,\ \text{at } y=0, \\ &u\to U_\infty,\ T\to T_\infty,\ C=C_\infty,\ \text{as } y\to\ \infty. \end{aligned}\right\} \tag{4.5}$$

In 1904, Ludwig prandtl first defined the aerodynamic boundary layer at the third International Congress of Mathematician in Heidleberg Germany. After that one of his student Henry Blasius presented the boundary layer approximation with similarity transformation. By Boundary layer approximation theory, here we have consider those terms which have greater impact of magnitude while eliminate those who have less impact of magnitude from th well known Navier-Stokes equations. In the above equations ω denotes the inclination angle of magnetic field, and the q_r known as Rosseland radiative heat flux which can be define as

$$q_r=\frac{-4\sigma^*\partial T^4}{3k^*\partial y}. \tag{4.6}$$

In this expression k^* (absorption coefficient) and σ^* (Boltzmann constant). By applying Taylor series, the temperature difference T^4 can be expanded about T_∞ which is ambient temperature.

$$T^4=T_\infty^4+4T_\infty^3(T-T_\infty)+\frac{12T_\infty^2}{2!}(T-T_\infty)^2+\frac{24T_\infty}{3!}(T-T_\infty)^3+...$$

By ignoring the higher order terms of temperature difference because its

impact is very small, so the reduced Taylor series gets the form

$T^4 = T_\infty^4 + 4T_\infty^3(T - T_\infty)$.

then

$$\frac{\partial T^4}{\partial y} = 4T^3 \frac{\partial T}{\partial y}. \tag{4.7}$$

Using Eq. (4.7) in Eq. (4.6) and then differentiate Eq. (4.6) with respect to y,

$$\frac{\partial q_r}{\partial y} = -\frac{16\sigma^* T_\infty^3}{3k^*} \frac{\partial^2 T}{\partial y^2}. \tag{4.8}$$

By using the similarity transformation Eq. (3.17), the partial differential equations converted into ordinary differential equations. Detailed procedure for the derivation of continuity equation and left hand side of momentum equation have been already discussed in the previous Chapter. So in order to derive the right hand side of Eq. (4.2) same procedure will be followed like in Chapter 3.

$$\begin{aligned} \frac{\mu_{nf}}{\rho_{nf}} \frac{\partial^2 u}{\partial y^2} &= \frac{\mu_{nf}}{\rho_{nf}} \frac{\partial}{\partial y}(Bxf''(\eta)) \sqrt{\frac{B}{\nu_f}}, \\ &= \frac{\mu_{nf}}{\rho_{nf}} \frac{B^2 x}{\nu_f} f'''. \end{aligned} \tag{4.9}$$

$$\begin{aligned} \sqrt{2}\frac{\mu_{nf}}{\rho_{nf}} \Gamma \frac{\partial u}{\partial y} \frac{\partial^2 u}{\partial y^2} &= \sqrt{2}\frac{\mu_{nf}}{\rho_{nf}} \Gamma \left(Bxf'' \sqrt{\frac{B}{\nu_f}} \right) \left(\frac{B^2 x}{\nu_f} f''' \right), \\ &= \sqrt{2}\frac{\mu_{nf}}{\rho_{nf}} \Gamma \frac{B^{\frac{7}{2}} x^2}{\nu_f^{\frac{3}{2}}} f'' f'''. \end{aligned} \tag{4.10}$$

Next

$$\begin{aligned} -\frac{\mu_{nf}}{\rho_{nf} k_p}(U_e - u) &= -\frac{\mu_{nf}}{\rho_{nf} k_p}(Ax - Bxf'), \\ -\frac{\sigma B_0^2}{\rho_{nf}}(U_e - u)\sin^2\omega &= -\frac{\sigma B_0^2}{\rho_{nf}}(Ax - Bxf')\sin^2\omega. \end{aligned} \tag{4.11}$$

Similarly

$$\begin{aligned} U_e \frac{\partial U_e}{\partial x} &= Ax \frac{\partial}{\partial x}(Ax). \\ &= A^2 x. \end{aligned} \tag{4.12}$$

Substituting Eq. (3.19) and Eq. (4.9)-(4.12) in Eq. (4.2)

$$\begin{aligned} B^2x(f'^2 - ff'') = \quad & \frac{\mu_f}{(1-\phi)^{2.5}((1-\phi)\rho_f + \phi\rho_s)}\frac{B^2x}{\nu_f}\left(f''' + \sqrt{2}\Gamma f'''f''\sqrt{\frac{B^3}{\nu_f}}\right) \\ & + \frac{\mu_f}{(1-\phi)^{2.5}((1-\phi)\rho_f + \phi\rho_s)k_p}(Ax - Bxf') + A^2x \\ & + \frac{\sigma B_0^2}{(1-\phi)\rho_f + \phi\rho_s}(Ax - Bxf')\sin^2(\omega). \end{aligned} \tag{4.13}$$

Dividing B^2x on both sides of Eq. (4.13)

$$\begin{aligned} f'^2 - ff'' = \quad & \frac{\mu_{nf}}{\rho_f(1-\phi)^{2.5}((1-\phi) + \phi\frac{\rho_s}{\rho_f})}\frac{1}{\nu_f}(f''' + \lambda f'''f'') \\ & + \frac{\mu_f}{\rho_f(1-\phi)^{2.5}((1-\phi) + \phi\frac{\rho_s}{\rho_f}Bk_p)}\left(\frac{A}{B} - f'\right) + \frac{A^2}{B^2} \\ & + \frac{\sigma B_0^2 Bx}{((1-\phi)\rho_f + \phi\rho_s)B^2x}\left(\frac{A}{B} - f'\right)\sin^2(\omega), \end{aligned}$$

$$\begin{aligned} f'^2 - ff'' = \quad & \frac{1}{\phi_1}(f''' + \lambda f'''f'') + \frac{\nu_f}{\phi_1 Bxk_p}\left(\frac{A}{B} - f'\right) \\ & + \frac{A^2}{B^2} + \frac{\sigma B_0^2 x}{\rho_f\phi_2 Bx}\left(\frac{A}{B} - f'\right)\sin^2(\omega), \end{aligned} \tag{4.14}$$

$$\begin{aligned} f'^2 - ff'' = \quad & \frac{1}{\phi_1}(f''' + \lambda f'''f'') + \frac{1}{K\phi_1}(E - f') \\ & + E^2 + \frac{M}{\phi_2}(E - f')\sin^2(\omega). \end{aligned} \tag{4.15}$$

Hence the final dimensionless form is

$$f'''(1 + \lambda f'') - \phi_1\left(f'^2 - ff'' - E^2 - \frac{M}{\phi_2}(E - f')\sin^2\omega\right) + \frac{1}{K}(E - f') = 0.$$

Next converting the dimensional temperature equation into the non-dimensional form. Calculating the temperature component along x and y direction as

$$\begin{aligned} & u\frac{\partial T}{\partial x} = (Bxf'(\eta))\frac{\partial}{\partial x}\left[g(\eta)(T_w - T_\infty) + T_\infty\right], \\ & = (Bxf'(\eta))(0), \\ & = 0. \end{aligned} \tag{4.16}$$

$$\begin{aligned} v\frac{\partial T}{\partial y} &= (-\sqrt{Bv_f}f(\eta))\frac{\partial}{\partial y}\left[g(\eta)(T_w - T_\infty) + T_\infty\right], \\ &= (-\sqrt{Bv_f}f(\eta))g'(\eta)(T_w - T_\infty)\sqrt{\frac{B}{\nu_f}}, \\ &= -Bf(\eta)g'(T_w - T_\infty). \end{aligned} \tag{4.17}$$

Adding both equations (4.16) and (4.17), it becomes

$$u\frac{\partial T}{\partial x} + v\frac{\partial T}{\partial y} = -Bf(\eta)g'(T_w - T_\infty). \tag{4.18}$$

Furthermore, all expressions on the right side of temperature equation have been transformed into the dimensionless form individually as stated below:

$$\frac{\partial^2 T}{\partial y^2} = g''(T_w - T_\infty)\frac{B}{\nu_f} \tag{4.19}$$

$$\left(\frac{\partial u}{\partial y}\right)^2 = \frac{B^3x^2}{\nu_f}f''^2 \tag{4.20}$$

$$\frac{\partial C}{\partial y}.\frac{\partial T}{\partial y} = \frac{B}{\nu_f}(T_w - T_\infty)(C_w - C_\infty)\varphi' g' \tag{4.21}$$

$$\left(\frac{\partial u}{\partial y}\right)^3 = \frac{B^{\frac{9}{2}}x^3}{\nu_f^{\frac{3}{2}}}f''^3 \tag{4.22}$$

$$\left(\frac{\partial T}{\partial y}\right)^2 = g'^2(T_w - T_\infty)^2\frac{B}{\nu_f} \tag{4.23}$$

$$(u - U_e)^2 = (Bxf' - Ax)^2 \tag{4.24}$$

$$\frac{\partial q_r}{\partial y} = \frac{-16\sigma^*}{3k^*}T_\infty^3 g''(T_w - T_\infty)\frac{B}{\nu_f} \tag{4.25}$$

Substituting all these equations (4.19)-(4.25) in the right hand side

$$\begin{aligned} = \; & \alpha_{nf}g''(T_w - T_\infty)\frac{B}{\nu_f} + \frac{\mu_{nf}}{(\rho C_p)_{nf}}\frac{B^3x^2}{\nu_f}f''^2 + \frac{1}{\sqrt{2}}\frac{\mu_{nf}}{(\rho C_p)_{nf}}\Gamma\frac{B^{\frac{9}{2}}x^3}{\nu_f^{\frac{3}{2}}}f''^3 \\ & + \frac{(\rho C_p)_f}{(\rho C_p)_{nf}}\left(D_B\frac{B}{\nu_f}(T_w - T_\infty)(C_w - C_\infty)\varphi' g' + \frac{D_T}{T_\infty}g'^2(T_w - T_\infty)^2\frac{B}{\nu_f}\right) \\ & + \frac{\sigma B_0^2}{(\rho C_p)_{nf}}\sin^2\omega(Bxf' - Ax)^2 - \frac{1}{(\rho C_p)_{nf}}\frac{-16\sigma^*}{3k^*}T_\infty^3 g''(T_w - T_\infty)\frac{B}{\nu_f}. \end{aligned}$$

Combining both left hand side and right hand side

$$
\begin{aligned}
-Bf(\eta)g'(T_w-T_\infty) &= \alpha_{nf}g''(T_w-T_\infty)\frac{B}{\nu_f}+\frac{\mu_{nf}}{(\rho C_p)_{nf}}\frac{B^3x^2}{\nu_f}f'''^2 \\
&+\frac{1}{\sqrt{2}}\frac{\mu_{nf}}{(\rho C_p)_{nf}}\Gamma\frac{B^{\frac{9}{2}}x^3}{\nu_f^{\frac{3}{2}}}f'''^3+\frac{(\rho C_p)_f}{(\rho C_p)_{nf}}\left(D_B\frac{B}{\nu_f}\right. \\
&\left.(T_w-T_\infty)(C_w-C_\infty)\varphi'g'+\frac{D_T}{T_\infty}g'^2(T_w-T_\infty)^2\frac{B}{\nu_f}\right) \\
&+\frac{\sigma B_0^2}{(\rho C_p)_{nf}}\sin^2\omega(Bxf'-Ax)^2 \\
&-\frac{1}{(\rho C_p)_{nf}}\frac{-16\sigma^*}{3k^*}T_\infty^3g''(T_w-T_\infty)\frac{B}{\nu_f}.
\end{aligned}
$$

Dividing this term $B(T_w-T_\infty)$ on both sides

$$
\begin{aligned}
-f(\eta)g'(\eta) &= \alpha_{nf}g''\frac{1}{\nu_f}+\frac{\mu_{nf}}{(\rho C_p)_{nf}}\frac{B^2x^2}{\nu_f(T_w-T_\infty)}f'''^2 \\
&+\frac{2\Gamma}{2\sqrt{2}}\frac{\mu_{nf}}{(\rho C_p)_{nf}}\frac{B^{\frac{7}{2}}x^3}{\nu_f^{\frac{3}{2}}(T_w-T_\infty)}f'''^3 \\
&+\frac{(\rho C_p)_f}{(\rho C_p)_{nf}}\left(D_B\frac{1}{\nu_f}(C_w-C_\infty)\varphi'g'+\frac{D_T}{T_\infty}g'^2(T_w-T_\infty)\frac{1}{\nu_f}\right) \\
&+\frac{\sigma B_0^2x^2}{(\rho C_p)_{nf}B(T_w-T_\infty)}\sin^2\omega(Bf'-A)^2 \\
&-\frac{1}{(\rho C_p)_{nf}}\frac{-16\sigma^*T_\infty^3}{3k^*\nu_f}g''.
\end{aligned}
$$

Multiplying both sides with $\frac{(\rho C_p)_{nf}}{\rho C_p)_f}$

$$
\begin{aligned}
-f(\eta)g'(\eta)\frac{(\rho C_p)_{nf}}{(\rho C_p)_f} &= \frac{k_{nf}}{k_f}\frac{k_f\rho_f}{\mu_f(\rho C_p)_f}g''+\frac{\mu_{nf}}{(\rho C_p)_{nf}}\frac{(\rho C_p)_{nf}}{(\rho C_p)_f}\left(\frac{B^2x^2}{\nu_f(T_w-T_\infty)}f'''^2\right. \\
&\left.+\frac{\Gamma}{2}\frac{\sqrt{2B^3}\nu_fx}{(T_w-T_\infty)}f'''^3\right)+\frac{(\rho C_p)_{nf}}{(\rho C_p)_f}\frac{(\rho C_p)_f}{(\rho C_p)_{nf}}\left(D_B\frac{1}{\nu_f}\right. \\
&\left.(C_w-C_\infty)\phi'g'+\frac{D_T}{T_\infty}g'^2(T_w-T_\infty)\frac{1}{\nu_f}\right) \\
&+\frac{(\rho C_p)_{nf}}{(\rho C_p)_f}\frac{\sigma B_0^2x^2}{(\rho C_p)_{nf}B(T_w-T_\infty)}\sin^2\omega(f'-E)^2 \\
&-\frac{(\rho C_p)_{nf}}{(\rho C_p)_f}\frac{1}{(\rho C_p)_{nf}}\frac{-16\sigma^*T_\infty^3}{3k^*\nu_f}g''.
\end{aligned}
$$

Using dimensionless constants

$$
-\phi_3fg' = \frac{k_{nf}}{k_f}g''+\frac{\phi_3}{\phi_4}E_c(f'''^2+\frac{\lambda}{2}f'''^3)+\phi_3(N_b\varphi'g'
$$

$$+N_t g'^2) + ME_c(f' - E)^2 \sin^2\omega + \frac{4R}{3P_r} g''.$$

Hence the non-dimensional form of Eqn. (4.3)

$$g''\left(\frac{k_{nf}}{k_f} + \frac{4}{3}R\right) + \phi_3 P_r\left(fg' + f''^2\frac{E_c}{\phi_4} + f''^3\frac{\lambda E_c}{2\phi_4} + N_b\varphi' g' + N_t g'^2\right)$$
$$+ME_c P_r(f' - E)^2\sin^2\omega = 0. \tag{4.26}$$

Next, we include the procedure for the conversion of (4.4) into the dimensionless form. The left hand side of Eq. (4.4) into the dimensionless form is similar to that discussed in Chapter 3. To convert the right side of concentration equation into the dimensionless form, steps proceed as follows:

$$\begin{aligned} D_B\frac{\partial^2 C}{\partial y^2} &= D_B\frac{\partial}{\partial y}\left(\varphi'(\eta)(C_w - C_\infty)\sqrt{\frac{B}{\nu_f}}\right), \\ &= D_B\varphi''(\eta)(C_w - C_\infty)\frac{b}{\nu_f}. \qquad (4.27) \\ \frac{D_T}{T_\infty}\frac{\partial^2 T}{\partial y^2} &= \frac{D_T}{T_\infty}\frac{\partial^2}{\partial y^2}(g(\eta)(T_w - T_\infty) + T_\infty), \\ &= \frac{D_T}{T_\infty}g''(\eta)(T_w - T_\infty)\frac{B}{\nu_f}. \qquad (4.28) \\ -k_1(C - C_\infty) &= -k_1(\varphi(\eta)(C_w - C_\infty) + C_\infty - C_\infty), \\ &= -k_1\varphi(\eta)(C_w - C_\infty). \qquad (4.29) \end{aligned}$$

Using (4.27)-(4.29) in the right side of concentration equation,

$$D_B\frac{\partial^2 C}{\partial y^2} + \frac{D_T}{T_\infty}\frac{\partial^2 T}{\partial y^2} - k_1(C - C_\infty) = \quad D_B\varphi''(\eta)(C_w - C_\infty)\frac{B}{\nu_f} + \frac{D_T}{T_\infty}g''(\eta)$$
$$(T_w - T_\infty)\frac{B}{\nu_f} - k_1\varphi(\eta)(C_w - C_\infty).$$

Therefore the dimensionless form of (4.4) becomes:

$$\begin{aligned} -Bf(\eta)\varphi'(\eta)(C_w - C_\infty) &= D_B\varphi''(\eta)(C_w - C_\infty)\frac{B}{v_f} + \frac{D_T}{T_\infty}g''(\eta)(T_w - T_\infty)\frac{B}{v_f} \\ &\quad -k_1\varphi(\eta)(C_w - C_\infty). \\ -f(\eta)\varphi'(\eta) &= D_B\varphi''(\eta)\frac{1}{v_f} + \frac{D_T}{T_\infty}g''(\eta)\frac{(T_w - T_\infty)}{(C_w - C_\infty)}\frac{1}{v_f} - \frac{k_1}{B}\varphi(\eta). \end{aligned}$$

Multiplying each term by $\frac{\nu_f}{D_B}$

$$-\frac{\nu_f}{D_B}f(\eta)\varphi'(\eta) = \varphi''(\eta) + \frac{D_T}{D_B T_\infty}g''(\eta)\frac{(T_w - T_\infty)}{(C_w - C_\infty)} - \frac{k_1\nu_f}{BD_B}\varphi(\eta).$$

Hence the required equation of concentration is

$$\varphi''(\eta) + S_c\varphi'(\eta)f(\eta) + \frac{N_t}{N_b}g''(\eta) - K_1\varphi(\eta) = 0. \tag{4.30}$$

Now for converting the extended associated boundary conditions into the dimensionless form, the following steps have been implemented as:

$$\begin{aligned}
&u \to U_e, \qquad \text{at} \quad y \to \infty,\\
&\Rightarrow Bxf'(\eta) \to Ax, \qquad \text{at} \quad \eta = 0,\\
&\Rightarrow \frac{Bx}{Bx}f'(\eta) \to \frac{Ax}{Bx}, \qquad \text{at} \quad \eta = 0,\\
&\Rightarrow f'(0) \to \frac{A}{B},\\
&\Rightarrow f'(0) \to E.
\end{aligned}$$

The final non-dimensional form of the governing equation is:

$$\begin{aligned}
&f'''(1+\lambda f'') - \phi_1\left(f'^2 - ff'' + \frac{M}{\phi_2}(E - f')\sin^2\omega\right)\\
&-\frac{1}{K}(E - f') = 0,
\end{aligned} \tag{4.31}$$

$$\begin{aligned}
&g''\left(K_0 + \frac{4}{3}R\right) + \phi_3 P_r\left(fg' + f''^2\frac{E_c}{\phi_4} + f''^3\frac{\lambda E_c}{2\phi_4} + N_b\varphi' g' + N_t g'^2\right)\\
&+ME_cP_r(f' - E)^2\sin^2\omega = 0,
\end{aligned} \tag{4.32}$$

$$\varphi''(\eta) + S_c\varphi'(\eta)f(\eta) + \frac{N_t}{N_b}g''(\eta) - K_1\varphi(\eta) = 0. \tag{4.33}$$

The transformed boundary conditions (4.5) formulated as:

$$\left.\begin{aligned}
&f(0) = 0,\ f'(0) = 1,\ g(0) = 1,\ \varphi(0) = 1,\\
&f'(\infty) \to E,\ g(\infty) \to 0,\ \varphi(\infty) \to 0.
\end{aligned}\right\} \tag{4.34}$$

In the above equations the dimensionless quantities are formulated as:

$E = \frac{A}{B}$, (Stretching ratio parameter)

$R = \frac{4\sigma^* T_\infty^3}{k^* k}$, (Thermal radiation parameter)

$M = \frac{x\sigma B_0^2}{U_w \rho_f}$, (Magnetic parameter)

$\lambda = \Gamma x \sqrt{\frac{2B^3}{\nu_f}}$, (Non-Newtonian parameter)

$N_b = \frac{D_B}{\nu_f}(C_w - C_\infty)$, (Brownian motion parameter)

$N_t = \frac{D_T}{\nu_f T_\infty}$, (Thermopheroesis parameter)

$E_c = \frac{U_w^2}{(T_w - T_\infty)(C_p)_f}$, (Eckert number)

$S_c = \frac{\nu_f}{D_B}$, (Schmidt parameter)

$K_1 = \frac{k_p \nu_f}{B D_B}$, (Chemical reaction parameter)

The values of fluid properties 3.16 and nanoparticles volume fraction 3.33 are identical in this Chapter.

4.2 Numerical Technique

To obtain the numerical solution for the system of ordinary differential equations (4.31)- (4.33) subject to boundary conditions Eq. (4.34), shooting method is used. First, the momentum equation is solved independently. Following notations have been considered for further procedure:

$$f = h_1$$
$$f' = h_1' = h_2$$
$$f'' = h_2' = h_3$$
$$f''' = h_1''' = h_2'' = h_3'$$

Rewriting these representation with boundary conditions, we acquire the system of first order ordinary differential equations:

$$h_1' = h_2, \qquad h_1(0) = 0,$$
$$h_2' = h_3, \qquad h_2(0) = 1,$$

$$h_3' = \frac{1}{(1+\lambda h_3)}\Bigg[\phi_1(h_2^2 - h_1h_3 - E^2 - \frac{M}{\phi_2}\sin^2\omega(E-h_2)) \\ - \frac{1}{K}(E-h_2)\Bigg], \qquad h_3(0) = \alpha$$

Differentiating with respect to α,

$$\frac{\partial f}{\partial \alpha} = h_4$$
$$\frac{\partial f'}{\partial \alpha} = h_5$$
$$\frac{f''}{\partial \alpha} = h_6$$

Similarly,

$$h_4' = h_5, \qquad h_4(0) = 0$$
$$h_5' = h_6, \qquad h_5(0) = 0$$
$$h_6' = \frac{1}{(1+\lambda h_3)^2}\Bigg[\phi_1(2h_2h_5 - h_4h_3 - h_1h_6 - E^2 - \frac{M}{\phi_2}\sin^2\omega(E-h_2)) \\ - (\phi_1(h_2^2 - h_1h_3 - E^2 + \frac{M}{\phi_2}sin^2\omega) - \frac{1}{K}(E-h_2))\Bigg] \\ - \frac{1}{K}(E-h_2)\Bigg], \qquad h_6(0) = 1$$

The above IVP has been tackled by using the RK4 method and their missing condition is α. The Newton's scheme is given by the following iterative scheme

$$\alpha^{(n+1)} = \alpha^{(n)} - \frac{(h_2(\eta_\infty)) - E}{\frac{\partial(h_2(\eta_\infty - E))}{\partial \alpha}},$$

$$\alpha^{(n+1)} = \alpha^{(n)} - \frac{(h_2(\eta_\infty)) - E}{(h_5(\eta_\infty))}, \ n = 0, 1, 2, 3...$$

To execute the numerical procedure, the problem domain was taken as $[0, 1]$. An asymptotic convergence of the numerical results is observed by enlarging the value of η_∞. For the shooting method, the stoping criteria is defined as follows

$$|(h_2(\eta_\infty) - E)| < \epsilon,$$

where ϵ is a small positive real number.

To numerically solve the coupled equations, the missing initial condition at $g(0)$ is β and $\varphi(0)$ is ξ. The following representation are considered:

$$\left.\begin{aligned} g = H_1,\ g' = H_2,\ \varphi = H_3,\ \varphi' = H_4,\ \frac{\partial g}{\partial q} = H_5,\ \frac{\partial g'}{\partial q} = H_6,\ \frac{\partial \varphi}{\partial q} = H_7, \\ \frac{\partial \varphi'}{\partial q} = H_8,\ \frac{\partial g}{\partial r} = H_9,\ \frac{\partial g'}{\partial r} = H_{10},\ \frac{\partial \varphi}{\partial r} = H_{11},\ \frac{\partial \varphi'}{\partial r} = H_{12} \end{aligned}\right\} \quad (4.35)$$

Using these notations, we obtain a system of first order ordinary differential equations which are given below

$$H_1' = H_2, \qquad H_1(0) = 1,$$

$$H_2' = \frac{1}{\left(\frac{k_{nf}}{k_f} + \frac{4R}{3}\right)}\left[-\phi_3 P_r\left(h_1 H_2 - + h_3^2\left(\frac{E_c}{\phi_4}\right) + h_3^3\left(\frac{\lambda E_c}{2\phi_4}\right)\right.\right.$$

$$\left.\left. + N_b H_2 H_4 + N_t H_2^2\right) - E_c M P_r (h_2 - E)^2 \sin^2(\omega)\right], \qquad H_2(0) = \beta,$$

$$H_3' = H_4, \qquad H_3(0) = 1,$$

$$H_4' = -S_c h_1 H_4 + \frac{\left(\frac{N_t}{N_b}\right)}{\left(\frac{k_{nf}}{k_f} + \frac{4R}{3}\right)}\left[-\phi_3 P_r\left(h_1 H_2 - + h_3^2\left(\frac{E_c}{\phi_4}\right) + h_3^3\right.\right.$$

$$\left.\left.\left(\frac{\lambda E_c}{2\phi_4}\right) + N_b H_2 H_4 + N_t H_2^2\right) - E_c M P_r (h_2 - E)^2 \sin^2(\omega)\right] + K_1 H_3, \quad H_4(0) = \xi,$$

$$H_5' = H_6, \qquad H_5(0) = 0,$$

$$H_6' = \frac{1}{\left(\frac{k_{nf}}{k_f} + \frac{4R}{3}\right)}\left[-\phi_3\left\{h_1 H_6 + N_b(H_6 H_4 + H_2 H_8)\right\}\right.$$

$$\left. + N_t(2H_2 H_6)\right], \qquad H_6(0) = 1,$$

$$H_7' = H_8, \qquad H_7(0) = 0,$$

$$H_8' = -S_c h_1 H_8 + \frac{\left(\frac{N_t}{N_b}\right)}{\left(\frac{k_{nf}}{k_f} + \frac{4R}{3}\right)}\left[-\phi_3\left(h_1 H_6 + N_b(H_6 H_4 + H_2 H_8) + \right.\right.$$

$$\left.\left. N_t(2H_2 H_6)\right) + K_1 H_7\right], \qquad H_8(0) = 0,$$

$$H_9' = H_{10}, \qquad H_9(0) = 0,$$

$$H_{10}' = \frac{1}{\left(\frac{k_{nf}}{k_f} + \frac{4R}{3}\right)}\left[-\phi_3\left\{h_1 H_{10} + N_b(H_{10} H_4 + H_2 H_{11})\right\}\right.$$

$$\left. + N_t(2H_2 H_{10})\right], \qquad H_{10}(0) = 0,$$

$$H_{11}' = H_{12}, \qquad H_{11}(0) = 0,$$

$$H_{12}' = -S_c h_1 H_{12} + \frac{\left(\frac{N_t}{N_b}\right)}{\left(\frac{k_{nf}}{k_f} + \frac{4R}{3}\right)} \left[-\phi_3 \left\{h_1 H_{10} + N_b(H_{10}H_4 + H_2 H_{12}) + \right.\right.$$

$$\left.\left. N_t(2H_2 H_{10})\right\}\right] K_1 H_{11}, \qquad H_{12}(0) = 1.$$

The RK4 scheme has been adopted for tackling the above initial value problem. To get the approximate solution, the domain of the problem has been taken as $[0, \eta_\infty]$ instead of $[0, \infty)$, where η_∞ is an appropriate finite positive real number. The missing conditions β and ξ in the above system of equations, are to be chosen such that

$$H_2(\eta_\infty, \beta, \xi) = 0, \quad H_4(\eta_\infty, \beta, \xi) = 0$$

For the improvement of the missing condition, Newton's method has been implemented which is conducted by the following iterative scheme:

$$\begin{bmatrix} \beta^{(n+1)} \\ \xi^{(n+1)} \end{bmatrix} = \begin{bmatrix} \beta^{(n)} \\ \xi^{(n)} \end{bmatrix} - \begin{bmatrix} H_5 & H_9 \\ H_7 & H_{11} \end{bmatrix}^{-1} \begin{bmatrix} H_1 \\ H_3 \end{bmatrix}_{(\beta^{(n)}, \xi^{(n)}, \eta_\infty)}$$

The following steps are involved for the accomplishment of the shooting method.

1. Choice of the guesses $\beta = \beta^{(0)}$ and $\xi = \xi^{(0)}$.
2. Choice of a positive small number ϵ. If $max(|H_1(\eta_\infty)|,\ |H_3(\eta_\infty)|) < \epsilon$, come to end the procedure or else go to 3.
3. Compute the $\beta^{(n+1)}$ and $\xi^{(n+1)}$, $n = 0, 1, 2, 3....$
4. Repeat 1 and 2 until the values of β and ξ are within the specified degree of accuracy.

4.3 Graphical Results

The aim of this section is to analyze the numerical results of velocity, temperature and concentration profile with the help of graphs and table by using different parameters.

4.3.1 Skin Friction Coefficient, Nusselt Number and Sherwood Number

P_r	R	S_c	N_t	M	$-(f''(0)+\frac{\lambda}{2}f''^2(0))$	$-g'(0)$	$-\varphi'(0)$
6.2	0.5	10	0.1	0.1	0.7774	1.1585	2.9579
4					0.7774	1.0064	2.9930
7					0.7774	1.1922	2.9546
9					0.7774	1.2450	2.9610
	0.0				0.7774	1.2622	2.9738
	1.0				0.7774	1.0449	2.9824
	1.5				0.7774	0.9477	3.0104
		0.2			0.7774	1.4731	-0.1632
		0.3			0.7774	1.4650	-0.1203
		0.4			0.7774	1.4566	-0.0753
			0.2		0.7774	0.9997	2.8203
			0.3		0.7774	0.8677	2.8105
				0.2	0.8171	1.1399	2.9350
				0.3	0.8545	1.1222	2.9133

TABLE 4.1: Computed numerical data of Sherwood number, skin friction coefficient and Nusselt number for $K = 2$, $\lambda = 0.3$, $\phi_1 = \phi_2 = \phi_4 = 0.1$, $\phi_3 = 1$, $K_1 = 0.5$, $N_b = 0.1$, $\omega = \frac{\pi}{3}$ and $E = 0.01$.

Table 4.1 describes the computed numerical results of C_f, Nu_x and Sh using different values of physical parameters given in the table. The skin friction coefficient

is $f''(0) + \frac{\lambda}{2} f''^2(0)$, Nusselt number is $-g'(0)$ and the Sherwood number is $-\varphi'(0)$. By altering the diverse parameters the values of skin friction coefficient, Nusselt parameter and Sherwood number changes. As given in table, the skin friction coefficient gradually depressed by enhancing values of magnetic number. However, for Prandtl number, Schmidt number, thermophoresis parameter, and thermal radiation parameter no change has been observed for skin friction coefficient. For the local Nusselt number diminish behaviour have been shown for various physical parameters, but opposite trend is noticed for growth of Sherwood number and Prandtl number reduces against physical parameters while in case of thermal radiation parameter Sherwood number slightly escalates.

4.3.2 Influence of Stretching Ratio Parameter E

Figure 4.2 shows the impact of stretching ratio parameter on the velocity parameter. It can be seen from the curve that the velocity profile decreases for boosting values of E. Actually, the mounting values of E induces more pressure on the flow as a result, the non-dimensional velocity profile reduces. To view the effect of velocity ratio parameter on the dimensionless temperature profile Figure 4.3 is presented. Practically it is perceived that by escalating the amount of the stretching ratio parameter E temperature profile increases.

4.3.3 Influence of Inclined Angle ω

Figure 4.4 reflects the effect of inclination angle ω of magnetic field on the velocity field. It is noticed that, physically an increase in the inclination angle actually increases the Lorentz force which is friction forces thus correspondingly that decreases the velocity profile. Figure 4.5 is displayed temperature distributions for the boosting values of ω. Physically by increasing the inclination angle we are increase the Lorentz force which generate more heat and thus increase the temperature profile.

4.3.4 Influence of Non-Newtonian Williamson Parameter λ

Figure 4.6 stipulates the influence of non-Newtonian Williamson parameter on the velocity profile. It is portrayed that the velocity profile decrease by increasing the values of λ, which attains the physical significance of non-Newtonian Williamson fluids having larger λ that can be selected to govern the heat transfer rate.

4.3.5 Influence of Magnetic Parameter M

Figure 4.7 depicts the effect of magnetic parameter M on the velocity field. That employs viscous drag force on the flow which results in the deceleration of momentum, therefore with the increment of M the velocity boundary layer thickness increases. Velocity profile stipulated that with the increasing values of M the velocity increases.

4.3.6 Influence of Nanoparticles Volume Fraction ϕ_1

Figure 4.8 shows the impact of ϕ_1 on velocity profile of different volume fractions. According to this figure, in volume fraction, velocity distribution decreases with an increase in ϕ_1. Due to accelerating amount of ϕ_1, the motion of particles will be more intense and the molecular force will be reduced. Therefore, fluid movement becomes easier. Hence, it is analyzed that an rise in nanoparticles volume fraction, fall in velocity profile. Graph describe the physical behaviour of the nanofluid. This is due to the fact that the velocity of the nanofluid is reciprocally proportional to the size of fluid particles.

4.3.7 Influence of Porosity Parameter K

Figure 4.9 demonstrates the variation of porosity parameter K, with in the boundary layer. It is found that increasing the values of K fluid velocity increases in

the boundary layer. Physically, the permeability reduces resistance of the porous medium against the flow which tend to increase the velocity of fluid. Figure 4.10 illustrates the impact of K on the temperature field. It is observed that by increasing the variation of K causes thickness of thermal boundary layer in dimensionless distribution of temperature. The similar behaviour of concentration distribution is noticed for the variation of K in Figure 4.11.

4.3.8 Influence of Brownian Motion Parameter N_b

Figure 4.12 depicts that rise in the N_b enhances the dimensionless temperature of fluid. Physically Brownian motion parameter associated with movement of the fluid nanoparticles. The fluid particles of kinetic energy accelerates with mounting alteration of N_b, so in this case temperature distribution of fluid escalates. Figure 4.13 is drawn to analyze the relationship between Brownian motion parameter and dimensionless concentration profile, which clearly proves the physical nature of N_b by enlargement of numerical values causes to reduce the concentration profile.

4.3.9 Influence of Thermophoresis Parameter N_t

Figures 4.14 and 4.15, it is clear that the dimensionless temperature and concentration increase with the gain in thermophoresis parameter N_t. Thermophoresis parameter assists to improve the thickness of the boundary layers of temperature and concentration. As a consequence, both profiles are raised. It is also present that the increasing in the temperature and concentration fields is high in nanofluid. Generally, thermophoresis is a mass transfer phenomena in which movement of small particles diminish thermal gradient. It causes the small particles to remain on the stretching surfaces.

4.3.10 Influence of Eckert Number E_c

Figure 4.16 shows a behaviour of the Eckert number E_c is given, that illuminates the reaction of the temperature area for the viscous dissipation and Joule heating circumstance. It is predominant to kept in mind that the appearance of heat dissipation is likely to lead to an increment of both the thickness of the thermal boundary layer and the temperature field. Physically, the implementation of convective heat is build up and then consequences in extent the thermal coating. Figure 4.17 is presented for different values of E_c against the concentration profile. For increasing values of Eckert number, it is observed that the concentration field declined.

4.3.11 Influence of Prandtl Number P_r

Figure 4.18 is sketched to visualize the variation in the dimensionless temperature profile for various values of P_r. The graph shows that the temperature decreases as the Prandtl number alteration rise at a fixed g value. This is attributed to the reason that a greater amount of Prandtl fluid has comparatively poor thermal conductivity, which lowers the conduction and hence the thickness of the thermal boundary layer and as a result, the temperature decelerate. Greater Prandtl number is to raise the rate of heat transfer at the surface as the temperature gradient at the surface increases.

4.3.12 Influence of Thermal Radiation Parameter R

Figure 4.19 elucidates the impact of thermal radiation parameter R on the temperature field. The dimensionless temperature profile and the thermal boundary layer thickness increase gradually with an increase in the values of the thermal radiation parameter R. Physically, it strengthen the fact that more heat is produced due to the radiation process which in response increases both the temperature distribution as well as the thermal boundary layer thickness.

4.3.13 Influence of Schmidt Parameter S_c

Figure 4.20 portrays the effect on concentration distribution over distinct values of S_c. The behaviour of Schmidt parameter against dimensionless concentration profile is decreased. Physically it attributes an inverse relation of mass diffusivity with S_c. The boosting numerical values of Schmidt number stipulated low mass diffusion and the concentration boundary layer thickness is reduced.

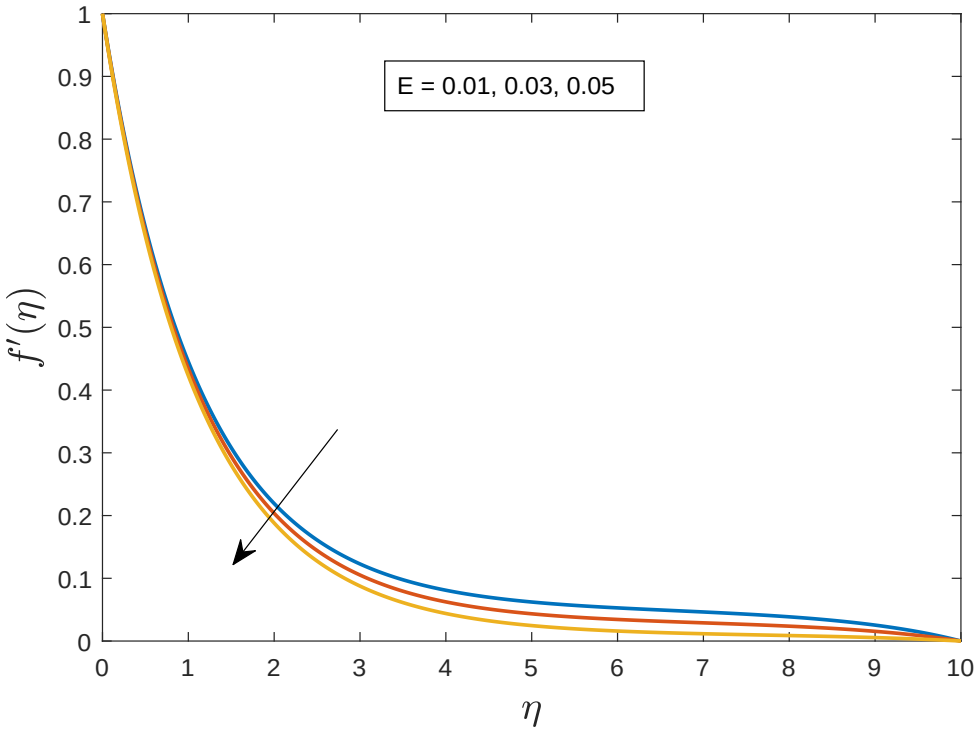

FIGURE 4.2: The impact of E on velocity profile is plotted against η.

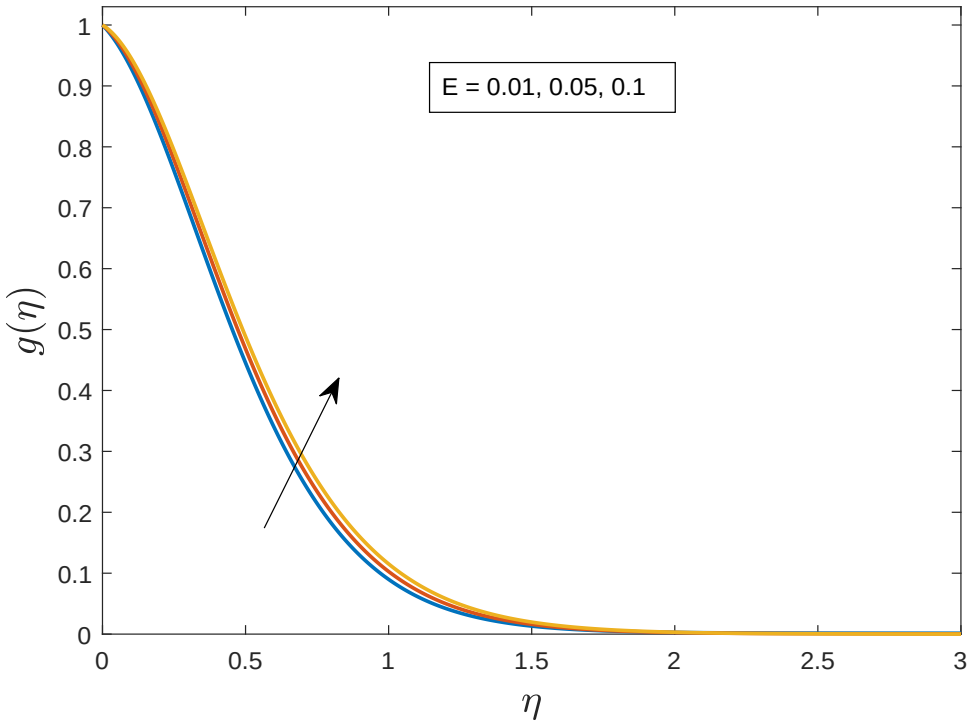

FIGURE 4.3: The impact of E on temperature profile is plotted against η.

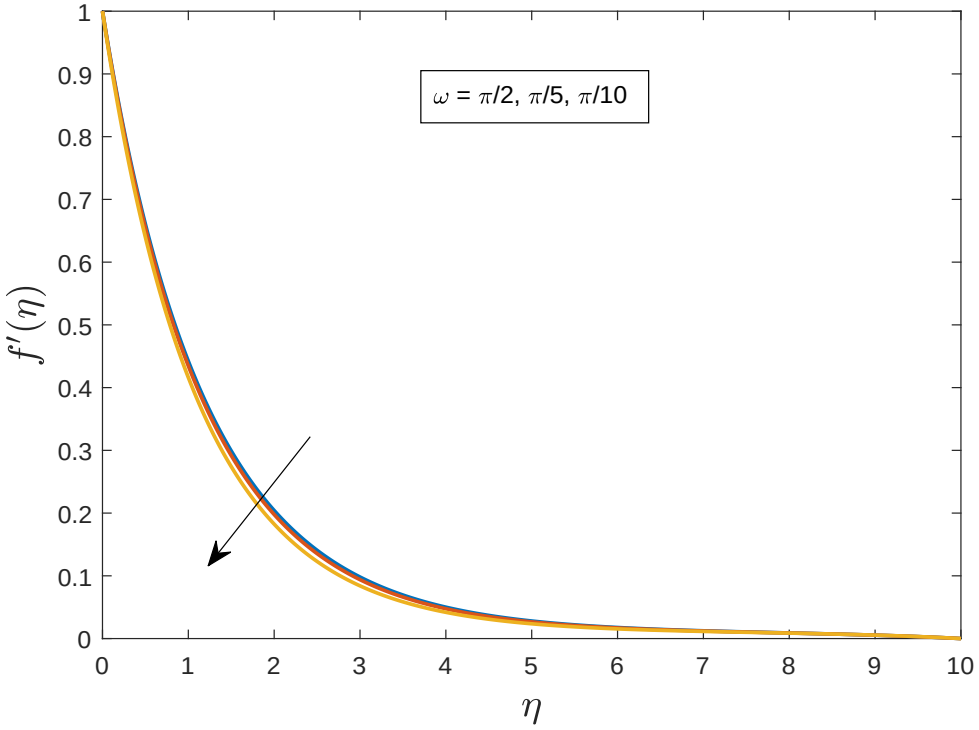

FIGURE 4.4: The impact of ω on velocity profile is plotted against η.

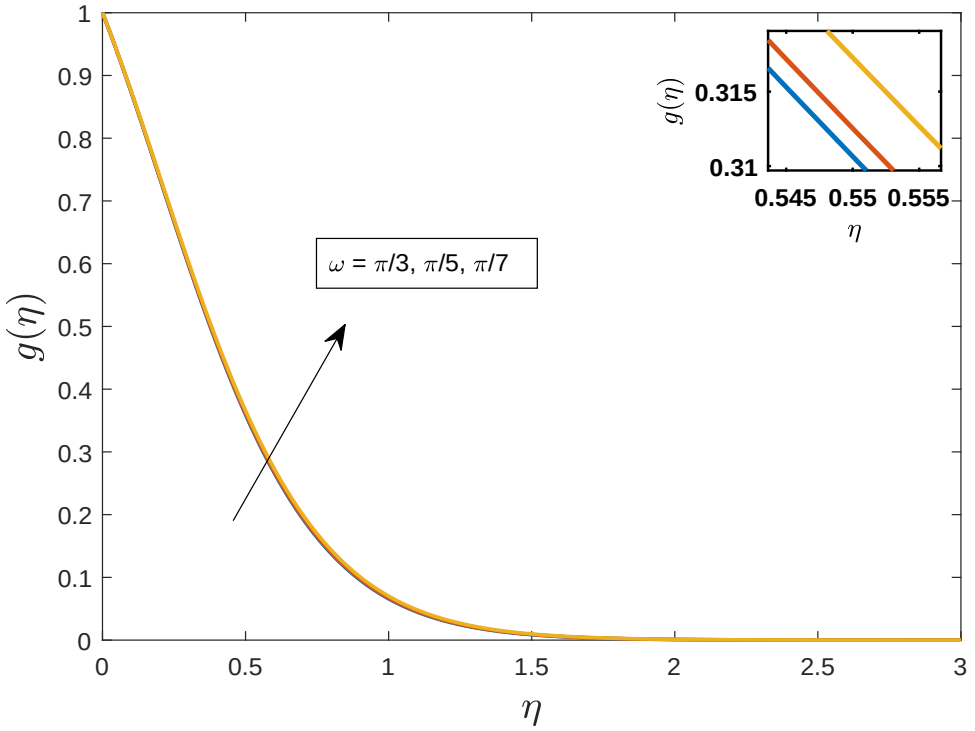

FIGURE 4.5: The impact of ω on temperature profile is plotted against η.

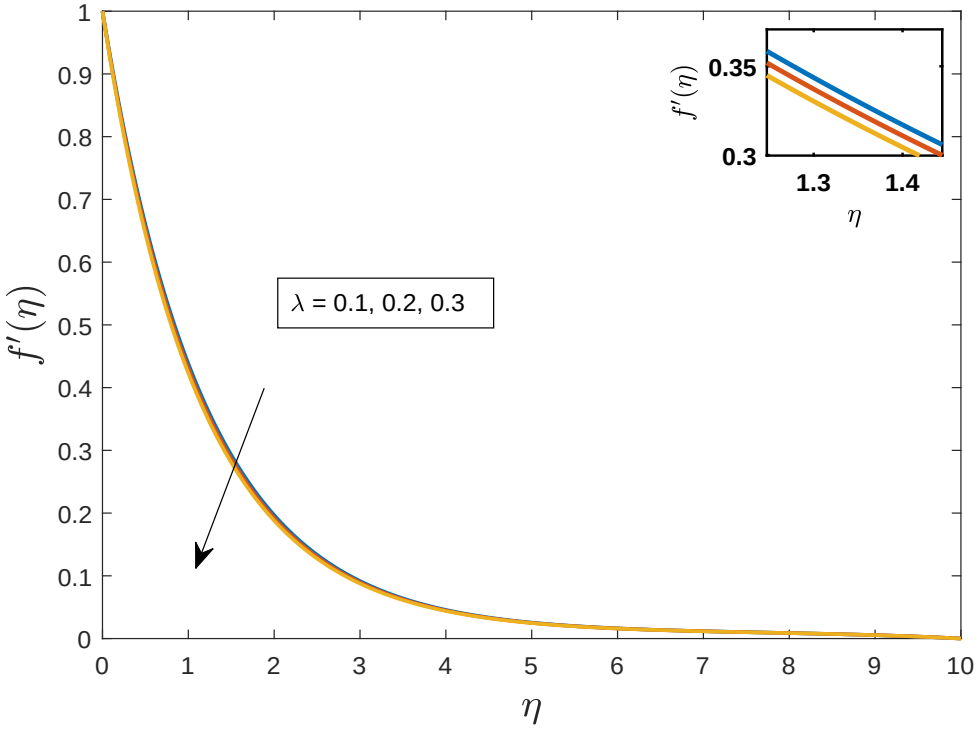

FIGURE 4.6: The impact of λ on velocity profile is plotted against η.

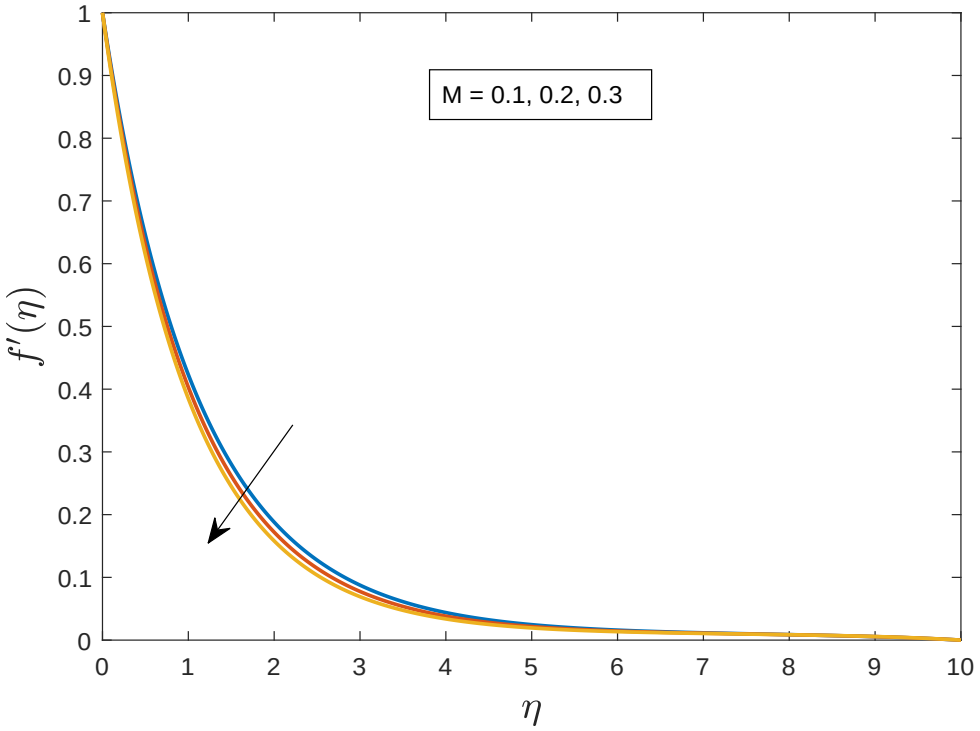

FIGURE 4.7: The impact of on M velocity profile is plotted against η.

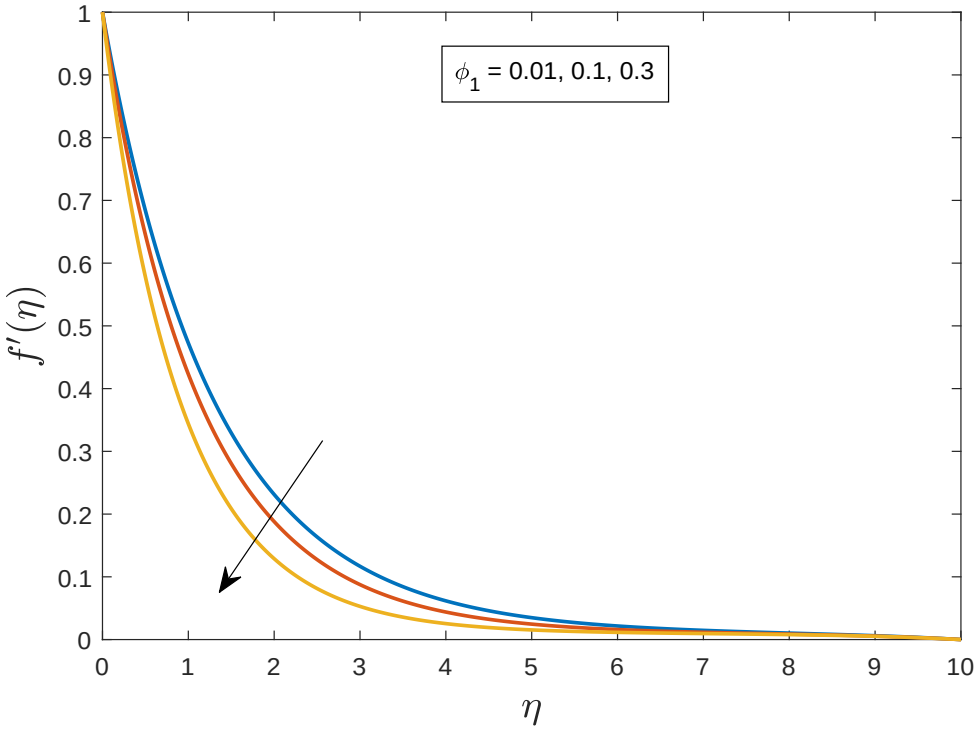

FIGURE 4.8: The impact of ϕ_1 on velocity profile is plotted against η.

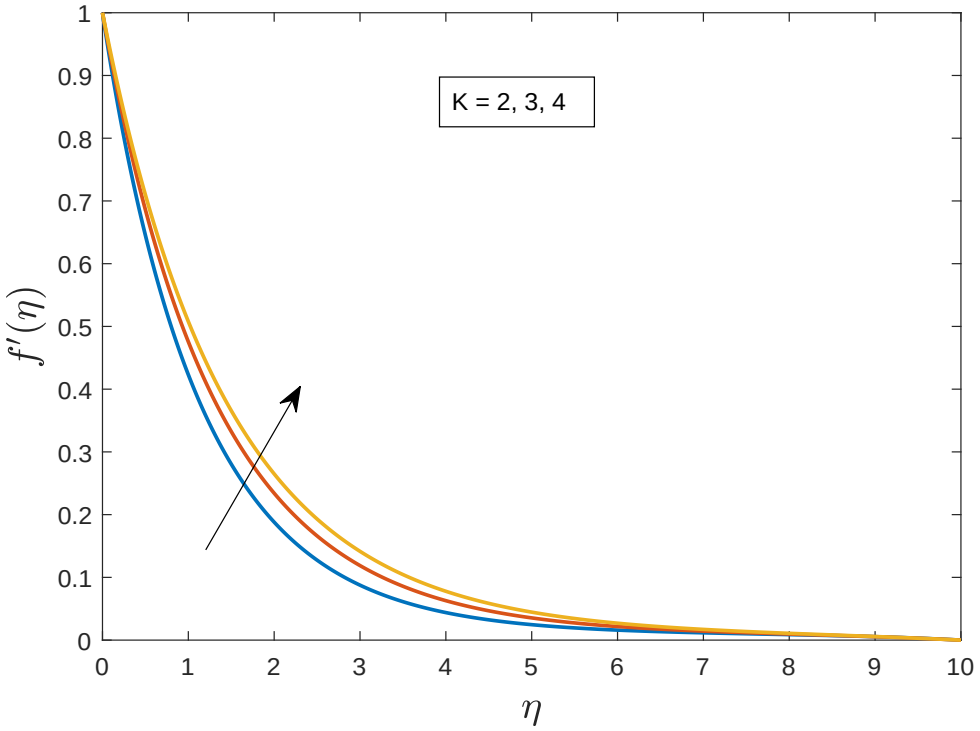

FIGURE 4.9: The impact of K on velocity profile is plotted against η.

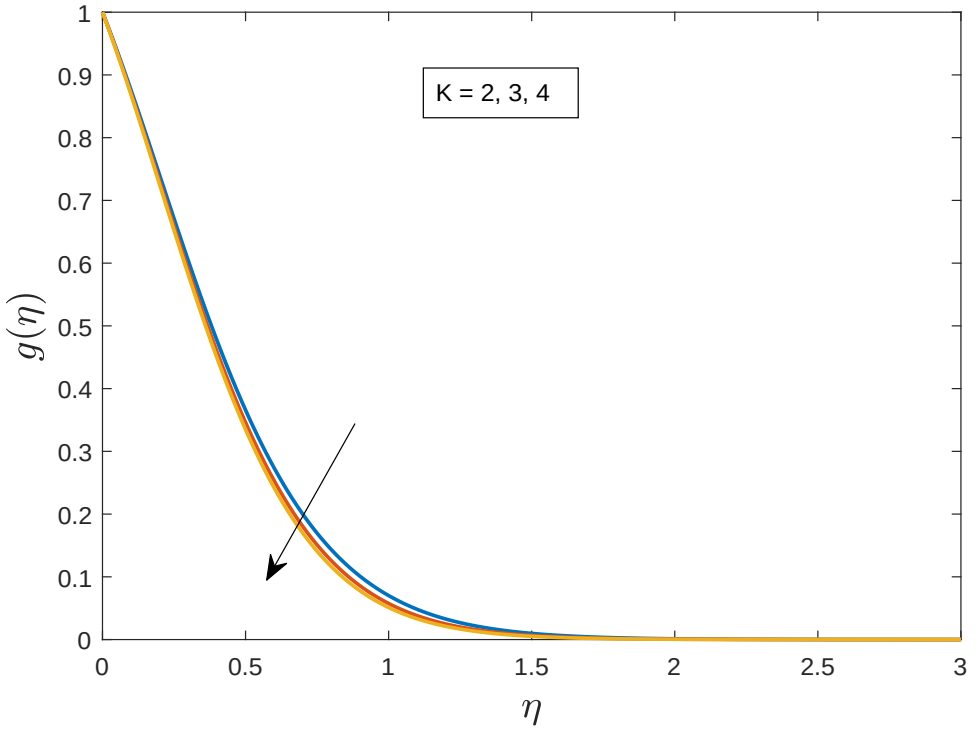

FIGURE 4.10: The impact of K on temperature field is plotted against η.

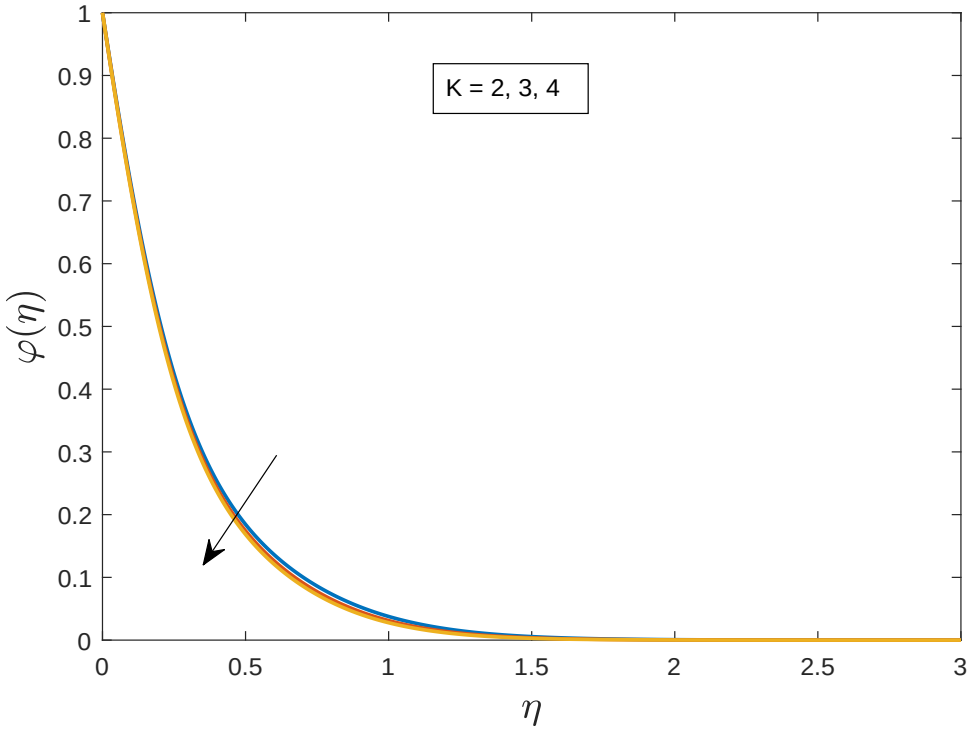

FIGURE 4.11: The impact of K concentration field is plotted against η.

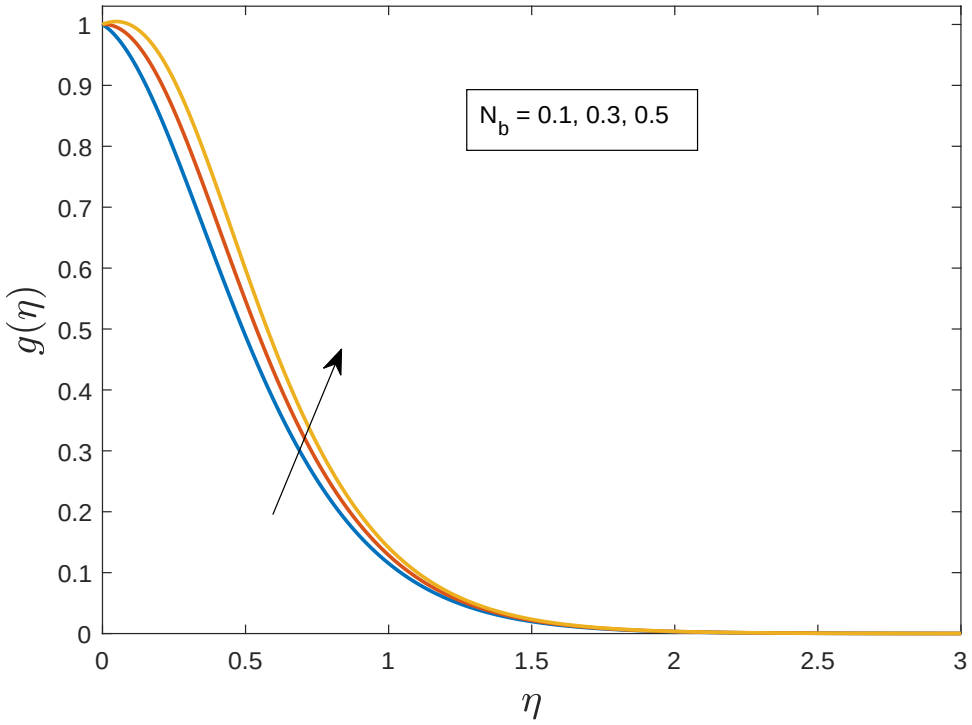

FIGURE 4.12: The impact of N_b temperature field is plotted against η.

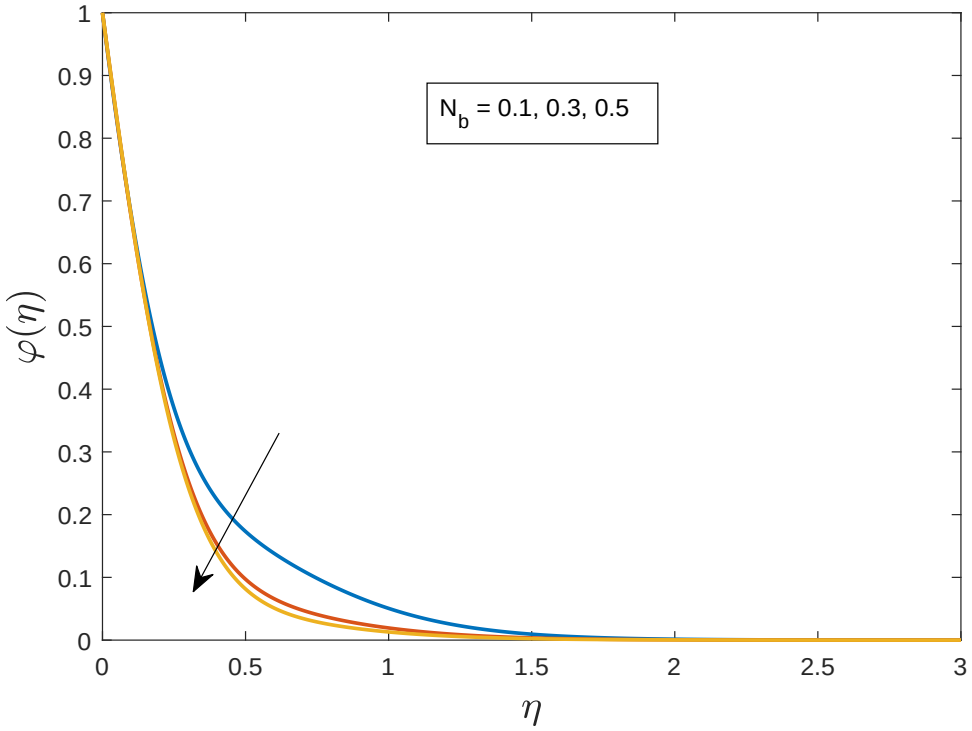

FIGURE 4.13: The impact of N_b concentration profile is plotted against η.

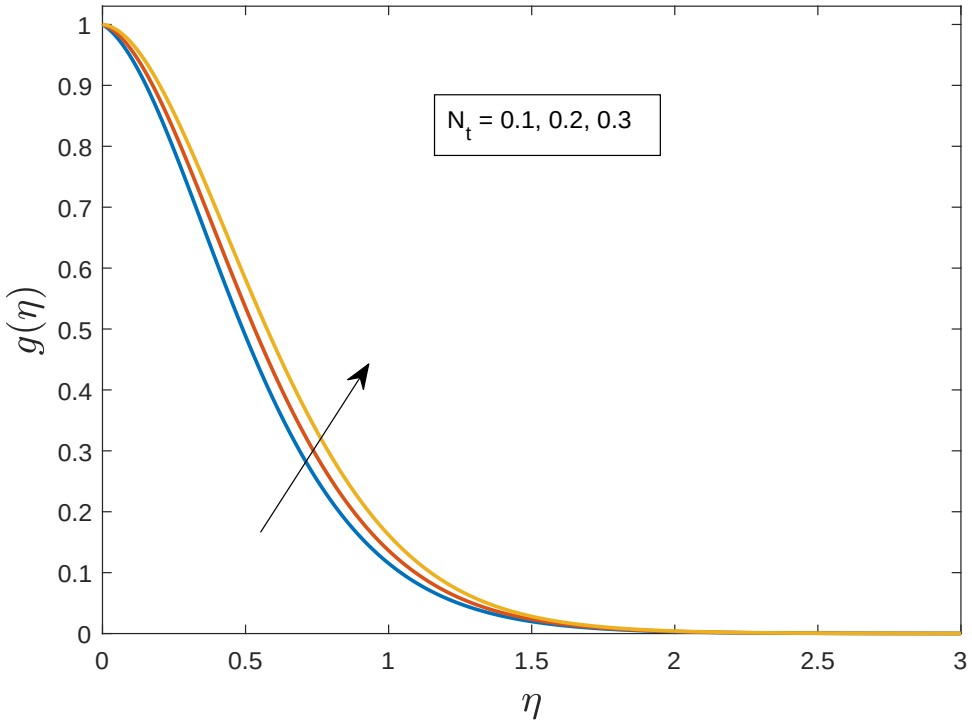

FIGURE 4.14: The impact of N_t on temperature field is plotted against η.

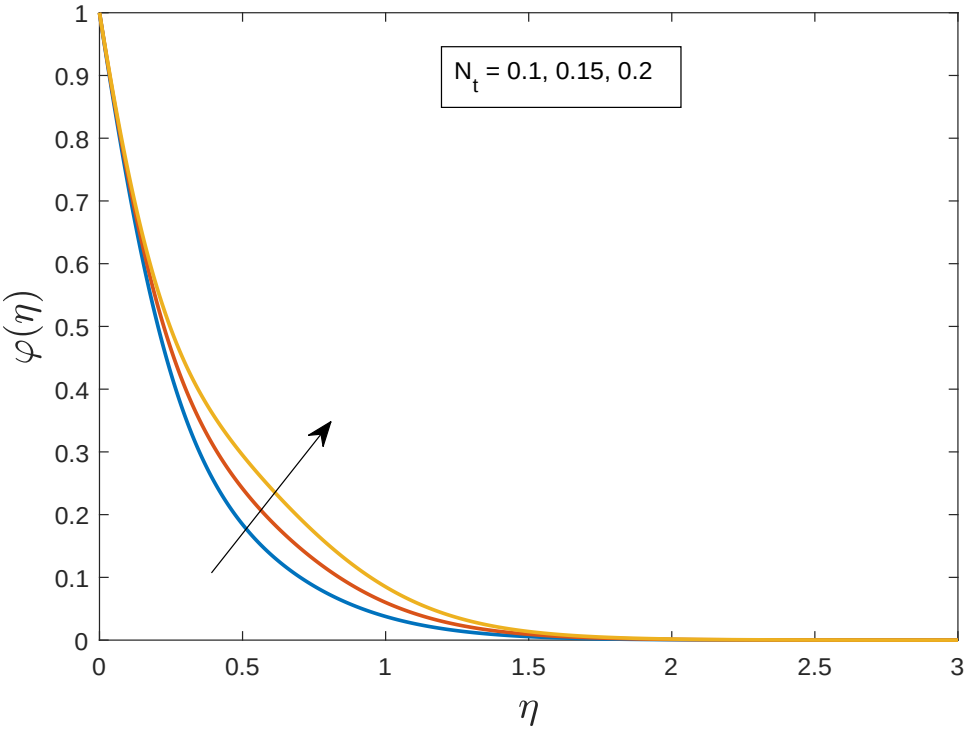

FIGURE 4.15: The impact of N_t concentration profile is plotted against η.

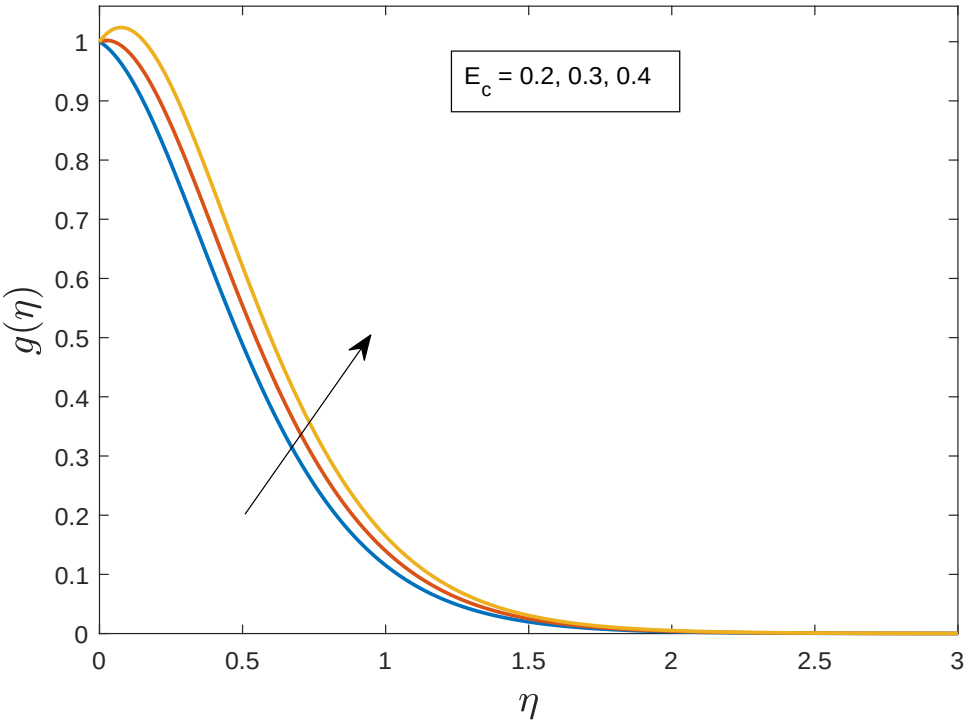

FIGURE 4.16: The impact of E_c on temperature field is plotted against η.

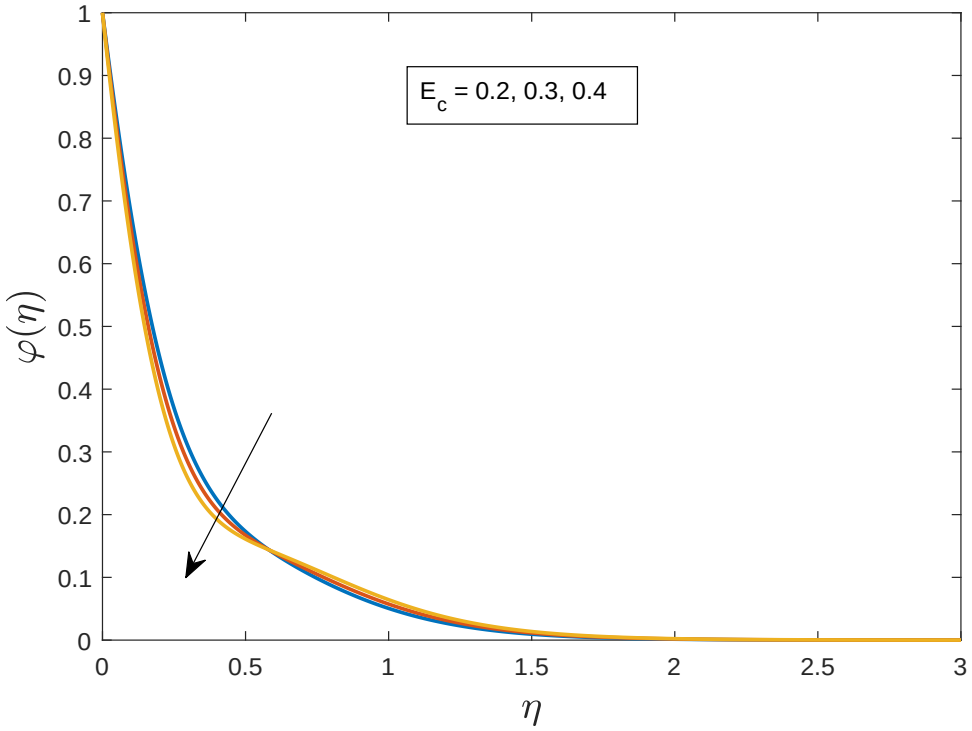

FIGURE 4.17: The impact of E_c on concentration profile is plotted against η.

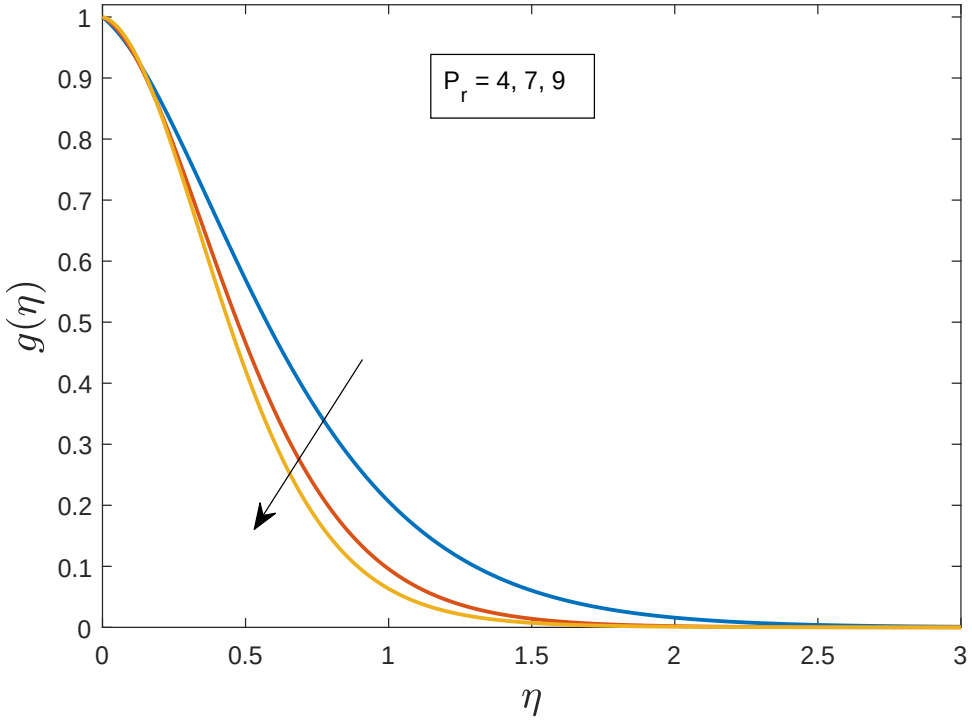

FIGURE 4.18: The impact of P_r on temperature field is plotted against η.

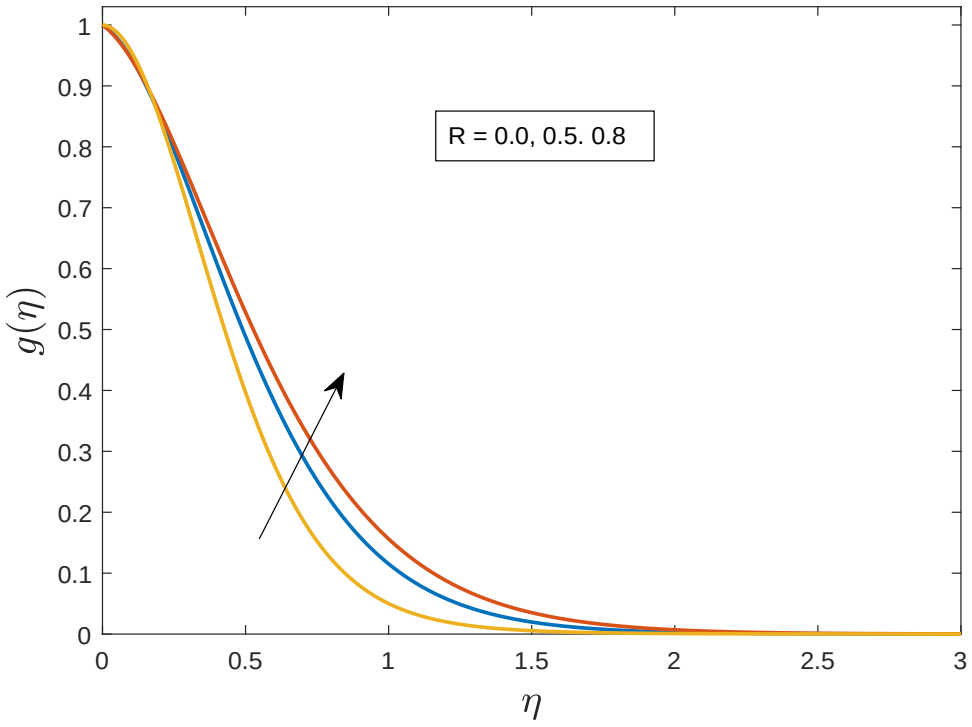

FIGURE 4.19: The impact of R on temperature field is plotted against η.

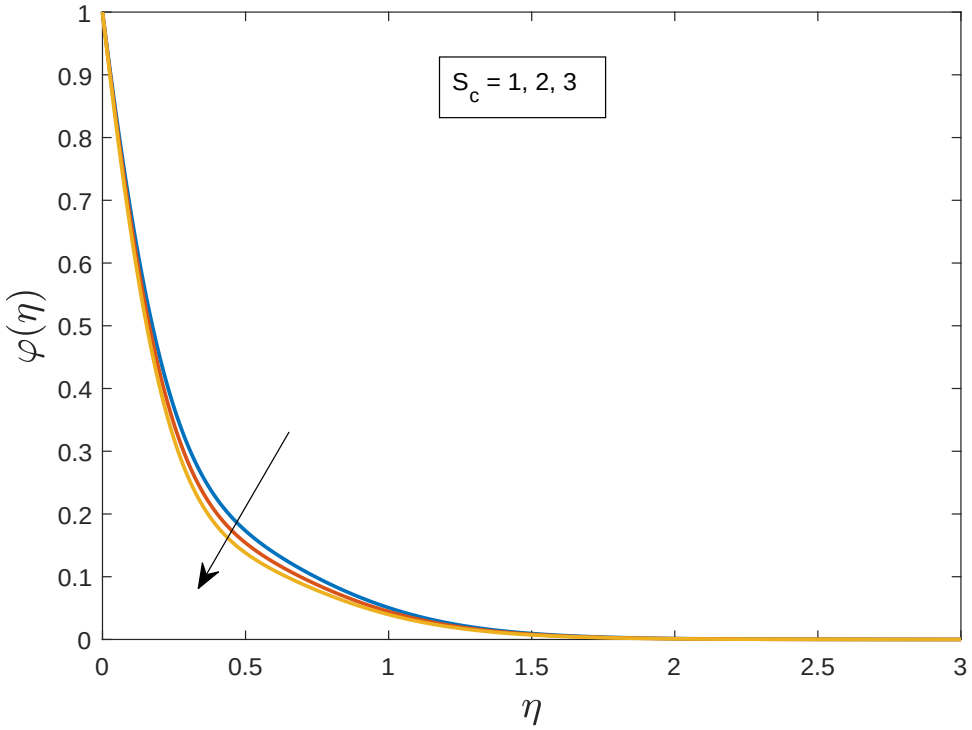

FIGURE 4.20: The impact of S_c on concentration gradient profile is plotted against η.

Chapter 5

Conclusion

In this thesis, a two dimensional incompressible and steady MHD stagnation point flow with the effect of thermal radiations, and inclined magnetic field with Joule heating is studied in an enclosure of stretching surface.

In this study, the work of Shawky *et al.* [25] is reviewed and extended with the concept of MHD stagnation point flow with effect of thermal radiations, stretching ratio parameter and inclined magnetic field with Joule heating to assimilate the momentum and energy equation. The influence of several physical parameters on velocity, temperature and concentration profiles is discussed graphically.
The skin fraction coefficient, Nusselt number and Sherwood number are investigated through table for the appropriate rate of the parameters using MATLAB.
From the current study that has been numerically analyzed the following worthy points can be concluded:

- Increasing the stretching ratio or velocity ratio parameter, temperature profile increases but the opposite trend is noticed for the dimensionless velocity field.
- The Eckert number accelerates the nature of temperature of nanofluid and thickness of thermal boundary layer extent. But the concentration profile decelerate by escalating the alteration of Eckert number.

- Raised up of thermal radiation has great influence on the maximum temperature gradient field and thermal boundary layer.
- Boosting value of inclined angle of magnetic field in response the temperature distribution increases while reverse behaviour is observed for velocity profile.
- Uprising the values of non-Newtonian Williamson parameter has inverse relation for non dimensional velocity of fluid.
- The velocity, temperature and concentration profiles escalate as the porosity parameter increases.
- Temperature distribution reduces by the enlargement of Prandtl number.
- Velocity of fluid field escalates as the magnetic parameter values increases and fall for various values of nanoparticles volume fraction.
- Brownian motion parameter enhances the temperature profile but opposing effect detected for dimensionless concentration field.
- The higher estimation of thermophoresis parameter tend to rise both the behaviour of dimensionless nanoparticles concentration and temperature profiles.
- The nanoparticles concentration profile declined for distinct values of Schmidt number.

5.1 Forthcoming Implementation

The study carried out in this thesis opens many gateways to new and innovative research directions, for example, the fluid model of Jeffery, Tangent hyperbolic nanofluid and Burger can be analyzed.

- It can also be analyzed the fluid by utilizing the various geometries as channel, cone, cylinder, wedge and squeezing flow etc.

- The problem can be developed by different physical parameters like Weisenberg number, Biot number, nth order chemical reaction parameter by assuming dust particles and suction or injection parameter.

Bibliography

[1] C. Hirsch, *Numerical computation of internal and external flows: The fundamentals of computational fluid dynamics*. Elsevier, 2007.

[2] J. D. Anderson and J. Wendt, *Computational fluid dynamics*, vol. 206. Springer, 1995.

[3] J. F. Wendt, *Computational fluid dynamics: an introduction*. Springer Science and Business Media, 2008.

[4] R. Agarwal, "Computational fluid dynamics of whole-body aircraft," *Annual review of fluid mechanics*, vol. 31, no. 1, pp. 125–169, 1999.

[5] F. J. Zajaczkowski, S. E. Haupt, and K. J. Schmehl, "A preliminary study of assimilating numerical weather prediction data into computational fluid dynamics models for wind prediction," *Journal of Wind Engineering and Industrial Aerodynamics*, vol. 99, no. 4, pp. 320–329, 2011.

[6] H. Okada, K. Mitsuhashi, T. Ohara, E. R. Whitby, and H. Wada, "Computational fluid dynamics simulation of high gradient magnetic separation," *Separation science and technology*, vol. 40, no. 7, pp. 1567–1584, 2005.

[7] J. Zhang, W. Johnson, and T. Plikas, "Application of computational fluid dynamics for solving ventilation problems in metallurgical industrial processes," *International Journal of Ventilation*, vol. 16, no. 3, pp. 200–212, 2017.

[8] K. Pavlov, "Magnetohydrodynamic flow of an incompressible viscous fluid caused by deformation of a plane surface," *Magnitnaya Gidrodinamika*, vol. 4, no. 1, pp. 146–147, 1974.

[9] K. H. Kabir, M. A. Alim, and L. S. Andallah, "Effects of viscous dissipation on MHD natural convection flow along a vertical wavy surface," *Journal of Theoretical and Applied Physics*, vol. 7, no. 1, pp. 1–8, 2013.

[10] T. Hayat, M. Waqas, M. I. Khan, and A. Alsaedi, "Impacts of constructive and destructive chemical reactions in magnetohydrodynamic (mhd) flow of Jeffrey liquid due to nonlinear radially stretched surface," *Journal of Molecular Liquids*, vol. 225, pp. 302–310, 2017.

[11] S. Nadeem, A. Hussain, and M. Khan, "HAM solutions for boundary layer flow in the region of the stagnation point towards a stretching sheet," *Communications in Nonlinear Science and Numerical Simulation*, vol. 15, no. 3, pp. 475–481, 2010.

[12] K. Hiemenz, "Die Grenzschicht an einem in den gleichformigen Flussigkeitsstrom eingetauchten geraden Kreiszylinder," *Dinglers Polytech. J.*, vol. 326, pp. 321–324, 1911.

[13] T. Grosan, I. Pop, C. Revnic, and D. Ingham, "Magnetohydrodynamic oblique stagnation-point flow," *Meccanica*, vol. 44, no. 5, p. 565, 2009.

[14] J. H. Merkin and I. Pop, "Stagnation point flow past a stretching/shrinking sheet driven by Arrhenius kinetics," *Applied Mathematics and Computation*, vol. 337, pp. 583–590, 2018.

[15] P. Weidman, "Hiemenz stagnation-point flow impinging on a uniformly rotating plate," *European Journal of Mechanics-B/Fluids*, vol. 78, pp. 169–173, 2019.

[16] T. R. Mahapatra and A. Gupta, "Stagnation-point flow of a viscoelastic fluid towards a stretching surface," *International Journal of Non-Linear Mechanics*, vol. 39, no. 5, pp. 811–820, 2004.

[17] Y. Lok, J. Merkin, and I. Pop, "MHD oblique stagnation-point flow towards a stretching/shrinking surface," *Meccanica*, vol. 50, no. 12, pp. 2949–2961, 2015.

[18] K. Kaladhar, K. Madhusudhan Reddy, and D. Srinivasacharya, "Inclined magnetic field, thermal radiation, and Hall current effects on mixed convection flow between vertical parallel plates," *Journal of Heat Transfer*, vol. 141, no. 10, 2019.

[19] T. Hayat, S. Bibi, M. Rafiq, A. Alsaedi, and F. Abbasi, "Effect of an inclined magnetic field on peristaltic flow of Williamson fluid in an inclined channel with convective conditions," *Journal of magnetism and magnetic materials*, vol. 401, pp. 733–745, 2016.

[20] N. Sandeep and V. Sugunamma, "Effect of inclined magnetic field on unsteady free convective flow of dissipative fluid past a vertical plate," *Open Journal of Engineering Technology*, vol. 1, no. 1, pp. 6–23, 2013.

[21] M. Rahman, "Convective flows of micropolar fluids from radiate isothermal porous surfaces with viscous dissipation and Joule heating," *Communications in Nonlinear Science and Numerical Simulation*, vol. 14, no. 7, pp. 3018–3030, 2009.

[22] M. I. Khan, T. Hayat, M. I. Khan, and A. Alsaedi, "A modified homogeneous-heterogeneous reactions for MHD stagnation flow with viscous dissipation and Joule heating," *International Journal of Heat and Mass Transfer*, vol. 113, pp. 310–317, 2017.

[23] M. Ilbas, "The effect of thermal radiation and radiation models on hydrogen-hydrocarbon combustion modelling," *International Journal of Hydrogen Energy*, vol. 30, no. 10, pp. 1113–1126, 2005.

[24] M. Waqas, M. I. Khan, T. Hayat, and A. Alsaedi, "Numerical simulation for magneto Carreau nanofluid model with thermal radiation: A revised model," *Computer Methods in Applied Mechanics and Engineering*, vol. 324, pp. 640–653, 2017.

[25] H. M. Shawky, N. T. Eldabe, K. A. Kamel, and E. A. Abd-Aziz, "MHD flow with heat and mass transfer of Williamson nanofluid over stretching

sheet through porous medium," *Microsystem Technologies*, vol. 25, no. 4, pp. 1155–1169, 2019.

[26] J. Kunes, *Dimensionless physical quantities in science and engineering*. Elsevier, 2012.

[27] R. Bansal, *A textbook of fluid mechanics and hydraulic machines*. Laxmi publications, 2004.

[28] J. M. C. Yunus A. Cengel, *Fluid Mechanics: Fundamentals and applications*. McGraw-Hill, 1st edition, 2006.

[29] F. M. White, *Fluid mechanics*. Tata McGraw-Hill Education, 1979.

[30] R. W. Lewis, P. Nithiarasu, and K. N. Seetharamu, *Fundamentals of the finite element method for heat and fluid flow*. John Wiley and Sons, 2004.

[31] A. J. Smits, *A physical introduction to fluid mechanics*. John Wiley New York, 2000.

[32] J. N. Reddy and D. K. Gartling, *The finite element method in heat transfer and fluid dynamics*. CRC press, 2010.

[33] T. Y. Na, *Computational methods in engineering boundary value problems*. Academic press, 1980.

[34] R. Williamson, "Flow of pseudoplastic materials.," *International Journal of Heat and Mass Transfer*, vol. 21, pp. 1108–1111, 1929.

[35] C. Vasudev, "Peristaltic pumping of Williamson fluid through a pourous medium in a horizontal channel with heat transfer: Problem formulation," *International Journal of Heat and Mass Transfer*, vol. 1, pp. 656–666, 2010.

[36] F. Hady, R. Mohamed, M. Abd-Elsalam, and A. Mostafa, "The Blasius and Sakiadis flow in a nanofluid through a porous medium in the presence of thermal radiation under a convective surface boundary condition," *International Journal of Engineering Innovative Technology*, vol. 3, no. 3, pp. 225–234, 2013.

[37] R. K. Tiwari and M. K. Das, "Heat transfer augmentation in a two-sided lid-driven differentially heated square cavity utilizing nanofluids," *International Journal of Heat and Mass Transfer*, vol. 50, no. 9-10, pp. 2002–2018, 2007.